ABSTRACT

AKDEMIR, KEREM ZIYA. Decarbonization Planning under Climate Change: An Open-Source Approach using Reduced Network Production Cost Models. (Under the direction of Dr. Jordan Kern and Dr. Jeremiah Johnson).

Electricity grids are undergoing significant transformation due to decarbonization and sectoral electrification efforts. On the other hand, extreme weather events strain the electricity grids by directly damaging or reducing the efficiency of energy infrastructure, increasing demand, and putting stress on transmission lines. There is a need to increase the share of renewable energy such as solar, wind, and wave power, and connect those resources by making efficient transmission investments. In this sense, the latest energy system models should consider all those factors while maintaining simulation times in reasonable ranges. However, this creates a computational modeling challenge. Developers must balance computational speed (i.e. runtime) with model fidelity (i.e. accuracy). The first chapter of this dissertation provides a more detailed outlook on these emerging needs. In the second chapter, a new framework for instantiating open-source production cost models (PCMs), called Grid Operations (GO), is presented. GO allows users to search across parameter spaces to identify model versions that appropriately balance computational speed and fidelity based on experimental needs and resource limits. Results of this chapter show that models with coarser network topologies can accurately mimic market operations, close to higher-resolution models. It is thus possible to conduct large simulation experiments that characterize risks related to climate and weather extremes while maintaining sufficient model accuracy. The third chapter investigates the possible benefits of wave energy in power system operations by utilizing the proposed framework. This chapter characterizes the inflection point beyond which wave integration starts impacting power system operations under the current transmission infrastructure. Furthermore, it considers the joint effects of wave energy

integration and system-wide transmission expansion as well as potential resilience scenarios such as wildfire-driven transmission contingencies and heat wave events. For this experiment, wave energy generation is integrated at carefully selected sites across the coastal areas of Washington, Oregon, and northern California of U.S. Western Interconnection. The results indicate that wave energy integration systematically reduces locational marginal prices (LMPs) of electricity and price volatility, especially during periods of high wave resource availability. The effects of wave energy integration can remain localized with existing transmission infrastructure. However, with concurrent transmission expansion, the impacts of wave energy integration are likely to have a higher geographical spread. The results also indicate that wave energy may be able to assist power system operations during resilience events such as major transmission contingencies. The last chapter examines the potential impact of cooperation in transmission expansion planning, using the proposed framework to simulate grid operations of U.S. Western Interconnection in 2019 and 2059 under different levels of collaboration between transmission planning regions. Also, two historical heat waves with varying spatial scope (local vs. widespread) in 2019 are replayed under future climate change in 2059 to assess the transmission cooperation benefits. The results show that cooperative transmission planning yields the best outcomes in terms of reducing wholesale electricity prices and minimizing energy outages both for the whole interconnection and individual transmission planning regions. It also helps decrease greenhouse gas emissions by reducing reliance on fossil fuel resources and/or increasing renewable energy utilization. However, the benefits of transmission cooperation diminish during widespread heat waves when all regions face extreme electricity demand due to space cooling needs. Despite this, cooperative transmission planning remains advantageous, particularly for California Independent System Operator (CAISO) with significant solar installations.

Decarbonization Planning under Climate Change: An Open-Source Approach using Reduced Network Production Cost Models

by
Kerem Ziya Akdemir

A dissertation submitted to the Graduate Faculty of
North Carolina State University
in partial fulfillment of the
requirements for the degree of
Doctor of Philosophy

Civil Engineering

Raleigh, North Carolina
2024

APPROVED BY:

_____	_____
Dr. Jordan Kern Committee Co-Chair	Dr. Jeremiah Johnson Committee Co-Chair
_____	_____
Dr. Gregory Characklis	Dr. John Baugh

DEDICATION

To my wife and family

BIOGRAPHY

Kerem Ziya Akdemir was born in Ankara, Turkey in 1995. He spent most of his childhood in Ankara and started to be interested in environmental issues. With this interest, he received a Bachelor of Science degree in Environmental Engineering from Middle East Technical University in June 2018. After his graduation, he worked at two consultancy companies on environmental impact assessment (EIA) of renewable energy projects, carbon abatement projects, voluntary carbon markets, and emission trading systems (ETS).

His interest shifted toward power systems, renewable energy, economics, modeling, optimization, and machine learning. In order to improve his abilities and knowledge on these topics, he received a Master of Science degree in Natural Resources at North Carolina State University in May 2021. Then, he continued with a Doctor of Philosophy degree in Civil Engineering at North Carolina State University to hone his skills further. After graduation, he plans to continue working on energy-related topics and be a part of the decarbonization efforts.

ACKNOWLEDGMENTS

Firstly, I would like to thank Dr. Jordan Kern, and Dr. Jeremiah Johnson for their valuable guidance and support that made this study a reality. Also, I would like to thank Dr. Gregory Characklis, and Dr. John Baugh for their insightful comments, contributions, and time, which enhanced the quality of this study significantly.

Next, I would like to share my gratitude to my family and friends. They have been by my side and never held back their support. Finally, I would like to thank my wife, Ece Ari Akdemir. Her endless love and support helped me to move forward positively throughout this journey, which was crucial for me to complete this dissertation.

This research was supported by the US Department of Energy, Office of Science, as part of research in the MultiSector Dynamics, Earth and Environmental System Modeling Program.

TABLE OF CONTENTS

LIST OF TABLES

LIST OF FIGURES

CHAPTER 1. INTRODUCTION

Climate change induced by increasing greenhouse gas emissions from burning fossil fuels is expected to have significant consequences on the environment and human well-being (Calvin et al., 2023; United Nations, 2023). Anthropogenic activities such as manufacturing, electricity generation, and transportation have caused global temperatures to increase by approximately 1.1°C, compared to preindustrial levels (IPCC, 2022; NASA, 2023). Maintaining global warming at levels below 1.5 °C or 2 °C entails reaching net-zero emissions by 2050 or 2070, respectively (IPCC, 2022).

A global transformation of the energy sector is required to diminish greenhouse gas (GHG) emissions and accomplish these climate goals (Guler et al., 2021; Lane et al., 2016; Rodríguez-Sarasty et al., 2021). Increasing the proportion of variable renewable energy sources such as solar and wind is pivotal for decarbonizing electricity grids (Arabzadeh et al., 2020; Golombek et al., 2022; Hamid et al., 2022; Liu et al., 2019). Apart from this, hydrometeorological conditions exert a substantial influence on electricity demands, system reliability, wholesale electricity prices, and GHG emissions in bulk power systems (Hill et al., 2021; Su, Kern, Reed, et al., 2020; Wessel et al., 2022). For example, the intensity and frequency of extreme weather events are intensifying due to climate change, and these types of events, like heatwaves and storms, disrupt electricity grids by demand spikes, physically damaging or reducing the effectiveness of the power plants and infrastructure (Akdemir et al., 2022; Matko et al., 2016). In addition, electrification of some areas such as transportation, space heating, and cooking is expected in the coming decades (Mai et al., 2018), which would increase the electricity demands substantially throughout the electricity grids in the world.

Given that grid operators confront these multiple challenges of decarbonization, sectoral electrification, and maintaining the reliability of power systems during extreme weather events, incorporating these several factors into power system modeling is of utmost importance (Dyreson et al., 2022). These challenges cause power system models to get more and more complex and arise a need to capture intersectoral dependencies in modeling studies (Antenucci et al., 2019). Therefore, power system researchers need to tailor the model complexity by striking a balance between tractability (i.e., computational complexity and run-time requirements) and fidelity (i.e., accuracy or ability to reproduce real-world outcomes) depending on the research question (Oikonomou et al., 2022). Furthermore, model simplification is also required for probabilistic assessments of weather and climate risks on power systems. Selecting a suboptimal modeling scale leads to oversimplified or overcomplex models, which either do not provide reliable results or waste too much resource and time.

This dissertation is prepared in response to these developments and needs. In the first chapter, we introduce our newly developed open-source framework to balance model fidelity and runtimes in production cost models (PCMs), which is called Grid Operations (GO). This framework helps researchers to create simplified representations of the three major interconnections of the United States (U.S.) from synthetic TAMU networks (Birchfield et al., 2017; Electric Grid Test Case Repository, 2017a, 2017b, 2018) by trying different parameters including number of nodes, mathematical formulation, transmission line limit scaling factors and hurdle rate scaling factors. Having an embedded PCM, users can model power system operations of three major interconnections of the U.S. However, the focus of this dissertation is modeling U.S. Western Interconnection by utilizing GO WEST, which is a sub-model of GO. The first chapter explores the impact of modeling parameters (e.g., number of nodes and mathematical

formulation) on modeling accuracy and runtimes, which lays the foundation for the upcoming chapters about renewable energy integration and power transmission investments.

The second chapter of this dissertation analyzes the economic and reliability opportunities of integrating wave energy into U.S. Western Interconnection. By utilizing the GO WEST model, the impacts of integrating different wave energy capacities under stationary and dynamic transmission line capacities are explored. Moreover, the benefits of wave power under contingency events like wildfire-induced transmission line outages are investigated. Finally, we determine the potential effects of hypothetical wave power during 2020 California heat wave event.

The third chapter of this dissertation explores the potential advantages of cooperative transmission expansion planning within U.S. Western Interconnection. Using a historical heat wave event and replaying that heat wave 40 years into the future under different climate change scenarios, we compare the individual (i.e., current planning practice) vs. cooperative (i.e., authorities working together to minimize investment and operation cost for the whole interconnection, rather than planning locally) transmission expansion planning in terms of wholesale electricity prices and reliability (e.g., unserved energy). In this chapter, on top of the GO WEST model, we developed a transmission expansion planning (TEP) model as well as some supplementary models to determine transmission line capacities under different scenarios, predict hourly electricity loads, generate future generation capacity additions and fuel prices, site the future generators to appropriate locations, and determine solar and wind generation profiles for the future years. Our hope is that this dissertation would help power system researchers by offering a new open-source PCM modeling framework and guiding the research community on the ways of using this framework to answer research questions about the future of the electricity grids.

CHAPTER 2. MODELING CONTRIBUTION: GRID OPERATIONS (GO) MODEL

2.1. Background

There is growing concern about the vulnerability of bulk electric power systems to weather and climate variability and extremes (Akdemir et al., 2022), which can strain the grid through demand spikes, generator outages and deratings, and other equipment failures, and cause reliability impacts and volatility in electricity markets (Hill et al., 2021; Oikonomou et al., 2022; Su, Kern, Denaro, et al., 2020; van Vliet et al., 2016). Correspondingly, there is growing interest in incorporating these stressors (alongside the effects of decarbonization) into operational studies using production cost models (PCMs) (Mideksa & Kallbekken, 2010; Oikonomou et al., 2022; Panteli & Mancarella, 2015; Pleßmann & Blechinger, 2017; Su, Kern, Denaro, et al., 2020). Numerous previous studies have used PCMs to simulate bulk power system operations on the interconnection scale (Behboodi et al., 2017; Brouwer et al., 2016; Cohen et al., 2022; Deane et al., 2014; Ibanez et al., 2014; Jorgenson et al., 2018; Nsanzineza et al., 2017; O'Connell et al., 2019; Samaan et al., 2015; Voisin et al., 2016), and a subset of these explicitly focus on vulnerability to weather and climate variability and extremes. Most of these previous studies employ commercial grid simulation software. Commercial models have several advantages, including shorter runtimes. However, they also have important limitations (e.g., the opacity of numerical approaches and license restrictions, etc.) that do not always allow for the large stochastic simulations needed to characterize weather and climate-related operational risks in power systems.

Take, for example, a hypothetical experiment in which a commercial PCM is used to characterize uncertainty in grid performance under future climate change. Given uncertainties in future greenhouse gas emissions pathways, along with uncertainties across climate models (including downscaling approaches), even a modestly scoped analysis may involve running the

PCM for 1000s-10,000s of individual weather years (Hill et al., 2021; Su, Kern, Denaro, et al., 2020). What if the commercial PCM comes with a license that limits its use to serial processing (one model run at a time)? If the modeler is further constrained by a computational budget (e.g., total wall clock runtime limit of L), the largest simulation ensemble possible is L divided by R, where R is the average run time of the PCM for a single year. The model runtime R becomes limiting in the experimental design if the quotient $\frac{L}{R} \ll 10{,}000$.

Thanks to the development of open-source grid asset databases like the Electric Grid Test Case Repository (Electric Grid Test Case Repository, 2022) and OpenStreetMap (OpenStreetMap Foundation, 2023), developing open-source grid operation models is now possible and several have emerged in recent years (Brown et al., 2018; Exascale Computing Project, 2023; NREL, 2022). Open-source models allow for flexible design and simultaneous batch processing of multiple model runs in high-performance computing (HPC) environments – both of which support stochastic simulation. For example, to increase simulation size and expand capabilities for uncertainty characterization and sensitivity analysis, developers can reduce the runtime of an open-source PCM (i.e., increase *L/R*) by simplifying core process representations. Several options exist to do this, including (but not limited to) aggregating across model features and space/time, network reduction, and relaxation of binary variables (Biener & Garcia Rosas, 2020; Galván et al., 2022; Oh, 2010; Shawhan et al., 2014; Svendsen, 2015).

A broad literature exists on navigating the model fidelity and computational speed tradeoff in PCMs and power system expansion models (Bistline, 2021; Daraeepour et al., 2019; Dranka et al., 2021; Hamilton et al., 2020; Jiang et al., 2020; Krishnan et al., 2016; LaRocca et al., 2015; Oikonomou et al., 2022; O'Neill et al., 2013; Schyska et al., 2021). For instance, the authors in (Schyska et al., 2021) developed a method to investigate the sensitivity of power system expansion

models to various parameters and model structures. They found out that temporal resolution is the leading sensitivity factor in power system models. The authors in (Bistline, 2021) analyze the effects of temporal resolution in power sector investments under different technology and policy scenarios. They argue that simplifying the temporal variability used in integrated power sector investment models might lead to deteriorations in model quality. Models should be neither oversimplified (e.g., unable to capture realistic behaviors of the grid in response to hydrometeorological stressors) nor overly complex (e.g., computational runtimes that limit experiment size and exploration of uncertainty) (Lara et al., 2020). Yet, a comprehensive framework for customizing open-source PCMs based on these recommendations is generally lacking in the literature.

In this chapter, we introduce the GO (Grid Operations) family of models, which allows for the easy training and testing of PCMs constructed around open-source synthetic grid databases. The main novelty of the GO software is that it establishes a pipeline from open-source energy data to the instantiation and calibration of PCMs. Furthermore, GO gives users the ability to vary the network topology and mathematical model formulation, as well as model parameters such as transmission line limits and economic hurdle rates. Users can then identify a model version that meets their experimental needs (e.g., resource limitations) in a robust and reproducible manner.

GO is available for all three interconnections of the U.S. (Western Interconnection, Eastern Interconnection, and Texas Interconnection). In this chapter, we demonstrate our approach over the Western Interconnection, a large and diverse system with previously demonstrated sensitivity to weather and climate variability and extremes (Cohen et al., 2022; O'Connell et al., 2019; Voisin et al., 2018). We conduct an evaluation of 100s of model versions and demonstrate quantitively that models with coarser topologies and lower runtimes can capture system dynamics adequately,

unlocking expanded capabilities for stochastic simulation. This chapter doubles as a detailed roadmap for how to use GO's flexible platform to design scale-adaptive model versions that balance computational complexity and fidelity.

2.2. Methods

In this chapter, we start with a general description of the GO framework, including its approaches for calibrating PCMs. Then we demonstrate how GO can be implemented in a real system, the U.S. Western Interconnection.

2.2.1. The Generalizable GO Framework

The GO software, written in Python, is based on synthetic grid databases of generators and system topologies created by Texas A&M University (TAMU) (Birchfield et al., 2017; Electric Grid Test Case Repository, 2017a, 2017b, 2018). GO instantiates simpler modeled versions of interconnection scale PCMs in four steps: 1) nodal selection; 2) network reduction; 3) data allocation and file setup; and 4) simulation using PCMs. Figure 1 summarizes the generalizable GO framework.

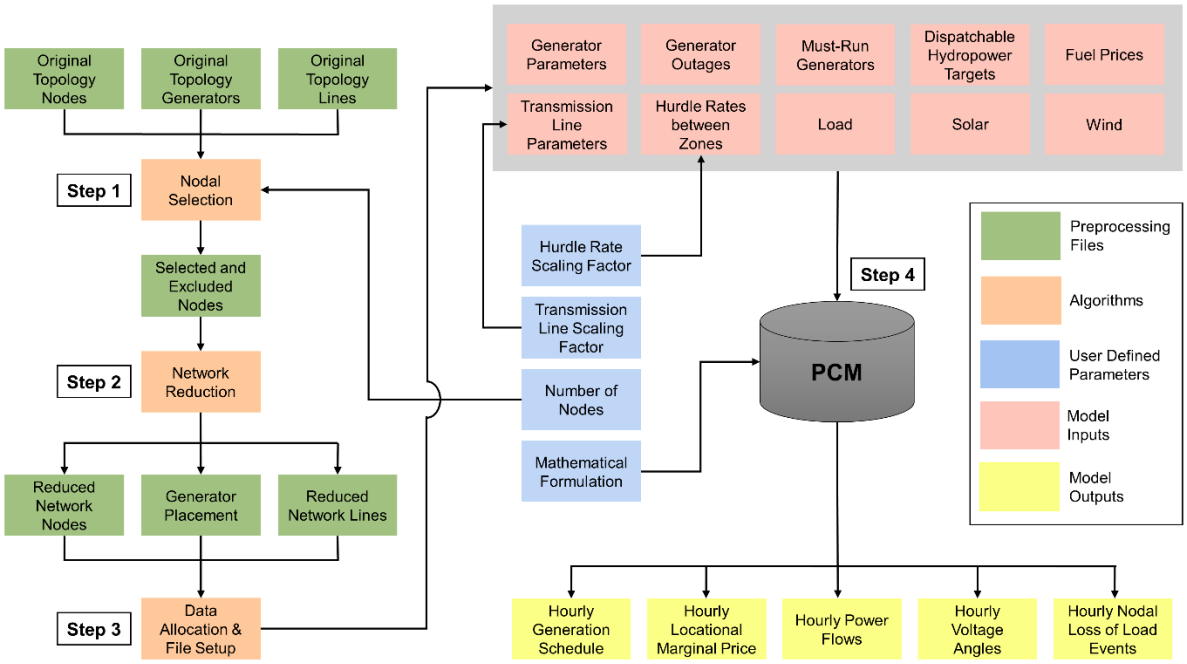

Figure 1: Flowchart of GO software including preprocessing files, algorithms, user-defined parameters, inputs, and outputs.

2.2.1.1. Step 1: Nodal Selection

GO allows users to train, test, and select a PCM version by searching over four user-defined parameters (see blue boxes in Figure 1). One of these parameters is the number of nodes that should form the final, simplified network. For example, if the full TAMU network representation has 10,000 nodes, a user could specify that they want to reduce this to a simpler, 'backbone' network made up of 100 nodes. After specifying this number, the first step in GO is a nodal selection algorithm that identifies which nodes to preserve from the full synthetic TAMU dataset. There are three types of node classifications in the original TAMU dataset: demand nodes (each of which comes with an estimated average load), generation nodes (each of which is assigned a total generation capacity), and transmission nodes (each of which is assigned a voltage level). Several criteria are applied to identify the most critical nodes in the network and guarantee minimum requirements to electrically connect and geographically cover interconnection scale systems.

First, for each unique balancing authority (BA) and state pairing, the node with the largest average demand is selected (BAs are entities which are responsible for balancing electricity supply and demand over distinct geographical areas). After removing these from the set, the remaining nodes are selected in equal numbers across the three different node classifications, though this ratio can be altered if desired. The algorithm selects demand nodes starting from the one with the highest electricity demand and moving to nodes with lower demands. Likewise, the algorithm selects generation nodes starting from the one with the largest generation capacity and moving to nodes with smaller generation capacities. After filtering nodes by voltage level (>345 kV), the algorithm selects transmission nodes starting from the node with the highest demand and moving to lower demands. Throughout the nodal selection process, a distance threshold (e.g., 5 km) restricts the algorithm from selecting any two nodes that are within that threshold from each other (this threshold can be changed by the user).

2.2.1.2. Step 2: Network Reduction

After selecting which nodes to preserve from the original TAMU network, GO uses a network reduction algorithm (Shi et al., 2012) to generate a new, simplified network equivalent topology. The algorithm first moves all generators to nodes selected in Step 1 based on the shortest electrical distance. It then recalculates nodal loads to compensate for the movement of the generators, such that estimated power flows on the preserved lines exactly match those in the full system. For other lines, the algorithm creates "equivalent" lines and associated impedances based on Ward's equivalent circuit calculation (Ward, 1949). Using distances and impedance values typical for high-voltage transmission lines, GO computes the per-distance impedance value (Ω/km), which we then associate with line flow capacities according to the transmission line loadability curve (Kundur & Malik, 2022). See (Shi et al., 2012) for more details about the network

reduction process used by GO. For a general review of network reduction methods, also see (Zhu & Tylavsky, 2018).

2.2.1.3. Step 3: Data Allocation and File Setup

After using the network reduction algorithm to create a simplified network, a data allocation algorithm disaggregates BA-level time series inputs, such as electricity load and solar and wind generation, and assigns these values to individual nodes. BA-level time series inputs are gathered from the U.S. Energy Information Administration (EIA) (EIA, 2022b). This process also creates job folders, which include all inputs and scripts necessary to run the simulations on a desktop computer or in an HPC environment.

In order to disaggregate BA-level load time series to each of the nodes in the reduced topology, nodal load weights are calculated within each BA by using the average load information from the TAMU dataset for each node in the reduced topology. In the TAMU dataset, a representative average nodal load value is assigned to each node. These nodal load values are used to calculate nodal load weights. BA nodal load weights are calculated by dividing the average nodal load of a specific node (from TAMU) by the sum of the average nodal load values of every node (from TAMU) in that specific BA. Nodal load weights are then multiplied by the load time series for their respective BAs to come up with the nodal loads for each hour. Available BA solar/wind generation is allocated to each node by calculating a weight reflecting the installed solar/wind capacity at each node. These weights are then multiplied by the solar/wind generation time series for their respective BA to get nodal solar/wind generation time series.

2.2.1.4. Step 4: Production Cost Model

After nodal selection, network reduction, and data allocation and file setup, GO simulates grid operations using the resultant production cost model (PCM). The PCM can simulate bulk

electricity grid operations using either linear programming (only economic dispatch) or mixed integer linear programming (both unit commitment and economic dispatch) formulations. The PCM is written in the Pyomo mathematical optimization package and can be solved using open-source (e.g., HiGHS, SCIP) or commercial solvers (e.g., CPLEX, Gurobi). All results shown in this chapter were produced by pairing GO's PCM with the Gurobi solver.

The objective function of the PCM is to minimize the system-wide cost of meeting fluctuating hourly electricity demand as well as cost of unserved energy, subject to several constraints such as individual generator capacities and ramp rates, thermal capacities of transmission lines, and Kirchoff's current and voltage laws using a DC power flow approximation. The PCM iteratively minimizes costs over a user-defined operating horizon (e.g., 24 – 168 hours) within which the modeled system operator has perfect foresight. Results presented in this chapter reflect an operating horizon of 24 hours. The decision variables consist of binary (if MILP is selected) and continuous electricity generation variables that control generator scheduling and dispatch, power flow between different nodes, voltage angles at each node, and loss-of-load variables at each node. Loss-of-load variables are units of last resort whose marginal cost is priced at $2000/MWh (the current loss of load price in several major markets (CAISO, 2022a)). Model outputs are hourly operating generation schedules of each power plant, hourly locational marginal prices (LMPs) at each node, simulated power flows on every transmission line, hourly voltage angle at each node, and (if applicable) hourly loss of load at each node.

Nuclear power plants are regarded as must-run resources apart from forced and unforced generator outages. The availabilities of solar and wind generation are represented by exogenously defined hourly time series, though the system operator can curtail both solar and wind if necessary. Weekly hydropower generation targets are collected from EIA-923 dataset (EIA, 2022a). From

weekly data, hourly minimum, hourly maximum, and daily allowed total hydropower generation is calculated and fed into the model. Then, PCM determines the optimal hourly hydropower schedule at each node.

Hourly generator outages are represented using data from the North American Electric Reliability Corporation's Generating Availability Data System (GADS) (NERC, 2022). Estimated lost capacity due to generator outages is subtracted from the nameplate generator capacities in each hour. Note that representation of both hydropower availability and unit outages can easily be substituted with alternative approaches, if desired. A more detailed discussion of GO's PCM modeling approach can be found in Appendices.

2.2.2. Model Calibration and Selection Process

GO allows users to calibrate and select a PCM version by searching over four user-defined parameters (see blue boxes in Figure 1):

Number of nodes: Users can select different numbers of nodes that will be in the final, simplified network representation of the PCM, thereby affording flexibility in the level of system granularity. As the number of nodes in the system increases, model runtimes generally increase as well because linear and mixed integer linear power system problems exhibit polynomial time complexity.

Mathematical formulation: Users can choose to implement only economic dispatch (ED) processes by using only linear programming (LP) or they can model both unit commitment (UC) and ED processes by using mixed-integer linear programming (MILP). MILP formulations entail higher runtimes due to the presence of binary generator on/off decision variables. On the other hand, MILP formulations allow for greater fidelity with respect to the operations of power plants (inclusion of startup costs, no load costs, and minimum-up and minimum-down times of

dispatchable generators). Capturing these generator characteristics can be important in accurately capturing the generation mix, power plant emissions, and electricity prices.

Transmission line capacity scaling factors: In GO, initial transmission line capacities are initially estimated by the network reduction algorithm. However, users can uniformly adjust transmission line capacities (+/- in MW) in the reduced network to increase model fidelity.

Hurdle rate scaling factors: Hurdle rates represent the cost of delivering 1 MWh of electricity from one balancing authority (BA) (i.e., a set of geographically clustered nodes representing quasi-independent grid operators) to another. Users can search over a range of different percentage scaling factors (+/- in %) to uniformly alter hurdle rates among BAs.

GO tracks the performance of the PCM by comparing simulated LMPs and generation mixes with historical data. Model performance is measured in terms of three fidelity metrics: mean absolute percentage errors in the interconnection scale yearly generation mix, and R^2 and root mean square error (RMSE) of daily LMPs at major pricing hubs/wholesale electricity markets.

Daily LMPs at major pricing hubs are calculated by taking a demand-weighted average of nodal LMPs within the geographic boundaries of each pricing hub (see Figure 3 for boundaries of pricing hubs). In order to calculate fidelity metrics on interconnection scale (i.e., for Eastern Interconnection and Western Interconnection), daily LMPs for multiple pricing hubs are utilized to calculate an aggregate (i.e., interconnection scale) R^2 and RMSE score by the demand-weighting average LMPs across all pricing hubs. For example, if the average loads in three different pricing hubs are: 10 GWh, 5 GWh, and 15GWh, and simulated vs. historical price comparisons in the same hubs yield R^2 values of 0.90, 0.85, and 0.95, the interconnection scale R^2 score for the PCM would be 0.9167.

GO numerically ranks each PCM tested (1=best) with respect to each individual metric (LMP R^2, LMP RMSE, and generation mix error), and then assigns each PCM an overall numerical ranking based on the sum of individual metric rankings. In this case, the model version with lowest sum of rankings would be the most accurate model among all created model versions. The model versions are sorted with respect to their sum of individual metric rankings and are given an ultimate fidelity ranking. This way, users can identify the highest-fidelity version of the PCM.

2.2.3. Demonstration of GO in Critical Test Bed: U.S. Western Interconnection

GO facilitates the quick development of open-source PCMs and evaluation of model performance over a wide parameter space, allowing users to find versions that sufficiently balance the tradeoff between model fidelity and computational speed. In the remainder of this chapter, we demonstrate these capabilities in a test bed of critical importance: the U.S. Western Interconnection, an interconnected system of 28 separate balancing authorities across the states of California, Oregon, Washington, Idaho, Nevada, Arizona, Utah, Wyoming, Montana, Colorado, and New Mexico (Figure 2). In this chapter, we use GO to (a) instantiate 540 different PCM models over a wide combinatorial parameter set; (b) measure model performance; and (c) identify models that demonstrate high fidelity and sufficient simulation speed. The 540 model versions are the combinations of:

- 9 different reduced networks (containing 100, 125, 150, 175, 200, 225, 250, 275, and 300 nodes) (see Figure 2c and Figure 2d)
- 2 different mathematical formulations (LP and MILP)
- 6 different transmission limit scaling factors (+0 MW (baseline), +500 MW, +1000 MW, +1500 MW, +2000 MW, +2500 MW)

- 5 different hurdle rate scaling factors (-100%, -50%, 0% (baseline), +50%, +100%). Baseline values of BA-to-BA hurdle rates are taken from the 2030 Anchor Data Set developed by the Western Electricity Coordinating Council (WECC) (WECC, 2021).

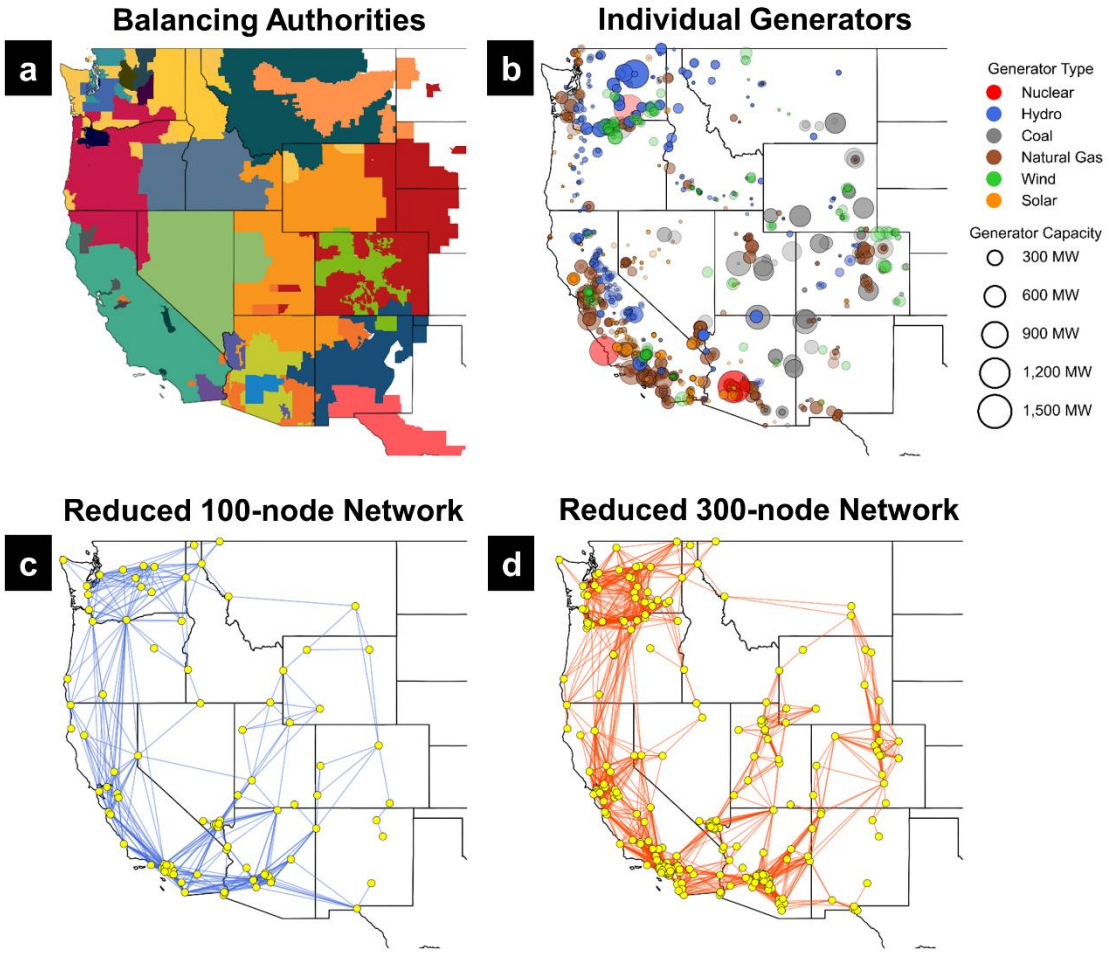

Figure 2: (a) 28 balancing authorities (BAs) in the Western Interconnection (each color represents a different BA) (Homeland Infrastructure Foundation-Level Data, 2022a); (b) all generator locations, types, and capacities in the Western Interconnection (Electric Grid Test Case Repository, 2017a); (c) 100-node reduced network; (d) 300-node reduced network.

Due to lack of open-source data and losing one-to-one node correspondence in a reduced network representation, it's not possible to conduct an LMP comparison for each node in the Western Interconnection. In this sense, LMP comparison is carried out for each pricing hub. We

have access to historical prices at five major pricing hubs in the Western Interconnection. Three are in California: Pacific Gas and Electric (PGAE), Southern California Edison (SCE), and San Diego Gas & Electric (SDGE) (CAISO, 2022b). The other two pricing hubs are the informal Mid-Columbia (MidC) trading hub in the Northwest and the Palo Verde trading hub in the Southwest (EIA, 2022c). Since the temporal resolution of historical LMPs in MidC and Palo Verde is daily, we aggregate LMPs simulated by the GO PCM to a daily time step for comparison. The boundaries of these five pricing hubs are shown in Figure 3.

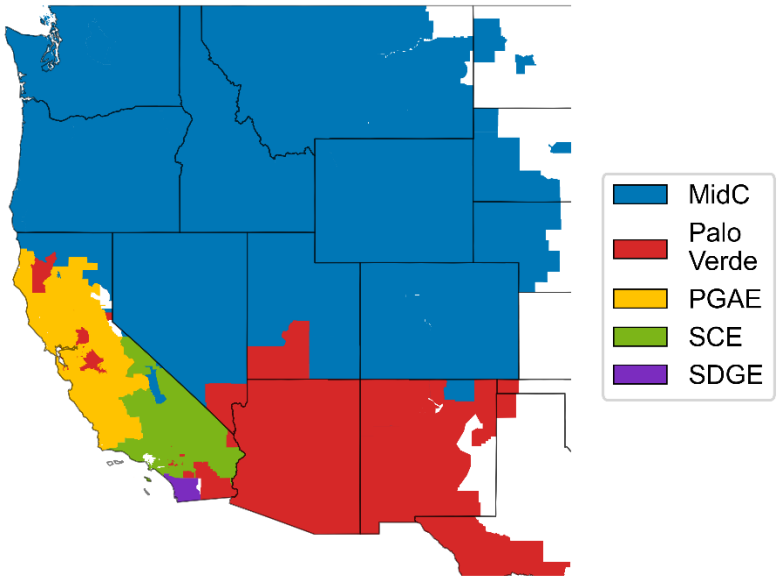

Figure 3: Boundaries of five pricing hubs used in this chapter. These pricing hub boundaries are constructed using geographical data from U.S. Department of Homeland Security (Homeland Infrastructure Foundation-Level Data, 2022b, 2022a) and pricing hub designations from EIA (EIA, 2022b) and CAISO (CAISO, 2022b).

2.3. Results and Discussion

2.3.1. Yearly Model Calibration and Selection Results

Historical operating data for every BA in the Western Interconnection are available for the years 2019-2021, so our parameter search (i.e., model calibration) focuses on this period. Figures 4a-d show the performance of all 540 model versions for the 2019 simulation year. The three dimensions measure model performance, and red stars at the origin show the ideal point

(minimized LMP RMSE and generation mix error, maximizing LMP R^2). LP formulations are shown with circles whereas MILPs are designated with crosses. In each respective panel, colors signify the number of nodes in the reduced network, transmission limit scaling factors, hurdle rate scaling factors, and wall-clock runtime.

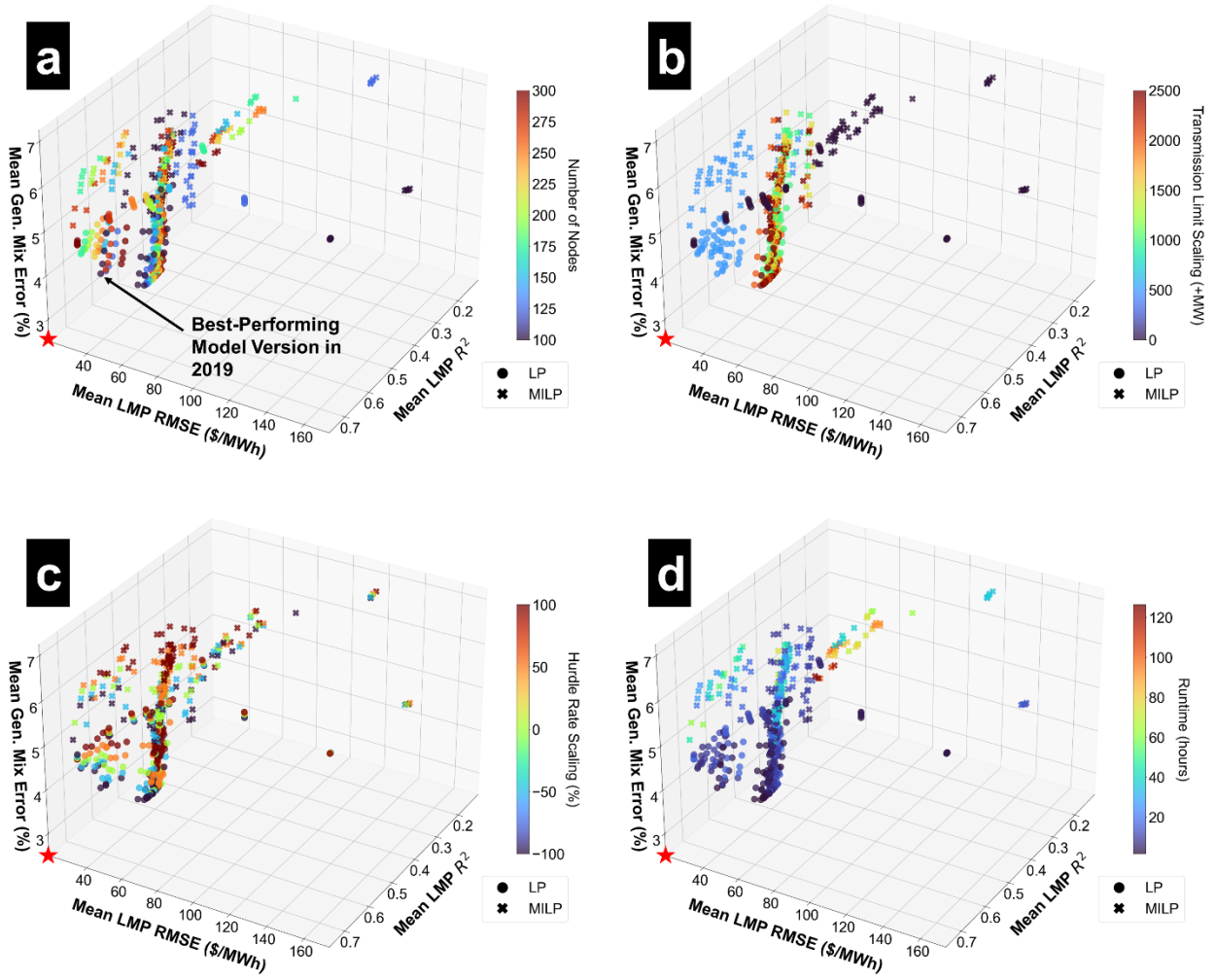

Figure 4: 3D model performance plots for the 2019 simulation year showing the influence of choices regarding (a) number of nodes, (b) transmission limit scaling factors, and (c) hurdle rate scaling factors. Panel (d) shows runtimes in hours. Each point represents one model version out of 540. Circles represent LP versions whereas crosses represent MILP versions. Red stars show the best possible solution on these figures.

Figure 4a shows that there is not a straightforward relationship between the number of nodes and model fidelity. While the expectation is generally that greater model complexity (i.e., larger numbers of nodes) should yield greater model accuracy, we see that some models with fewer

nodes (blue colors tones) can also mimic grid operations relatively well. Figure 4b shows that lower transmission scaling factors (like +500 MW) do better in terms of LMP R^2 and RMSE values, but higher transmission scaling factors seem to be better at capturing generation mix. In general, we observe that a higher number of nodes can give better results when coupled with lower transmission scaling factors, and models with lower numbers of nodes require higher transmission scaling factors. This is because having more nodes in the reduced topology increases the electrical connectivity of individual nodes so that lower transmission scaling factors can suffice. When we evaluate model versions by hurdle rate scaling (Figure 4c), we can see that there is a consistent gradient in colors, indicating that lower hurdle rates increase model fidelity in 2019.

Figure 4d shows the same 540 model versions evaluated in terms of wall-clock runtime. Runtimes for a single year (8760 hours) vary between 2 and 120 hours depending on the number of nodes, mathematical formulation, and transmission scaling factors. Clearly, there are some less complex (lower node) LP formulations with shorter runtimes that can also do a good job of capturing LMPs and generation mix, indicated by numerous dark blue circles close to the ideal point (red star). In fact, the best-performing model version for 2019 only takes 2 hours to finish simulating 1 year of hourly grid operations.

Figure 5 compares runtimes for different model versions (varying the number of nodes in the reduced network, mathematical formulation, and transmission scaling factors), all assuming the same default hurdle rates. In general, increasing the number of nodes increases the model runtimes whereas increasing transmission line capacities decreases runtimes. However, after a certain threshold (around +2000 MW), increasing transmission line capacities does not significantly affect the runtimes because the model becomes mostly free of transmission capacity

limitations. In our simulations, changing hurdle rates did not have a significant impact on the runtimes.

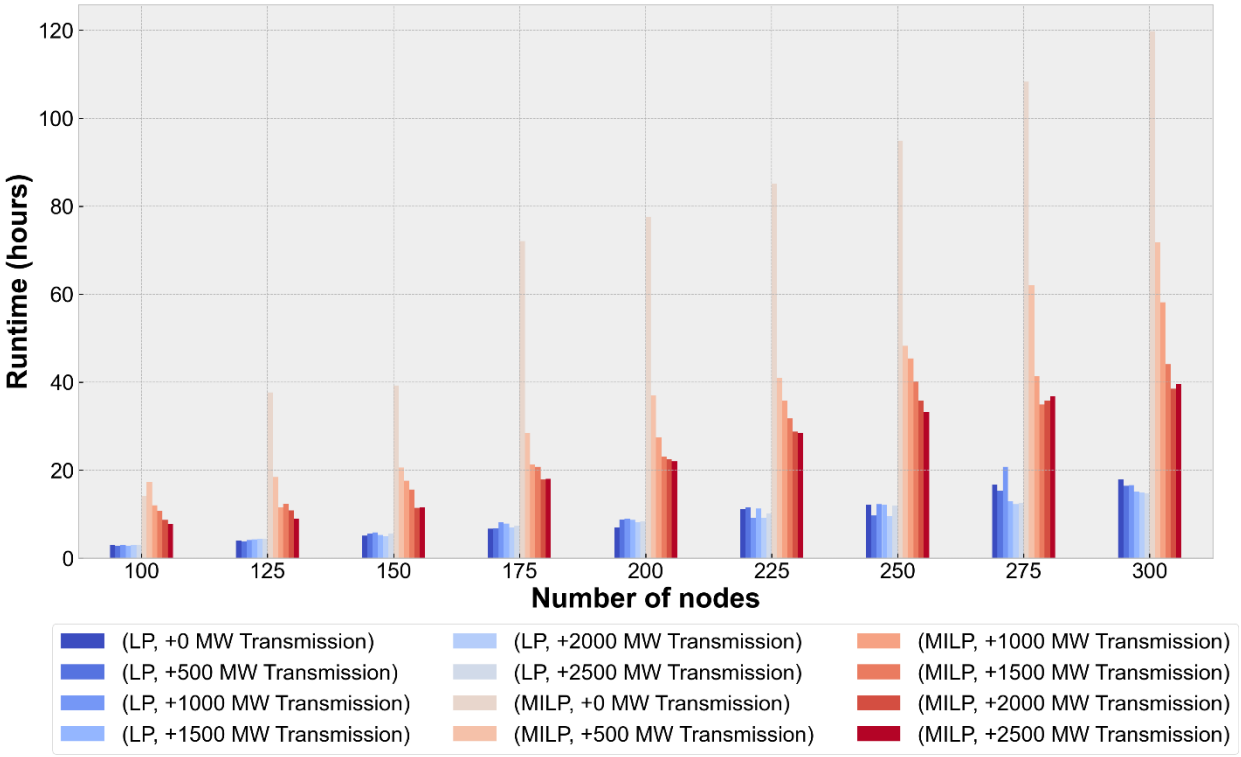

Figure 5: Model runtimes for different number of nodes, mathematical formulations, and transmission scaling factors in 2019. This figure includes 108 model versions out of 540 because hurdle rates do not have a noticeable impact on the model runtimes. In this figure, runtimes show the simulations with baseline hurdle rates (0% scaling).

Figure 6 shows an example of a generation mix comparison for the best-performing model version for the 2019 simulation year (which is also indicated in Figure 4a). Although there are some differences between historical and simulated daily generation mix, this model version captures yearly generation mix trends in the Western Interconnection to a certain extent. As the number of nodes and transmission lines retained in the system varies, generation mix estimates will fluctuate, which might seem to favor some generation sources more depending on the topology. If this behavior is observed, users are encouraged to compare different number of nodes

and mathematical formulations, and experiment with the weight of generation mix during the model selection stage to capture generation mix characteristics better.

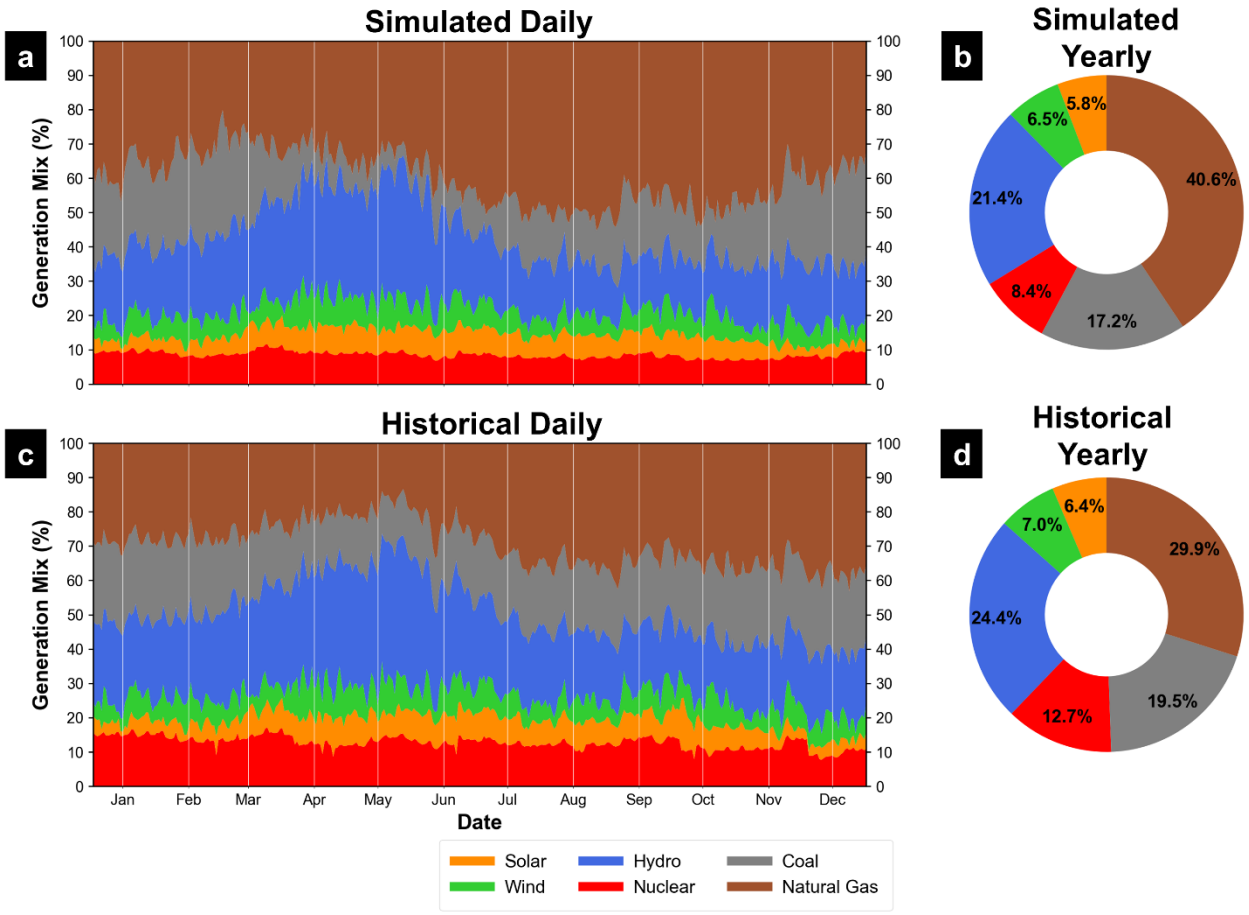

Figure 6: (a) Simulated daily total generation mix; (b) simulated yearly total share of each generation type; (c) historical daily total generation mix; (d) historical yearly total share of each generation type. Results are from the best-performing model version for the 2019 simulation year.

Figure 7 shows a visual comparison example of historical and simulated daily LMP time series from the same, best-performing model version for the 2019 simulation year. This model version does a good job capturing LMP variations in PGAE, SCE, and SDGE but it misses some oscillations in MidC and Palo Verde LMPs.

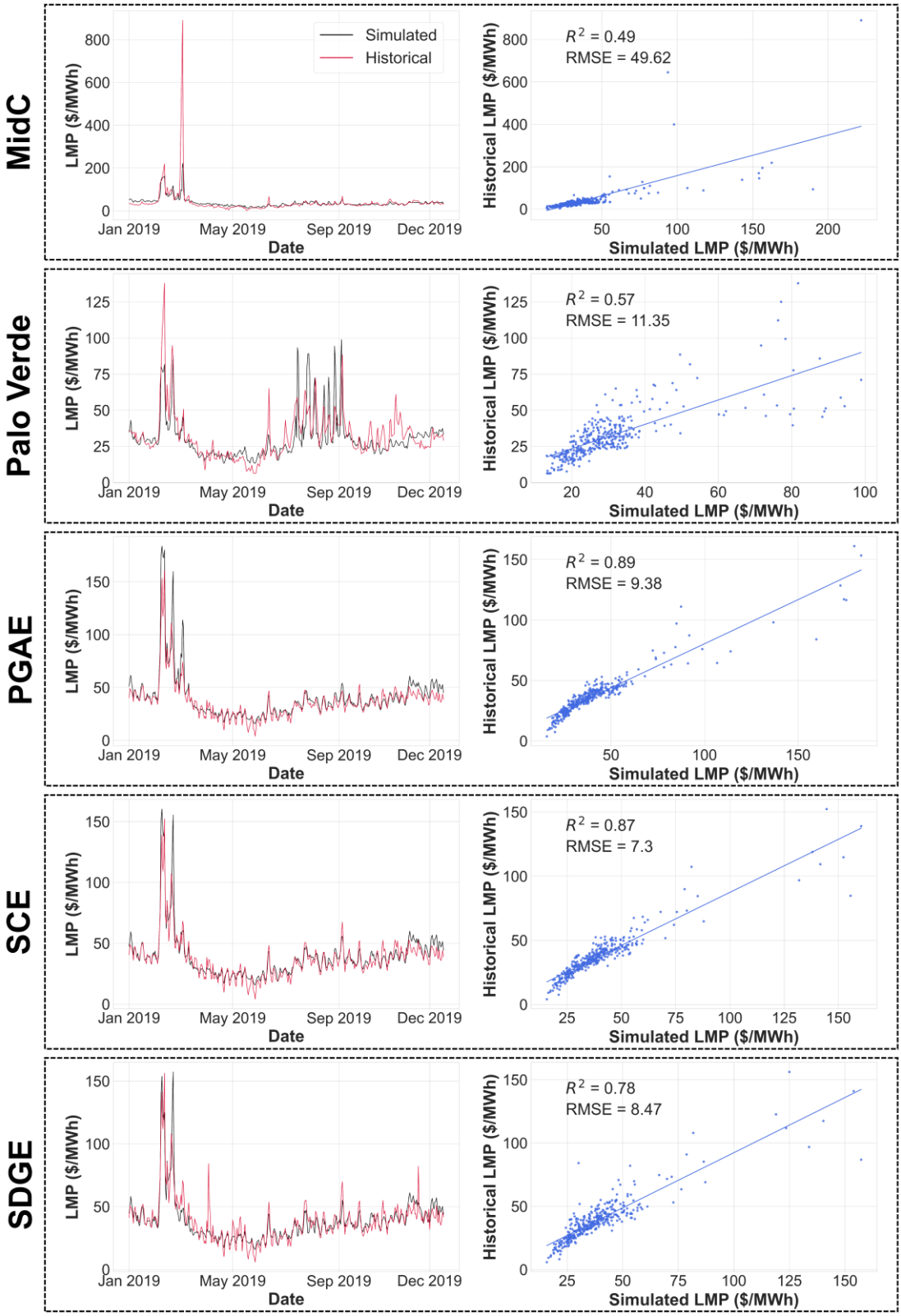

Figure 7: (Left) Simulated and historical daily LMP time series for each pricing hub; (right) distribution and best-fitting line of simulated and historical daily LMPs for each pricing hub. Results are from the best-performing model version for the 2019 simulation year.

We calibrated the PCM separately for 2019, 2020, and 2021, and then for all combinations of those years with a leave-one-year-out approach (e.g., train on 2019-2020, test on 2021; train on 2019 and 2021, test on 2020, etc.). We then compared the resultant LMPs and generation mixes with historical data and selected the best model version for each year combination. For 2019, a model with a 125-node topology, LP formulation, +500 MW transmission limit scaling, and -100% hurdle rate scaling yielded the best results. The best model version for 2020 has the same characteristics, except for the number of nodes (100 vs 125). The best-ranked model for 2021 includes a 225-node topology, a MILP formulation, +500 MW transmission limit scaling, and -100% hurdle rate scaling. See Figure 39 and Figure 40 in the Appendices for 3D model performance plots for 2020 and 2021. Table 1 lists all selected parameters of the best-ranked model versions for each set of training year(s). In general, an LP formulation with +500 MW transmission scaling and -100% hurdle rate scaling is the most robust model version.

Table 1: Selected parameters of the best model versions for each training set.

Training Set	Number of Nodes	Mathematical Formulation	Transmission Line Limit Scaling Factor	Hurdle Rate Scaling Factor
2019	125	LP	+500 MW	-100%
2020	100	LP	+500 MW	-100%
2021	225	MILP	+500 MW	-100%
2019 and 2020	125	LP	+500 MW	-100%
2019 and 2021	125	LP	+500 MW	-100%
2020 and 2021	125	LP	+500 MW	-100%
2019, 2020, and 2021	125	LP	+500 MW	-100%

2.3.2. Impact of User-Defined Parameters on Model Fidelity and Different Model Selection Methods

GO's flexibility allows users to instantiate hundreds of different model versions. In this chapter, we mine these simulation results for larger patterns in how parameters affect model performance. The panels in Figure 8 slice the 540 different model versions in several ways. Each column shows data for a different simulation year (2019, 2020, and 2021). The rows isolate the effects of changing each user-defined parameter. For example, in the first row, each box plot (color) shows distribution of performance rankings (1=best, 540=worst) of 60 unique model versions that share the same number of nodes but differ in terms of mathematical formulation, transmission line scaling, and/or hurdle rate scaling. There are 9 box plots, equaling the 540 total versions tested. Likewise, in the second row, each box plot (color) represents 270 out of 540 model versions, all of which share the same mathematical formulation (either LP or MILP).

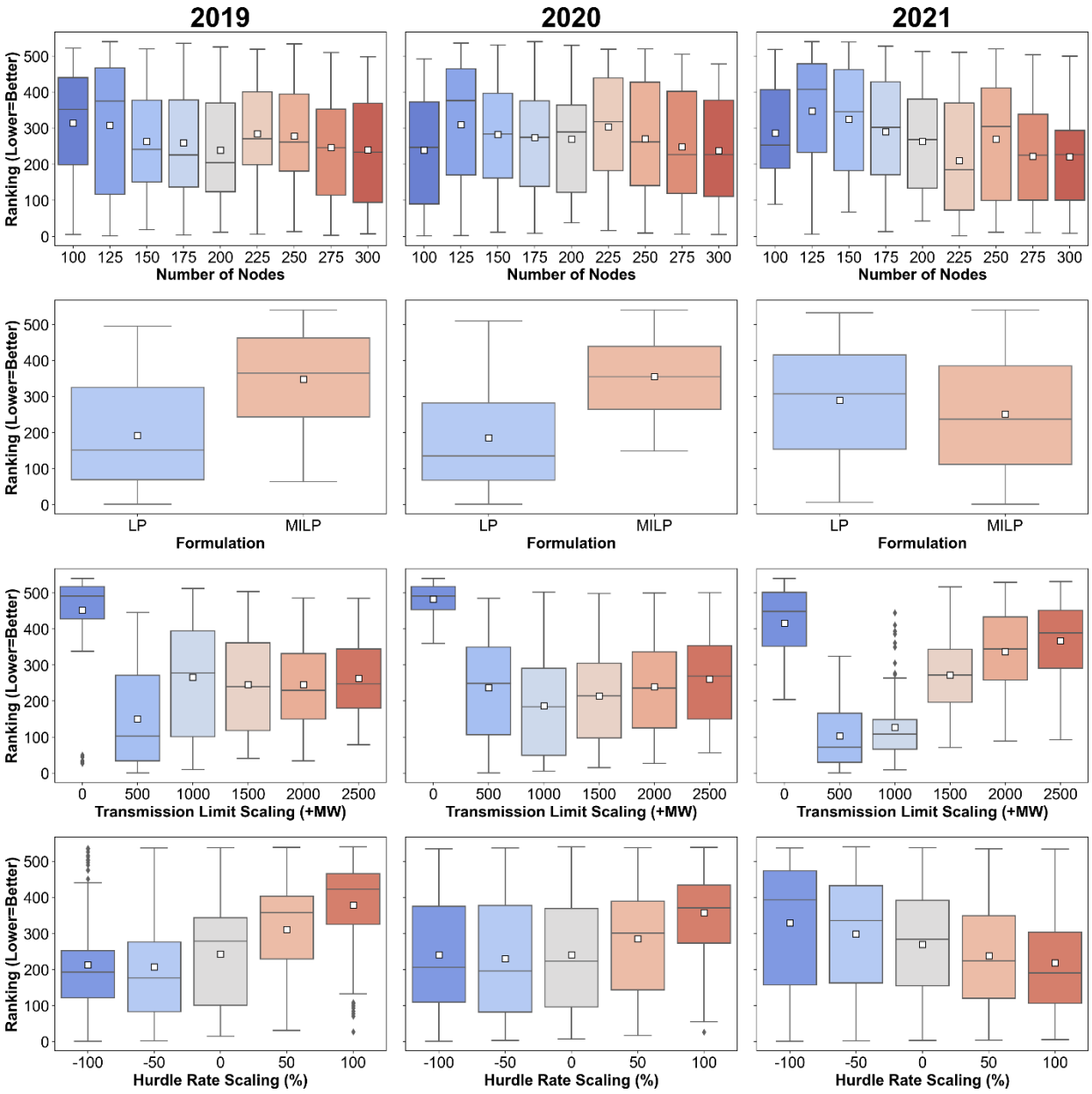

Figure 8: Model ranking distributions of number of nodes, model formulation, transmission limit scaling, and hurdle rate scaling in 2019, 2020, and 2021. White squares designate the average ranking for each parameter value.

The first row of Figure 8 shows a fairly consistent trend across all three simulation years: as the number of nodes increases, the *median* model ranking decreases (i.e., model fidelity increases). At first glance, this may seem to conflict somewhat with our finding that the best-ranked models generally have a smaller number of nodes (see Table 1). However, the lower whisker of each box plot falls close to zero, indicating that higher performing models are possible

for any number of nodes selected. The interquartile ranges (IQRs) of the boxplots also vary. For example, in 2019, models with between 150-250 nodes have smaller IQRs, indicating that the performance of these models is more stable across values of other parameters than model versions with a smaller/larger number of nodes. Looking at 2021, the opposite is true. In addition, the second row of Figure 8 indicates that LP versions did a better job in 2019 and 2020 but MILP versions performed better in 2021 on average.

Another finding illustrated by Figure 8 (third row) is that moderate levels of transmission line scaling typically yield more accurate models. In fact, we observe that high-performing (low-ranked) models become impossible to find for certain transmission line parameterizations. Zero transmission scaling consistently yields the least-accurate models. In addition, as we increase transmission line capacities above +500MW to +1000MW, the model becomes free of transmission restrictions and starts to utilize lower marginal cost power plants and transfer electricity more freely throughout the network, which causes inaccuracies in generation mix and LMPs in different regions In general, we find that model performance is the least sensitive to hurdle rate scaling (see Figure 41 in the Appendix B shows small changes in model selection metrics). Thus, we primarily focus our discussion on the other three, more impactful, parameters.

Figure 9 provides a deeper examination of the interactive effects of two key model parameters: the number of nodes in the network and transmission line scaling. In particular, we observe that having a higher number of nodes (warmer colored boxplots) becomes much more important to model accuracy if transmission lines are not scaled-up (panels on the left). Increasing the number of nodes enhances the connectivity of the reduced network, which prevents LMP spikes caused by activation of loss of load variables. However, if we scale transmission lines by more than +500 MW, we can create the same connectivity conditions with fewer nodes. In fact, at

higher transmission scaling levels, networks with lower numbers of nodes yield accurate models. In general, we find that transmission line and hurdle rate scaling factors interact like supporting calibration parameters (e.g., hyperparameters), with the nature of this interaction also dependent on the number of nodes and mathematical formulation selected.

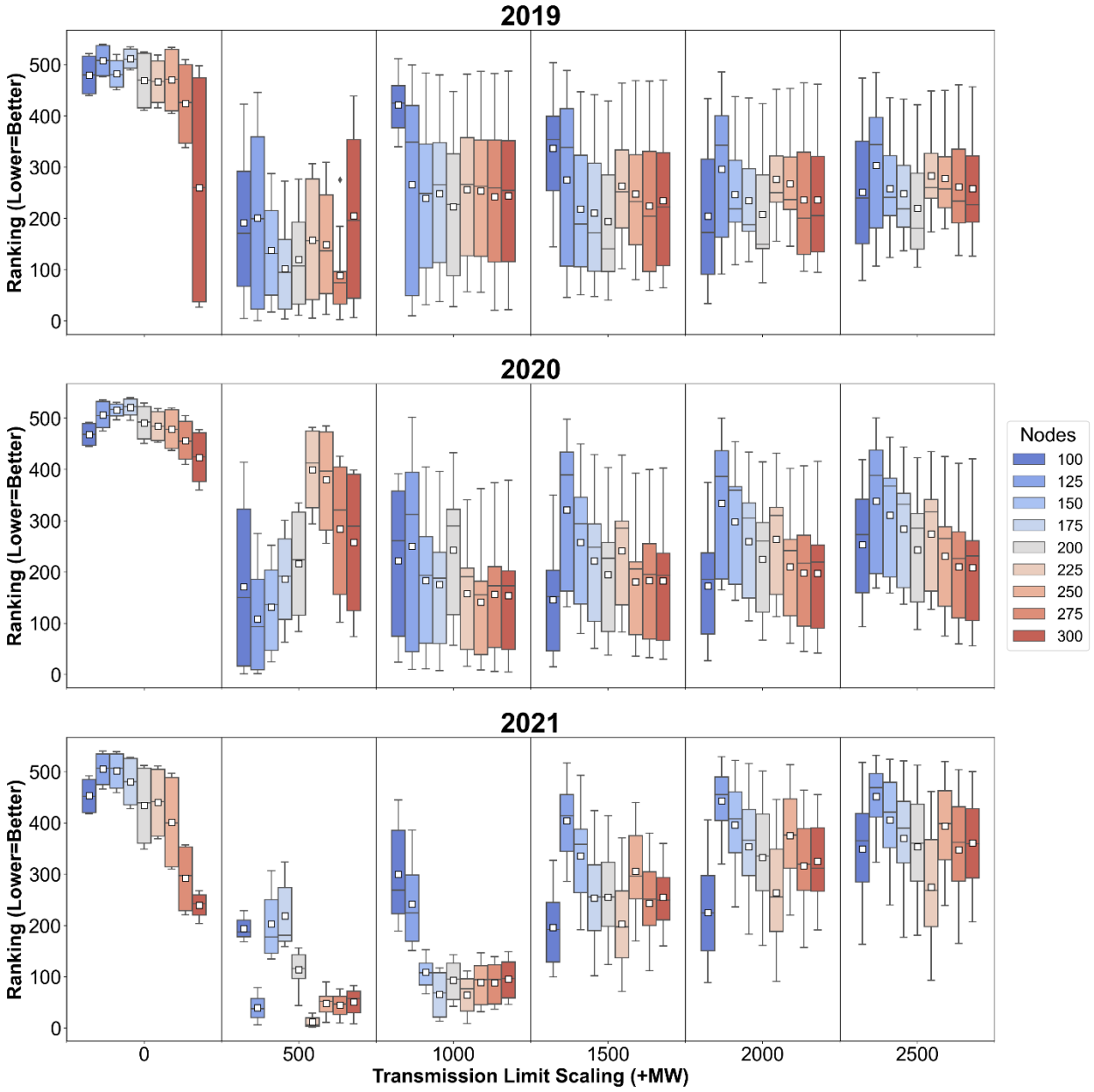

Figure 9: Model ranking distributions of number of nodes while keeping transmission limit scaling constant in 2019, 2020, and 2021. White squares designate the average ranking for each number of nodes.

2.3.3. Influence of Training and Testing Data on Model Selection

Table 2 lists model performance metrics and rankings (1=best) for all possible training and test year combinations, allowing us to observe how the choice of this data could impact model selection.

For example, when the 540 different versions of the PCM are used to simulate 2019, the version that performs the best also performs second best when tested in 2020 and the 16th best version when tested in 2021. When we train the PCM on all two and three-year combinations, the best-performing model version is the exact same version that performs best when simulating 2019 (see Table 1).

When the 540 different versions of the PCM are used to simulate 2020, the version that performs the best also does a good job of capturing 2019 grid dynamics, but it performs significantly worse at simulating grid operations in 2021. Likewise, when the PCM is trained only on 2021 data, it does a worse job simulating grid operations in 2019 and 2020. A possible reason is that the best model version in 2021 uses a MILP formulation. Among the 3 years, the highest average daily natural gas prices are observed in 2021 (5.42 $/MMBtu), which increases the marginal cost of natural gas power plants and generally favors coal plants in the dispatch order. However, without binary variables controlling the on/off status of coal power plants in LP versions, coal plants overproduce. An MILP formulation introduces new costs (like startup) and additional constraints (like minimum up and down time) for coal generators, which decreases their usage in the model yielding a closer match with the historical generation mix.

Table 2: Model performance metrics and rankings for different training and test years.

Training Years \ Test Year	2019				2020				2021			
	LMP R^2	LMP RMSE	Gen. Mix Error (%)	Rank	LMP R^2	LMP RMSE	Gen. Mix Error (%)	Rank	LMP R^2	LMP RMSE	Gen. Mix Error (%)	Rank
2019	0.62	30.35	3.56	1	0.62	29.69	2.91	2	0.31	52.64	3.04	16
2020	0.66	33.31	3.73	5	0.63	31.48	2.75	1	0.28	55.95	2.41	213
2021	0.58	32.19	5.58	221	0.42	35.48	5.08	468	0.27	52.22	1.73	1
2019-2020	0.62	30.35	3.56	1	0.62	29.69	2.91	2	0.31	52.64	3.04	16
2019-2021	0.62	30.35	3.56	1	0.62	29.69	2.91	2	0.31	52.64	3.04	16
2020-2021	0.62	30.35	3.56	1	0.62	29.69	2.91	2	0.31	52.64	3.04	16
2019-2020-2021	0.62	30.35	3.56	1	0.62	29.69	2.91	2	0.31	52.64	3.04	16

There are numerous possible ways to select the "best" model version, including using other metrics, changing the weights of each metric in the selection stage, and selecting different model versions for each pricing hub. For example, although the best model for 2019 accurately mimics the LMPs in three California pricing hubs, it misses some price oscillations in the MidC and Palo Verde hubs (Figure 7) If we only considered the MidC hub while selecting the best version, we would have chosen a model with 300-node topology, LP formulation, +0 MW transmission limit scaling, and 0% hurdle rate scaling. This would have increased the LMP R^2 of MidC from 0.49 to 0.74. On the other hand, a model with 100-node topology, LP formulation, +2000 MW transmission limit scaling, and 0% hurdle rate scaling would work better for the Palo Verde hub. This would have increased the LMP R^2 of Palo Verde from 0.57 to 0.7.

In addition, changing how we weigh the individual model performance metrics and/or which metrics are considered at all can strongly affect the PCM selection process. For instance, Figure 10 shows R^2 values from different model versions for each pricing hub as well as the demand-weighted average R^2 value for the entire Western Interconnection. The "best" model version for 2019 (i.e., the lowest ranked model when LMP R^2, LMP RMSE, and average generation mix are all considered) is designated with a red square. However, there are different model versions (like the 175-node MILP version with +500 MW transmission scaling or the 300-node LP version with +0 MW transmission scaling) with worse overall rankings but higher LMP R^2 values (these are indicated by orange squares).

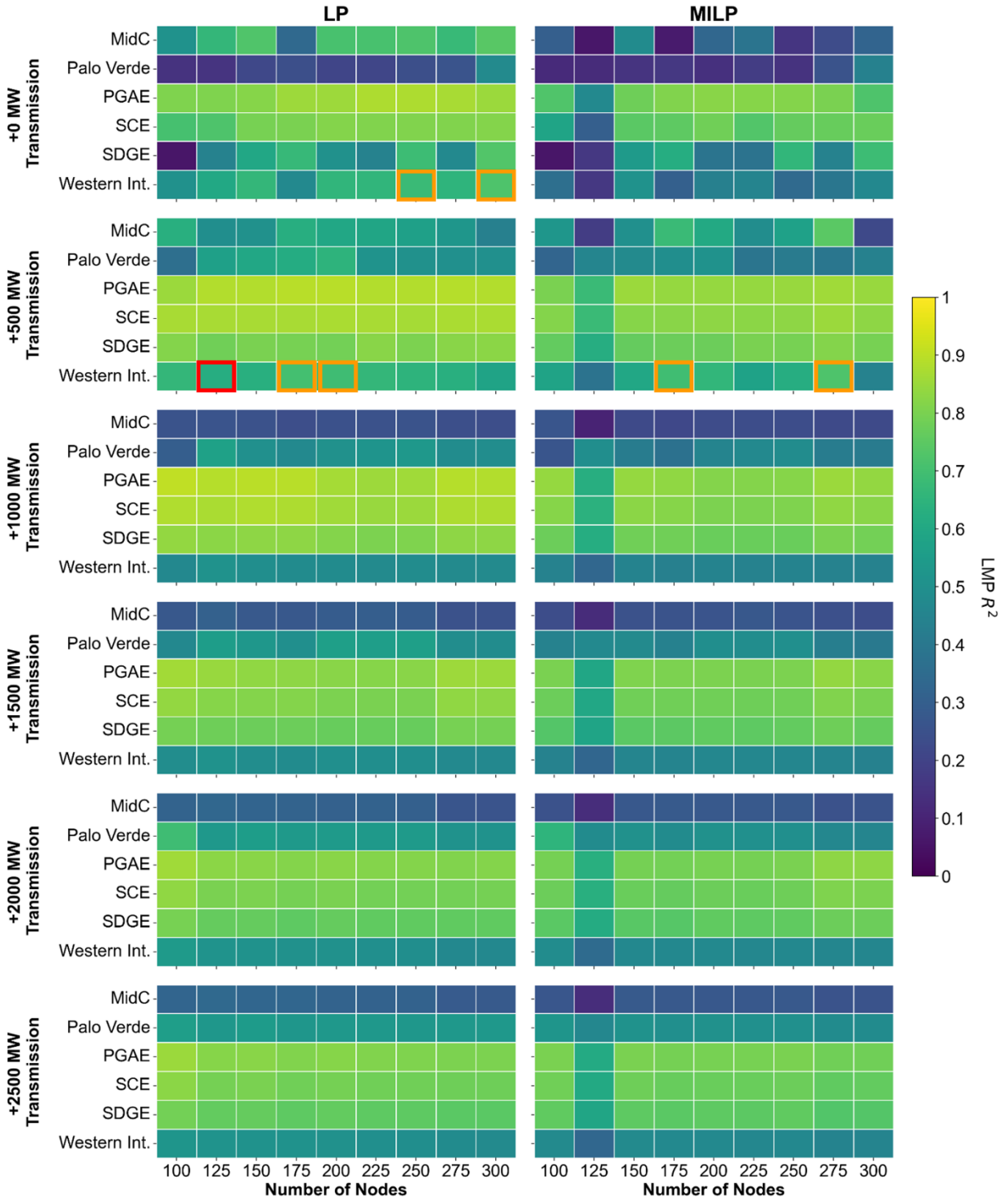

Figure 10: Color-mapped LMP R^2 scores for each pricing hub as well as demand-weighted average for the Western Interconnection. Values are grouped in terms of number of nodes, mathematical formulation, and transmission limit scaling factors. This figure includes 108 model versions (with -100% hurdle rate scaling) out of 540 in 2019. Red square designates the best model version in 2019 (with respect to LMP R^2, LMP RMSE, and average generation mix error) whereas orange squares designate the model versions where the demand-weighted average R^2 for the Western Interconnection is higher than the best model version in 2019.

An important feature of GO is its ability to help power system modelers navigate the tradeoff between model fidelity and computational speed. Figure 11 illustrates this tradeoff for all 540 model versions in 2021. It took nearly 40 hours for the best-performing model version to simulate 2021 grid dynamics on an hourly time step (cross in green box). As we can see, there are other possible versions in the orange box which have similar rankings (i.e., fidelity) but require much lower runtimes. The modeler might prefer another version in orange box to save computational time if the main interest of the research entails running the model hundreds or thousands of times to characterize system performance, e.g., under weather and climate variability and extremes. We can also see that if we also considered runtimes in model selection, the algorithm may have a tendency to select a version in orange box as those versions are closer to the red star which is the ideal point in this figure.

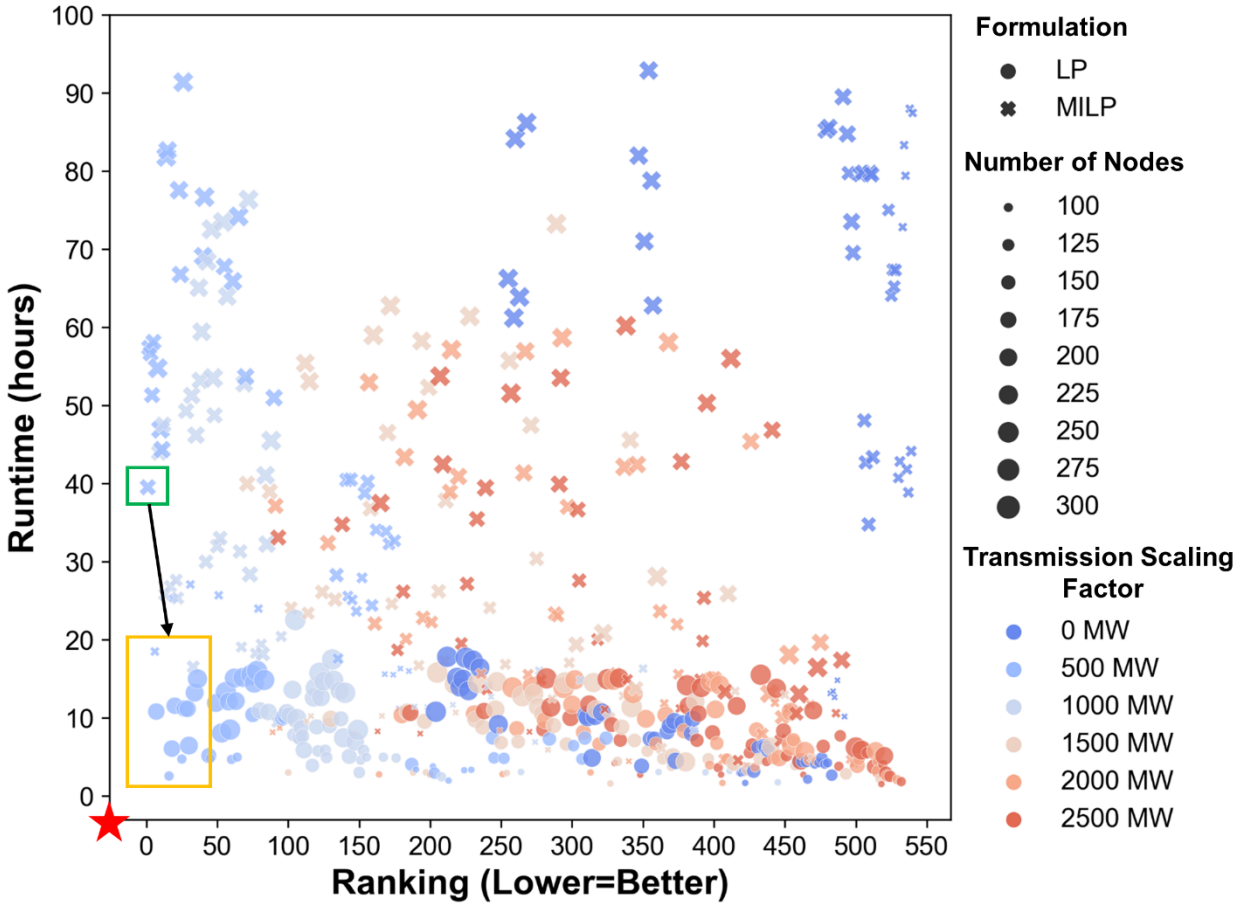

Figure 11: Tradeoff between model fidelity (ranking) and tractability (runtime) for 540 simulations of 2021. Each point represents one model version out of 540. Circles represent LP versions whereas crosses represent MILP versions. Size of the points represents the number of nodes whereas color of the points represents transmission scaling factors. Green box shows the best model version in 2021 and orange box designates other possible options with lower runtimes. Red star shows the optimal point on this figure.

2.3.4. Experimental Aims and Computational Limits

Ultimately, model selection should consider both the need for model fidelity and limitations on researchers' computational resources (e.g., available number of cores, memory size, runtime limitations, etc.). The GO framework supports researchers in developing specialized s for their research questions. For instance, if a user is interested in individual generator operations or air pollution emissions, choosing a MILP formulation may be more appropriate. Exploring weather and climate uncertainty may recommend and faster LP. To expand on this, we revisit the hypothetical example described in the introduction. Specifically, a researcher would like to explore

the impacts of future climate change on operations of the U.S. Western Interconnection, using an ensemble of different general circulation models (GCMs), and exploring a range of different shared socioeconomic pathways (SSPs) and representative concentration pathways (RCPs). In addition, for each unique climate state (GCM + SSP combination), the researcher would like to simulate grid operations using a 100-year Monte Carlo weather ensemble to explore stationary uncertainty.

The feasible scale of this experiment is likely to be constrained by available computational resources. For example, what if the hypothetical researcher can run 10 simulations simultaneously on an HPC cluster and has 45 days (or 1080 hours) to complete the experiment? Table 3 shows how GO can be used to identify the best PCM parameterization for five different experimental designs (columns in Table 3).

Table 3: Number of available model versions and parameters of the best available model version under varying numbers of runs for uncertainty analysis. The data in this table refers to 2021 simulation results.

		1 GCM, 1 RCP, 2SSPs, 100 weather years	**1 GCM, 2 RCPs, 2 SSPs, 100 weather years**	**2 GCMs, 2 RCPs, 2 SSPs, 100 weather years**	**1 GCM, 4 RCPs, 4 SSPs, 100 weather years**	**4 GCMs, 4 RCPs, 4 SSPs, 100 weather years**
	Runs Required	200	400	800	1600	6400
	Number of Feasible Model Versions	540	535	534	525	214
Parameters of the Best Feasible Model Version	**Number of Nodes**	225	125	225	125	100
	Mathematical Formulation	MILP	MILP	LP	LP	LP
	Transmission Scaling Factor	+500 MW	+500 MW	+500 MW	+500 MW	+1500 MW
	Hurdle Rate Scaling Factor	-100%	-100%	100%	-100%	-100%
	1-year runtime (hours)	39.5	18.5	10.8	2.6	1.6

Moving left to right, the number of runs required by each experiment increases. To meet this requirement while staying within the allotted computational time, a researcher would need

faster models that utilize lower number of nodes and sometimes LP formulations. For example, moving from an experiment that requires 200 runs to one that requires 400, the best available model (that is also feasible) uses an MILP formulation, but the topology must be reduced from 225 nodes to 125. For any experiment involving at least 800 runs, an LP model is needed to match the computational resource requirements. As the number of runs required increases further beyond this point, the best available models must utilize simpler networks. Transmission scaling factors increase slightly to create a less transmission-constrained system that can be solved more quickly.

2.4. Limitations and Future Work

GO comes with some limitations which double as areas for future work. First, transmission and hurdle rate scaling factors uniformly impact all lines and BA-to-BA power transactions. Although it may require more costly calibration efforts to search for an optimal scaling factor for each individual line and BA-to-BA transaction, selectively altering the individual transmission line capacities and hurdle rates might create a more accurate model version. Second, the GO PCM assumes a single, central operator with perfect foresight of load and generation resources beside the probabilistic outage. Integrating forecast errors and balancing (real-time) markets could improve realism in certain cases. Last, fuel price information for many BAs is limited. A spatial algorithm was used to generate fuel price time series for some BAs (see Appendix A for more details). Using more granular and reliable fuel price information would most likely enhance our ability to replicate LMPs more accurately.

2.5. Conclusion

Accurately representing power system dynamics over a wide range of operating conditions is critical for performing vulnerability analysis. This imposes a challenge on researchers with computational budgets to strike a balance between model fidelity and computational speed.

To that end, this paper introduces GO, a framework for training and testing scale-adaptive open-source PCMs on the U.S. interconnection scale. GO allows users to search over many parameterizations of a PCM and identify versions that adequately balance model fidelity and computational speed. In an application over the Western U.S., our results show that simplified PCMs utilizing linear programming formulations and significantly reduced networks can adequately capture LMPs and generation mix. This result quantitively supports the potential for large, stochastic simulation experiments using open-source PCMs, including experiments designed to characterize risks from climate and weather variability and extremes. Other findings of note include the interplay between transmission line scaling and network reduction in model calibration; essentially, transmission line scaling allows users to maintain network dynamics (and model accuracy) while reducing system complexity (and model runtimes). We also show that model selection is sensitive to choices around training data (e.g., weather year) and testing data (e.g., market or regional subsystem of interest). Finally, we provide a salient example of how experimental design (e.g., the scale of an uncertainty analysis), in the presence of limits on computational resources, can lead researchers to choose different versions of a PCM.

2.6. Software and Data Availability

The model is open-source and publicly available. All codes of the model and data used are available under MIT free software license (Akdemir, Oikonomou, et al., 2023b). All model outputs utilized in this chapter are available under Creative Commons Attribution 4.0 International license (Akdemir, Oikonomou, et al., 2023a).

CHAPTER 3. IMPACTS OF WAVE ENERGY INTEGRATION TO U.S. WESTERN INTERCONNECTION

3.1. Background

Renewable energy integration has been deemed critical for ensuring a sustainable and decarbonized future energy landscape (Arabzadeh et al., 2020; Hamid et al., 2022). As grids are decarbonized, grid operators need to come up with alternative methods to ensure reliability during normal operations as well as during extreme weather events (Akdemir et al., 2022). In this context, it is not only essential to develop key technologies that facilitate seamless and efficient integration of existing and technically advanced renewable generation resources (such as wind and solar), but also important to investigate relatively newer modes of renewable energy generation (Vargas et al., 2022), that may have potential for added benefits. Marine energy resources (including wave, tidal, and ocean currents) are one such group of resources that have significant potential to emerge as effective clean generation alternatives (Fairley et al., 2017; Moazzen et al., 2016; Reikard et al., 2015).

Authors in (Barstow et al., 2008) show that at a worldwide scale, ocean waves have a potential reserve of 2 TW of power, which is approximately equal to the global energy demand. For the United States (U.S.) alone, the projected wave energy content across the continental coastline is 2640 TWh/year (Jacobson et al., 2011), which is equal to approximately 65% of the country's total annual energy demand (Department of Energy, 2015; Lehmann et al., 2017). Compared to other renewable resources such as wind and solar, some forms of marine energy resources, such as wave energy and tidal energy are more periodic, persistent, and predictable (Bhattacharya et al., 2021; Fairley et al., 2020a). Researchers have studied the possible advantages of including wave and tidal energy within the generation portfolio on power system operations

(Pennock et al., 2022; Reikard et al., 2015; Soudan, 2019). Specifically, wave energy is observed to be the most scalable among marine energy resources and its integration in bulk power system operation has proven potential to reduce balancing requirements, improve effective load carrying capabilities, and also improve operational reliability and resiliency (Bhattacharya et al., 2021).

As marine energy is a relatively nascent technology when compared to wind and solar, a substantial body of work has focused on assessing its technical suitability (Armstrong et al., 2015; Göteman et al., 2020; Rasool et al., 2020; Said & Ringwood, 2021) economic viability (Lavidas & Blok, 2021; Robertson et al., 2020) and identifying development sites with optimal resource potential (Iglesias et al., 2009; Reikard et al., 2017; Xu et al., 2020). Although there has been a body of work investigating the possible impacts on power system operations, these analyses have been mostly performed in grid-abstracted settings that do not model power system specifics in detail or have focused on grid interconnection issues at the device/converter level (Dario Jaramillo & Garces, 2015; Halamay et al., 2011; Johnson & Cotilla-Sanchez, 2020; Matthew & Spataru, 2021). Additionally, the impact of wave power in transmission-constrained systems has been studied in (Moazzen et al., 2016), where authors posited that wave energy reduces the energy demand from other sources of generation. Even with this related body of work, there remains a need to further understand the value proposition of wave energy in continental-scale bulk power system operations, specifically, we need to quantitatively characterize its contribution to day-to-day operations as measured with key performance metrics such as operational and market dynamics, as well as the contribution during extreme events.

In this chapter, we investigate the potential impact of integrating marine energy-based generation resources on bulk-scale power system operations. Owing to considerable high-quality wave-based resource availability on the western coast of continental United States, we selected a

reduced order network model of the U.S. Western Interconnection as our test bed in this work (Akdemir, Oikonomou, Kern, Voisin, Ssembatya, et al., 2024). This power system model was equipped with wave energy generation at key points across the western coast of the United States (the states of Washington, Oregon, and California). Subsequently, we study the impact of the assumed wave generation on power system operations through an optimization-based unit commitment/economic dispatch (UC/ED) formulation, under several different types of operating conditions. Please note that the choice of wave as the studied resource is driven by the inherently scalable nature of wave energy technology. Other marine energy technologies such as tidal energy are largely restricted to localized impacts or are not as scalable as wave, and are hence not considered in this chapter.

The main contributions of our work are listed as follows. Firstly, to the best of our knowledge, this is the first-of-its-kind study to consider the impact of wave generation on bulk power system operations. Key insights are presented on how wave energy can bring down energy prices across critical demand locations across the power system. Secondly, our analysis also characterizes the spatial distribution of the benefits stemming from the aforementioned wave integration and analyzes transmission upgrade scenarios that can aid in translating the benefits of wave integration over a greater geographical spread. Thirdly, our work also investigates the role of wave energy on system operations under extreme weather events like heat waves and power system contingencies, and comments on the applicability of wave energy at scale to address power system resiliency issues.

The rest of the chapter is organized as follows. Chapter 3.2 provides a description of the grid operations model and marine energy (wave) generation data used for this chapter. Chapter 3.3 provides a description of the scenarios along with the details of the corresponding experimental

designs. All numerical results, including model validation and results from the designed experiments (as noted in Chapter 3.3) are presented in Chapter 3.4. Finally, we provide concluding remarks followed by limitations and future research directions in Chapter 3.5.

3.2. Methods

In this chapter, we provide a brief description of the unit commitment and economic dispatch (UC/ED) model used for simulating grid operations. Note that the main objective of this chapter is to employ this UC/ED framework to investigate the key opportunities that can be explored by integrating wave energy resources at scale to bulk-scale power system operations. Therefore, a model suitable for conducting experiments has to (a) represent power system operations for a realistic bulk power system and (b) have a geographical area of coverage that has sufficient good-quality wave resources. For the US, the western seaboard has some of the best wave resources in the country (Fairley et al., 2020b; Zheng, 2021), a balanced mix of major load centers located in close proximity to the coast as well as in more inland areas, away from the coast. Thus, we have selected the U.S. Western Interconnection as the candidate power system model in this chapter. In order to study the impact of marine renewable energy (MRE) resources on the overall U.S. Western Interconnection in a scalable manner, a systematic model reduction is performed to design an equivalent reduced topology network for the entire U.S. Western Interconnection. Criteria for selecting node locations in the reduced topology are subsequently described. Lastly, an overview of modeling the MRE resources is presented.

3.2.1. UC/ED Model Formulation

In this chapter, an open-source production cost modeling framework for the U.S. Western Interconnection called GO WEST (Akdemir, Oikonomou, Kern, Voisin, Ssembatya, et al., 2024) is used as a baseline to create the specific test case for wave energy integration.

Spanning over 4.66 million square kilometers, the U.S. Western Interconnection encompasses several U.S. states, Canadian provinces, and some parts of Baja California in Mexico. It provides electricity to approximately 80 million people (WECC, 2017). In 2018, the total nameplate capacity of all power plants in the U.S. Western Interconnection was 258,200 MW. The capacity mix is dominated by natural gas (38%) and hydroelectric power plants (27%), and they are followed by coal, nuclear, wind, and solar power plants (WECC, 2018).

GO WEST accounts for the grid operation in only the U.S. states of Western Interconnection, which include California, Oregon, Washington, Idaho, Nevada, Arizona, Utah, Wyoming, Montana, Colorado, and New Mexico. It is a Python-based software where the UC/ED mathematical optimization is solved by the solver Gurobi. Note that while the UC problem typically entails solving a mixed-integer linear program (MILP), the ED version is a pure linear program (LP). With GO modeling framework, users can choose between LP and MILP for their specific research study.

The model's objective is to minimize the total cost of providing necessary electricity to meet the total energy demand across the entire power system, subject to constraints that restrict the generator commitment and dispatch decisions such as generator ramp rate limits, maximum generator capacities, and minimum up and down times. There are also other constraints like thermal limits of the transmission lines and nodal power balances. The model operates on a user-defined 24-hour horizon and the temporal resolution of the model outputs is hourly.

Decision variables of the model consist of on/off status and electricity generation from each generator, voltage angle at each node, and power flow on each transmission line. There is one slack generator at each node that has an extremely high marginal cost of generation and is used only as a last resort. Slack generators are often used to detect loss of load events at any point in

time and account for power imbalances arising due to such events (Exposito et al., 2004). Model outputs include the generation schedule of each generator, power flow on each transmission line, locational marginal prices (LMP) at each node (typically characterized by the dual of power balance constraint at any node), voltage angles, and loss of load events at each node.

Scheduling and dispatch of thermal generators, like natural gas and coal, depends on several inputs like heat rates, fuel prices, and variable operation and maintenance costs as well as generator-related constraints. In the GO WEST model, nuclear power plants are considered as a must-run resource, except when there is a planned or forced generator outage. On the other hand, renewable generators are modeled differently. Historical hourly generation from solar and wind generators is gathered from EIA-930 dataset (EIA, 2022b) at the balancing authority scale and is remapped to the reduced nodal scale. Hourly available solar, wind, and wave generation at each node are provided as input to the model, which then decides how much of the available solar, wind, and wave power to dispatch. This means that the model might choose to curtail renewable generation depending on the grid conditions even though the marginal cost of renewable generators is low. On the other hand, a different approach is followed to model hydropower generators. Historical weekly hydropower datasets include generation targets as well as hourly minimum, hourly maximum, and daily maximum fluctuations. The generation targets are based on a modified version of EIA-923 dataset (EIA, 2022a), further downscaled based on USGS flows (Turner et al., 2022). The hydropower is dispatched hourly (with an operational daily maximum flow constraint) based on the power grid needs.

GO WEST uses a synthetic 10,000-node representation of U.S Western Interconnection (Birchfield et al., 2017; Electric Grid Test Case Repository, 2017a). Given that running a model of this scale would be both time- and resource-intensive, researchers often make use of simplified,

reduced-topology model versions of detailed power systems. In this regard, GO WEST allows users to select different number of nodes suitable for their studies, type of mathematical formulation (LP, i.e., only economic dispatch versus MILP, i.e., combined unit commitment and economic dispatch), transmission line scaling factors as well as hurdle rate scaling factors.

- **Number of nodes:** Users of GO WEST can select the number of nodes to retain from 10,000 nodal topology of the U.S. Western Interconnection (TAMU network). In this chapter, we selected 134 nodes to represent grid operations in Western Interconnection (see Chapter 3.2.2 for more details).
- **Mathematical formulations:** Although GO WEST allows both UC and ED formulations as discussed earlier, in this chapter, we selected the LP version (i.e., economic dispatch only) owing to its reasonable run times and comparable degree of accuracy, when compared with the results of the corresponding MILP (i.e., unit commitment) formulation (Akdemir, Oikonomou, Kern, Voisin, Ssembatya, et al., 2024).
- **Transmission line capacity scaling factors:** GO WEST determines the transmission line locations and thermal capacities for any reduced network automatically by utilizing a network reduction algorithm (Akdemir, Oikonomou, Kern, Voisin, Ssembatya, et al., 2024). However, additional calibration of transmission line capacities is necessary since there might be inconsistencies in the line limits calculated by the network reduction algorithm. In this chapter, thermal limits for congested lines over a pre-selected threshold were scaled up by a factor of 500 MW. All other lines retained their original thermal limits as prescribed by the network reduction algorithm.

- **Hurdle rate scaling factors:** A hurdle rate is defined by the cost of transferring 1 MW of power between two balancing authorities (BAs). A balancing authority oversees the electrical balance in its region. There are 28 BAs in GO WEST model. Original hurdle rates between BAs are gathered from Western Electricity Coordinating Council (WECC) Anchor Data Set (WECC, 2021). GO WEST model allows scaling hurdle rates up and down by user-defined percentages. In this chapter, we used the hurdle rates as reported by WECC and did not use hurdle rate scaling factors.

3.2.2. Nodal Topology Selection

In this chapter, we detail the steps of generating the 134-node reduced order model from the 10,000 parent topology. The metrics chosen for validation are (a) zonal LMPs and (b) system-wide generation portfolio composition (see Chapter 3.4.1 for numerical validation of the selected reduced topology model). Detailed node selection steps are enumerated below:

- Ten nodes throughout the Western Interconnection are selected specifically to host wave generation resources. Selection of the wave energy generator nodes is consistent with resource potential (wave power density), regions with existing infrastructure, and transmission capabilities across the western coast of continental U.S. (Yang et al., 2020). Specifically, two of these nodes are located in Washington, four in Oregon, and the last four nodes are placed in northern California. Note that in this chapter, we use wave energy as the only MRE resource since wave is considered to be the most scalable of the MRE resources (Bhattacharya et al., 2021; Jin et al., 2022).
- After selecting the wave generator nodes, nodes with the highest demand in each of the 28 balancing authorities (BA) are also added to the custom topology to represent high-load areas (e.g., cities) - this ensures at least one node in each state is selected.

- The remaining 96 nodes are uniformly divided into three categories; demand nodes, generation nodes, and transmission nodes. During the selection process of these nodes, a relatively higher priority is given to coastal states (Washington, California, and Oregon) to adequately capture wave power transmission ability to more inland nodes. Furthermore, demand and generation nodes are prioritized in proportion to their associated demand quantities and generation capabilities respectively. For transmission, the nodes having access to lines higher than 345 kV are prioritized.

Through the nodal selection procedure, two different distance thresholds are used. These thresholds make sure that the selected nodes are separated by a certain distance. We used a 30 km threshold while selecting a node in each BA, otherwise, an 80 km threshold is used elsewhere. The reason for using a 30 km threshold during node selection in each BA is to include at least one node in BAs that has a smaller service area. This approach allows a more dispersed topology while retaining the most important nodes (major demand centers, generation options, and transmission corridors). Figure 12 serves as a comparison of 10,000 nodal topology and 134 nodal topology we created for this chapter.

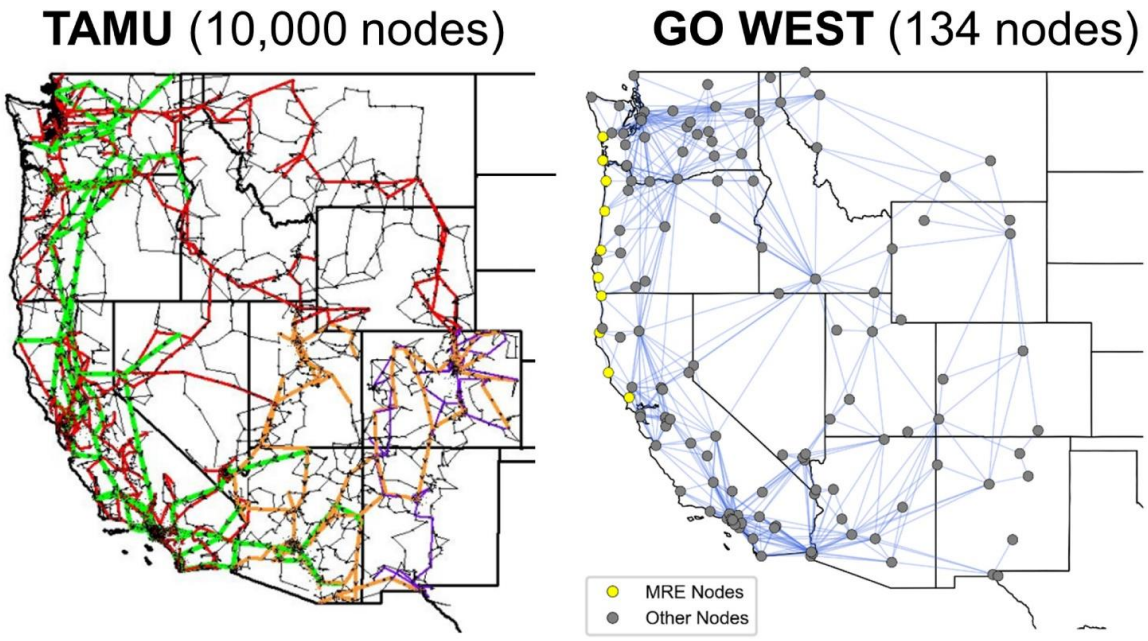

Figure 12: Comparison of the nodal topologies of the 10,000 node WECC representation (TAMU) and the reduced order 134 node representation developed for this chapter.

3.2.3. Wave Energy Modeling

The development of the necessary wave power (energy) generation characteristics for integration into the GO WEST model representation of the Western Interconnect is dependent on two major factors; the gross resource availability along the western seaboard of the U.S., and the conversion efficiency of the wave energy converters (WECs) from this gross resource into a usable net electrical power generation. A consistent, time-coherent, and well-validated dataset of the offshore wave energy gross resource characteristics is required to ensure the wave energy generation is well represented. Two data streams were used in this analysis.

Firstly, numerical wave propagation model outputs from a Simulating Waves Nearshore (SWAN) model (Booij et al., 1997) were utilized for the integration scenarios in 2019 (i.e., the representative year of chapter). This data included details on the significant wave height and wave energy period, as per International Electrotechnical Commission specifications (Robertson, Dunkle, et al., 2021). This data is publicly available from the National Renewable Energy

Laboratory's Marine Energy Atlas (NREL, 2021). Secondly, higher temporal resolution data which is time coherent with the respective demand data was needed for simulating wave power during California heat wave in 2020 (see Chapter 3.3 for more details on these scenarios). The necessary gross wave resource data for 2020 was harvested from in-situ device measurements, which are stored on National Data Buoy Center database for the following buoys: 46013, 46014, 46022, 46027, 46029, 46041, 46050. In order the quantify the conversion efficiency of the WECs, it was important to ensure that the results of this chapter were specific technology-agnostic. The conversion efficiency is needed to properly represent both existing WEC designs but also provide a reliable representation of possible future technologies. Utilizing the methodology developed by Robertson, et al. (Robertson, Bailey, et al., 2021), the conversion efficiency of the WECs was represented by a two parameter surface; with dependencies on both significant wave height and energy period. To ensure complementarity with existing renewables (i.e., wind and solar), the conversion efficiency surface includes 'cut-in' and rated power limits. Finally, the MRE generation profiles were developed by assessing the significant wave height and wave energy period at each location, for each hour, and identifying the appropriate conversion efficiency from the generic WEC representation. Normalized wave power outputs for the representative year of study (2019) at the 10 aforementioned locations (for locations, see Figure 13) selected for this chapter are shown in Figure 14.

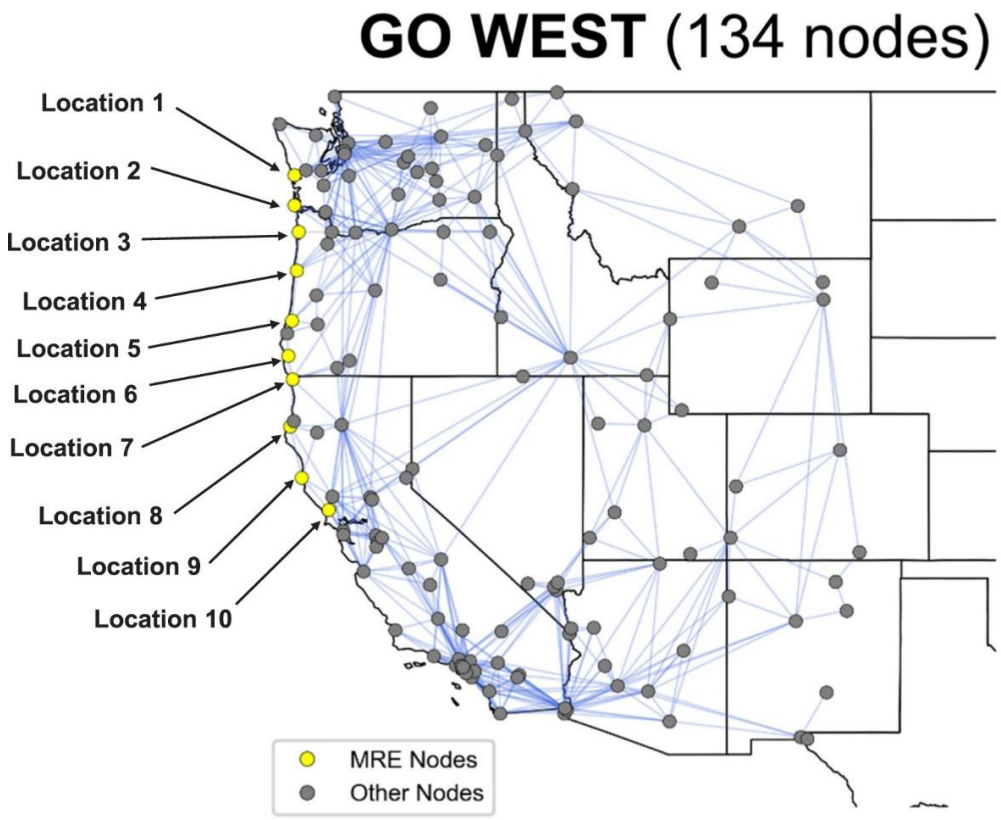

Figure 13: Locations of the selected nodes where wave energy-based generation is considered for installation.

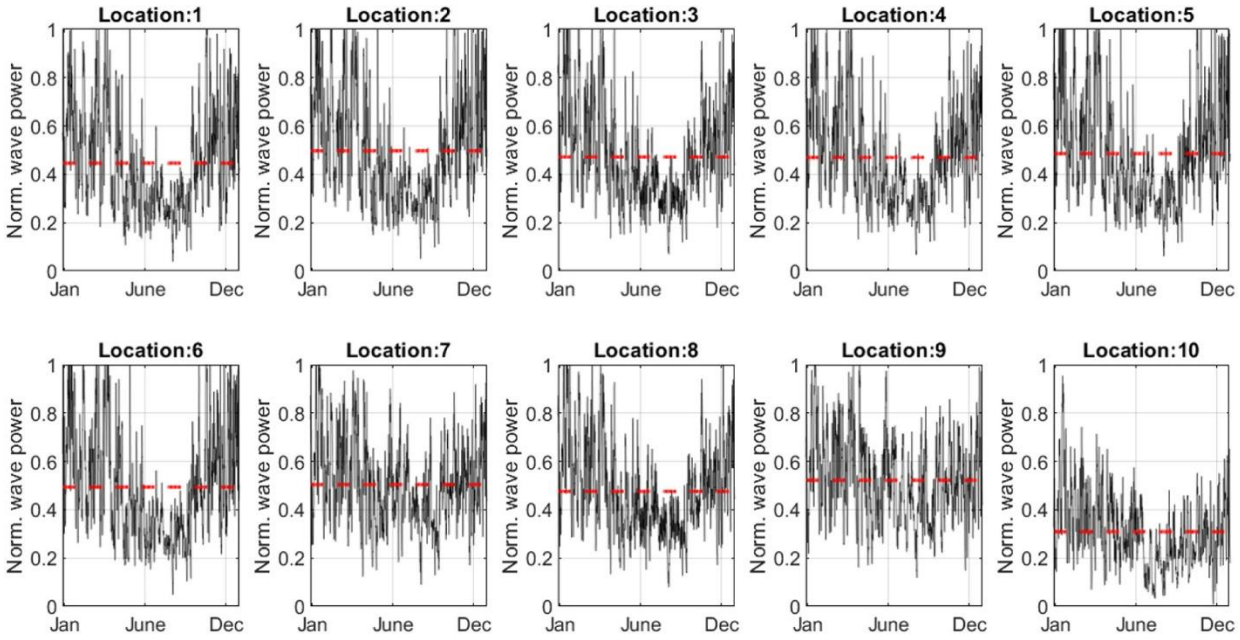

Figure 14: Normalized wave power outputs for the 10 selected locations, along with their yearly normalized average values (shown in red dotted line).

3.3. Scenarios and Experimental Design

In order to investigate the impacts of integrating MRE resources (wave energy) on bulk power system operations, a variety of scenarios were generated to help identify opportunities and challenges. The contribution of any new technology to bulk power grid operations is a function of the installed capacity. For a robust evaluation of the value proposition of wave energy to the contemporary grid of 2019 (our representative case study in this chapter), eight different wave energy capacity penetration scenarios are considered, with installed wave capacities of 10 MW, 20 MW, 50 MW, 100 MW, 200 MW, 300 MW, 400 MW, and 500 MW in each wave generation node. The operational and market impacts are analyzed both spatially and temporally.

As the integration of wave energy increases in the scenario, transmission constraints might limit the value proposition. Thus, we also study an alternate scenario where we increase the transmission line capacities equally by ＋500 MW throughout the Western Interconnection for each of the aforementioned wave energy penetration scenarios. The two sets of 8 scenarios provide a realistic evaluation of the potential contribution of wave energy to key performance metrics of the bulk power system, the first one relying on the 2019 infrastructure and the second set requiring an investment in transmission upgrades to achieve the full potential of the new technology.

Another opportunity of wave energy is to support power grid resilience. Specifically, we use two stress tests which are an artificial wildfire in August 2019 and a historical heat wave in August 2020, as described in Chapters 3.4.4 Impact of wave energy integration under resilience scenario: Wildfire contingency event, 4.5 Impact of wave energy integration during a heat wave scenario: 2020 California event respectively. Our selection of the wildfire event has been motivated by the observation that natural hazards (including forest fires) have significantly impeded power system operations in recent years (Tapia et al., 2021), with wildfire-driven

contingencies being of particular prominence in the Oregon/northern California region (Zanocco et al., 2023). Lastly, we analyzed the value of having wave power during the historical California heat wave that occurred between August 14, 2020 and August 19, 2020. This specific heat wave led to significant LMP spikes in California due to high electricity loads driven by extreme space cooling needs. During this extreme event, California Independent System Operator (CAISO) had to implement rotating outages to prevent more damage to the bulk electricity grid (CAISO, 2021).

3.4. Results and Discussion

3.4.1. Model Validation

Prior to detailed investigations into the impact of wave energy, it is important to ensure the baseline model well represents historical characteristics. The selected model version is validated by comparing simulated LMPs and generation mix with historical data in 2019. The left side of Figure 15 illustrates the LMP validation, which includes a time series comparison of simulated LMPs to historical LMPs in 2019. Daily LMP data for pricing hubs are calculated by taking a demand-weighted average of simulated LMPs at each node within each pricing hub. Relevant R^2 and root mean square error (RMSE) is calculated for each pricing hub. From Figure 15 (left-hand side plot), we can conclude that our version of the GO WEST model can capture LMPs appreciably well in all pricing hubs.

From the second plot (right-hand side) of Figure 15, we can infer that our model appreciably captures solar, wind, hydro, and nuclear generation. However, the over-utilization of natural gas plants more than historical data can be partly attributed to the inability of importing electricity from outside the U.S. (e.g., Canada). Therefore, our model has to generate more electricity from natural gas power plants to ensure adequate power balance. Another reason can be the lack of granular fuel price data for each balancing authority, which can impact the subsequent

merit order dispatch in the ED solution. Nevertheless, even with the aforementioned artifact, the selected topology captures the major generation mix in the U.S. Western Interconnection with reasonable accuracy.

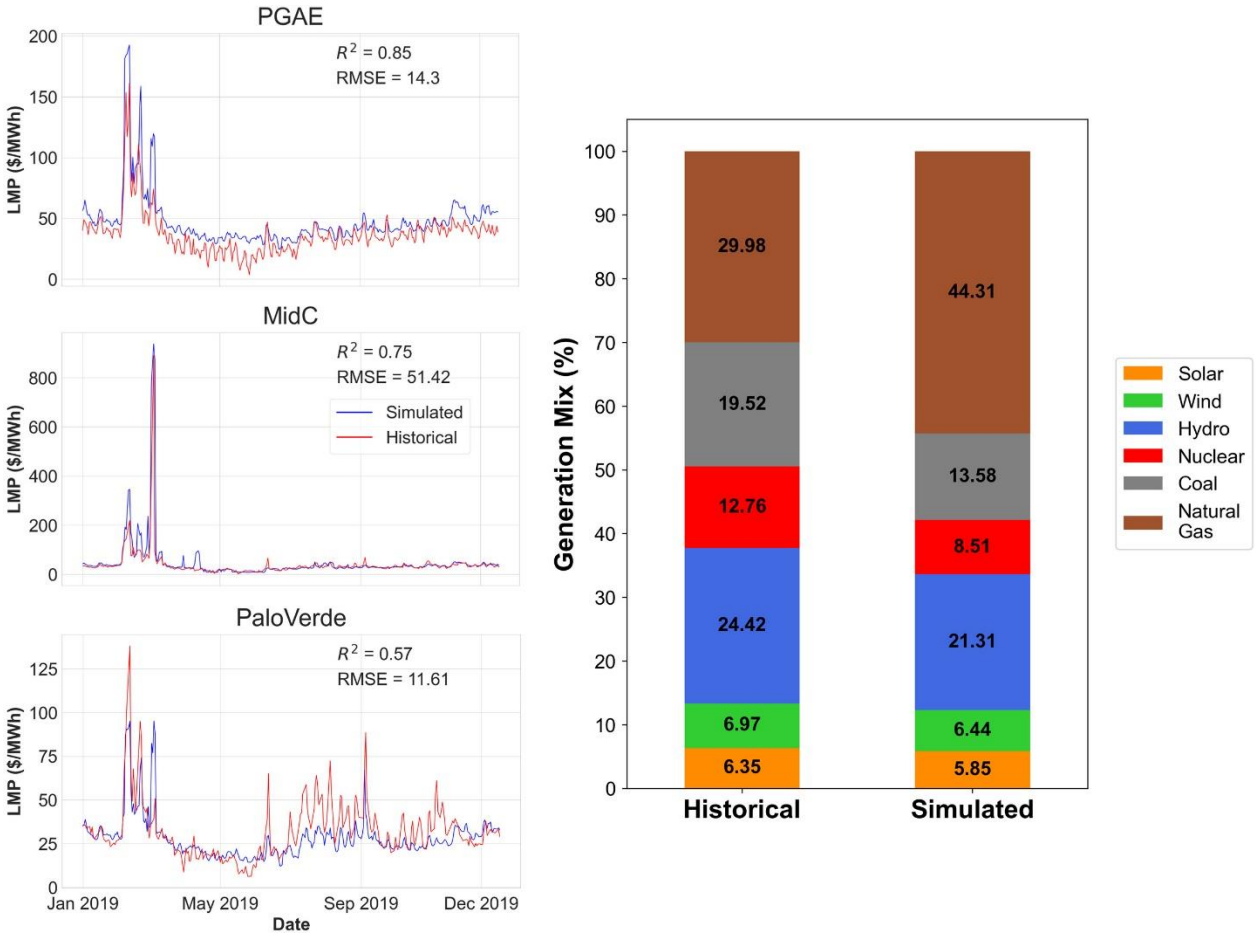

Figure 15: (Left) Historical and simulated daily LMPs for Mid-Columbia (MidC), Southwest (PaloVerde), and Pacific Gas and Electric (PGAE) in 2019; (right) comparison of historical and simulated generation mix percentages for the whole Western Interconnection in 2019.

3.4.2. Impacts of Integrating Different Wave Energy Capacities

In this chapter, we analyze the results of the 8760-hour economic dispatch with the selected topology (assuming 2019 operations) under eight different wave energy penetration scenarios where the installed capacities of wave energy in each MRE generator node were assumed to be 10 MW, 20 MW, 50 MW, 100 MW, 200 MW, 300 MW, 400 MW, and 500 MW. In these simulations,

the specified wave energy capacity is integrated into every MRE node simultaneously by the same amounts.

Hourly average, standard deviation, maximum, and minimum of LMPs for each scenario is listed in Table 4, which reflects the prices for overall Western Interconnection. Note that we calculated hourly LMPs for the whole Western Interconnection by taking a demand-weighted average of simulated LMPs at each node. Even though lower wave energy capacities do not have a significant impact on the LMPs, after reaching 50 MW wave capacity, we start to observe LMP reductions. Integrating 100 MW wave power decreases average LMPs by 0.91 $/MWh whereas 500 MW wave power leads to a reduction in average LMPs by 2.95 $/MWh. Furthermore, wave power decreases price volatility by reducing the standard deviation of LMPs. Adding 100 MW and 500 MW of wave capacity to each node diminishes the maximum LMPs observed in 2019 by 16.85 and 51.28 $/MWh, respectively. Additionally, beyond 200 MW wave integration, even minimum prices start to decrease as well.

Subsequently, we now study the temporal characteristics of the LMP reduction in Figure 16. We observe that before 50 MW wave power, there are minimal changes in LMPs when compared to the baseline configuration. After the 50 MW threshold, LMP reductions mostly occur in February and especially in March. This timing can be attributed to wave power being a stronger resource in winter months (Bhattacharya et al., 2021). Another likely contributing factor can be the higher-than-normal LMPs during the winter of 2019 due to supply constraints on natural gas and extremely cold temperatures (EIA, 2019). As wave power capacity grows, LMP depreciation becomes more pronounced. Beyond 200 MW wave integration, price reductions are observed in late fall and spring as well, in addition to winter months.

Table 4: Hourly LMP statistics for the whole Western Interconnection with and without wave energy integration in 2019.

Installed wave capacity per generator node (MW)	Average LMP ($/MWh)	Standard Deviation of LMPs ($/MWh)	Maximum LMP ($/MWh)	Minimum LMP ($/MWh)
0 (Baseline)	43.43	49.86	504.15	14.62
10	43.32	49.60	503.76	14.62
20	43.28	49.55	503.46	14.62
50	42.97	48.09	497.48	14.62
100	42.52	45.98	487.30	14.62
200	42.14	45.36	484.10	14.49
300	41.74	45.04	482.09	13.98
400	41.22	43.89	467.76	13.88
500	40.48	41.41	452.87	13.49

In Figure 17, we study the LMP reduction due to wave integration from a spatial viewpoint. Specifically, the reduction in LMPs in the individual nodes of our reduced topology model is plotted, from which we can clearly see that LMP reduction is more pronounced in the Pacific Northwest region (from coastal WA to northern CA), which is situated in close proximity to MRE generator nodes or has adequate transmission infrastructure for the benefits of wave generation to percolate inland.

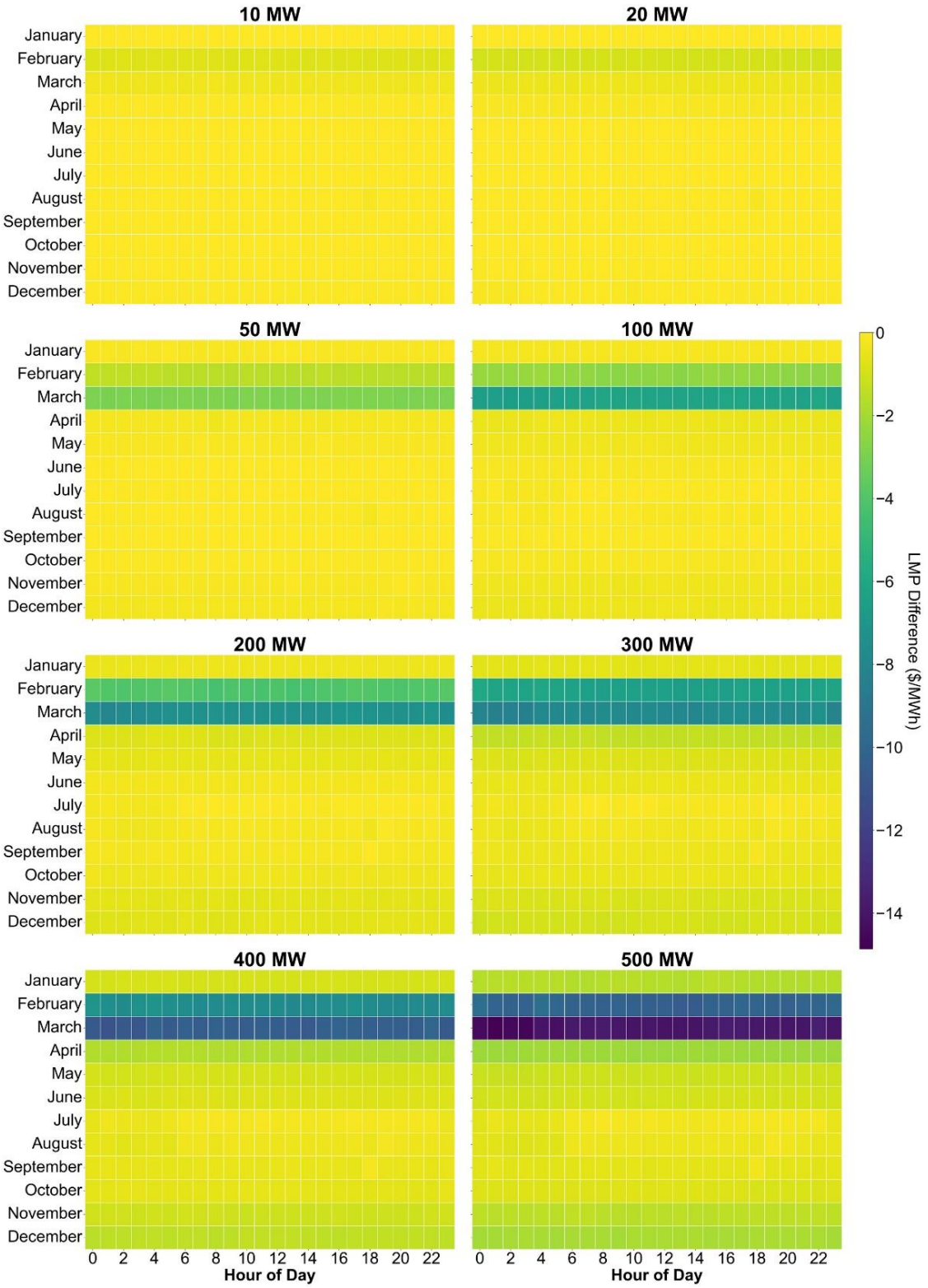

Figure 16: Fluctuation map of LMP changes due to wave power integration for each scenario. LMP difference designates the change in LMPs between the baseline scenario (0 MW wave power) and each MRE scenario. Negative values show LMP decrease due to wave power integration. Each row shows the hourly profile of an average day in different months of 2019.

Figure 17 demonstrates as integrated wave power capacity grows, the LMP depreciation also increases but only in a subset of nodes. Therefore, we can infer that if wave power integration is not accompanied by sufficient transmission infrastructure, the benefits of wave power will potentially remain localized.

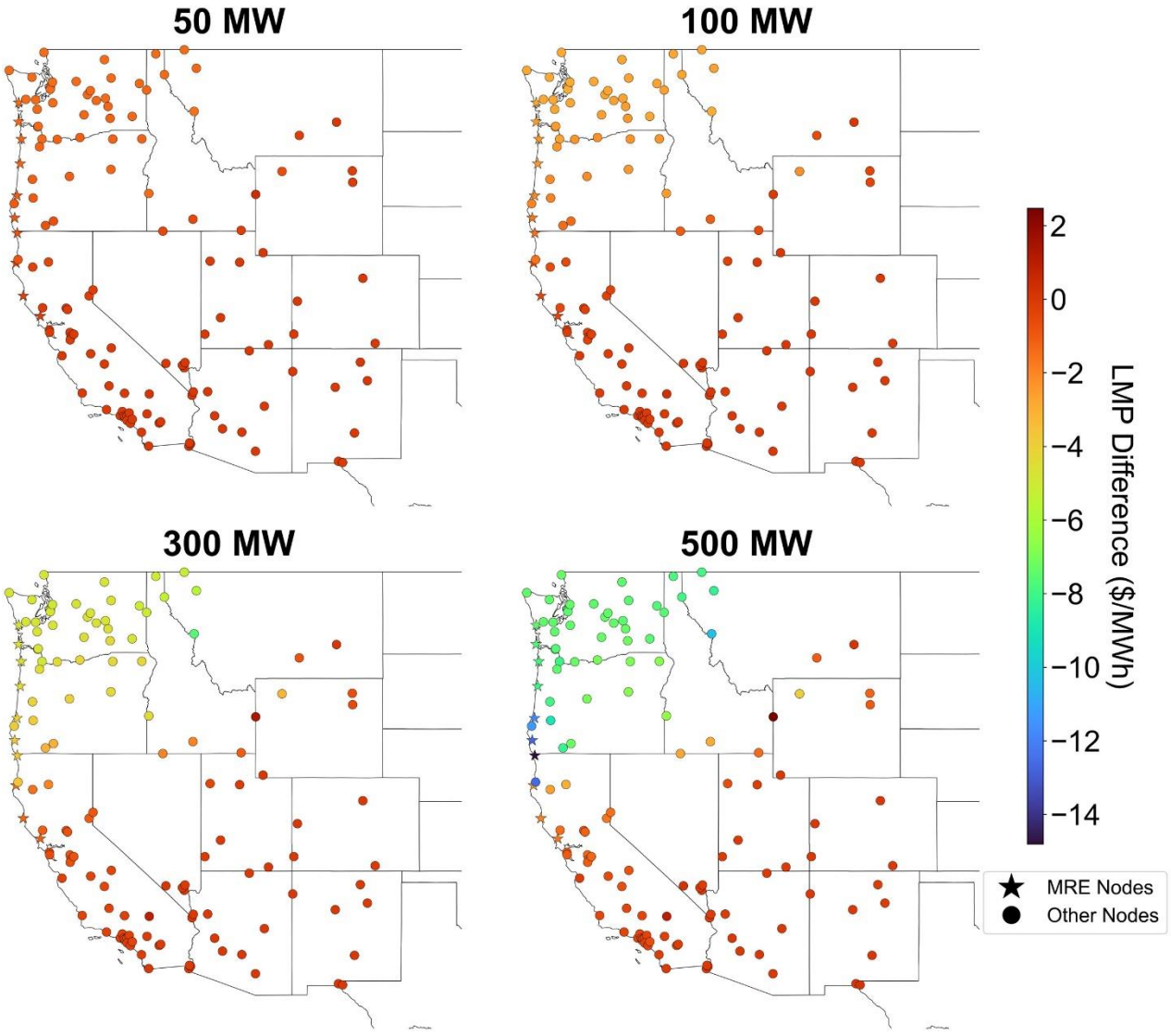

Figure 17: Average nodal LMP changes due to wave power integration for four selected scenarios in 2019. LMP difference designates the change in LMPs between the baseline scenario (0 MW wave energy capacity) and each wave integration scenario. Negative values show LMP decrease due to wave power integration. Color designates the magnitude of average LMP change at each node. MRE nodes are shown with stars whereas other nodes are shown with circles.

3.4.3. Impact of Concurrent Transmission Capacity Expansion and Wave Energy Integration

In this chapter, we repeat our experiments in Chapter 3.4.2 considering an increased transmission capacity (＋500 MW) across all transmission lines in the reduced topology network. For this chapter, LMP statistics in 2019 for the overall Western Interconnection under each wave penetration scenario are listed in Table 5. Again, we calculated hourly LMPs for the Western Interconnection by taking a demand-weighted average of simulated LMPs at each node. Since improving transmission capabilities enables inland nodes to take advantage of cheap electricity produced by wave resources, the overall price depreciation is much smaller due to the spread of the benefits. Even with 500 MW wave power, average LMPs reduce only by 1.05 $/MWh. Although price volatility in terms of standard deviation, maximum and minimum prices reduce with the integration of wave power, the amount of change is much lower than in the earlier case where an expanded transmission infrastructure was not considered.

Temporal LMP differences resulting from wave energy integration under each scenario are illustrated in Figure 18. No noticeable impact on the LMPs below 50 MW wave integration is observed, as was the case without transmission expansion. As wave power capacity grows, LMP reductions also increase and become dominant in February, which is also similar to our observation without transmission expansion in Chapter 3.4.2. In addition to winter months, LMP benefits from wave power start to emerge in late fall and spring after 200 MW integration case. In addition, higher LMP reductions occur between 7 PM and 8 AM since wave resources are more persistently available (at a relative scale when compared to wind and solar) during the night (Bhattacharya et al., 2021). Lastly, when compared to Figure 16, the boundary of LMP difference is narrower (i.e.,

maximum LMP reduction is lower) in Figure 18 due to the higher spatial spread of wave energy integration impact.

Table 5: Hourly LMP statistics for the whole Western Interconnection with and without wave energy integration in 2019. This table shows results for the case in which all transmission line capacities are additively scaled by +500 MW.

Installed wave capacity per generator node (MW)	Average LMP ($/MWh)	Standard Deviation of LMPs ($/MWh)	Maximum LMP ($/MWh)	Minimum LMP ($/MWh)
0 (Baseline)	33.98	15.44	158.11	16.36
10	33.96	15.42	158.11	16.36
20	33.94	15.42	158.16	16.36
50	33.87	15.38	158.18	16.36
100	33.76	15.33	157.1	16.36
200	33.57	15.22	156.72	16.2
300	33.37	15.06	155.59	16.17
400	33.15	14.9	155.43	16.17
500	32.93	14.77	155.18	16.17

From a spatial viewpoint, the LMP reduction effect is observed to be significantly more spread out over a wider geographical extent, thereby highlighting the benefits of concurrent transmission expansion in leveraging the benefits of wave energy. Figure 19 verifies that wave power's positive impacts (e.g., LMP reductions) can reach inland nodes when coupled with transmission investments. On the other hand, LMP depreciation in most of the nodes becomes relatively lesser due to the benefit now spreading over a greater geographical region with increased transmission capabilities. In order to understand the scale of the wave power integration for this chapter, it should be noted that the total capacity of integrated wave power (5000 MW from the 10 wave energy generator nodes) corresponds to 1.9% of the total installed capacity in the U.S. Western Interconnection.

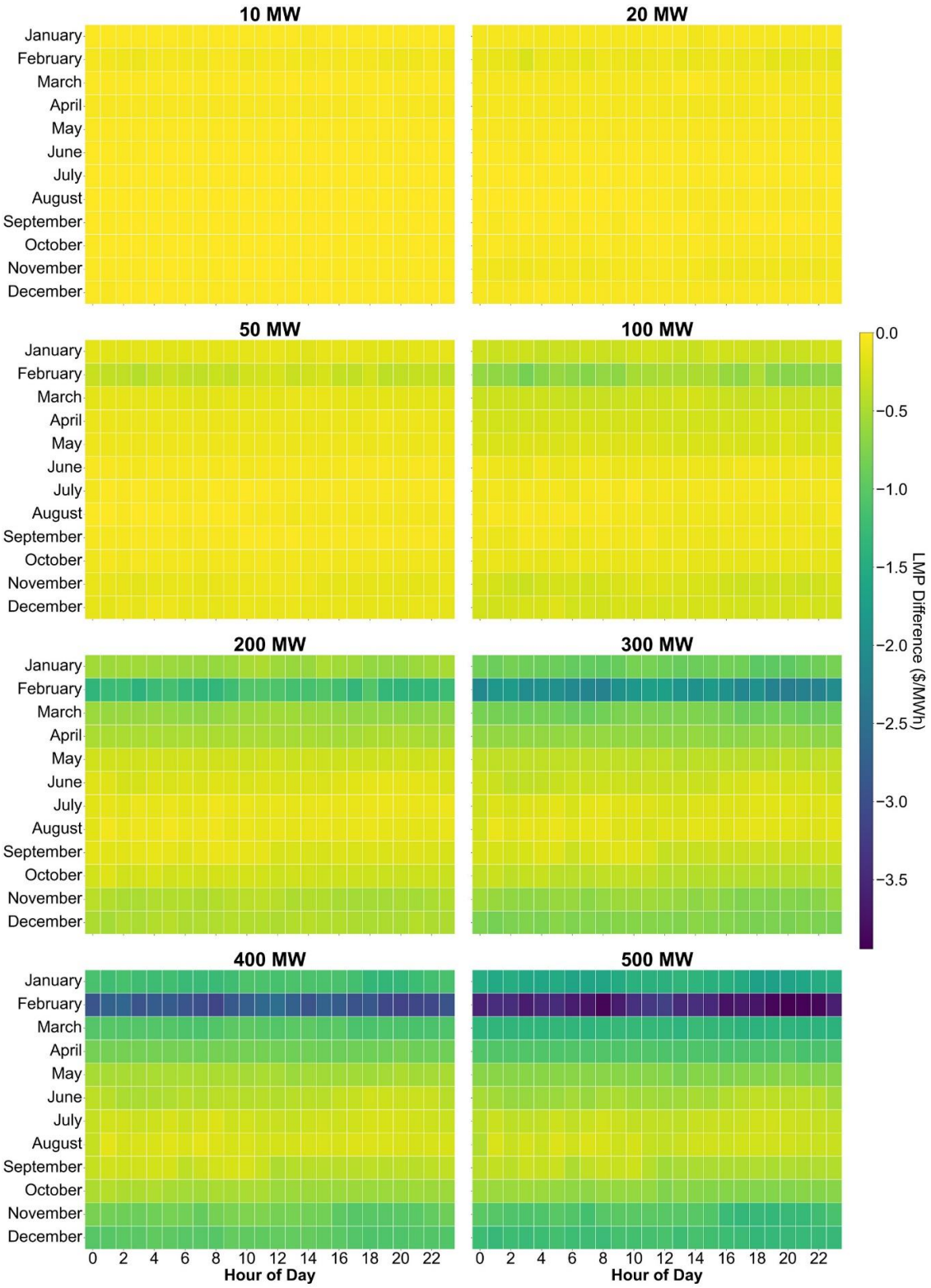

Figure 18: Fluctuation map of LMP changes due to wave power integration for each scenario. LMP difference designates the change in LMPs between the baseline scenario (0 MW MRE) and each MRE scenario. Negative values show LMP decrease due to wave power integration. Each row shows the hourly profile of an average day in different months of 2019. In this figure, all transmission lines are scaled by ＋500 MW.

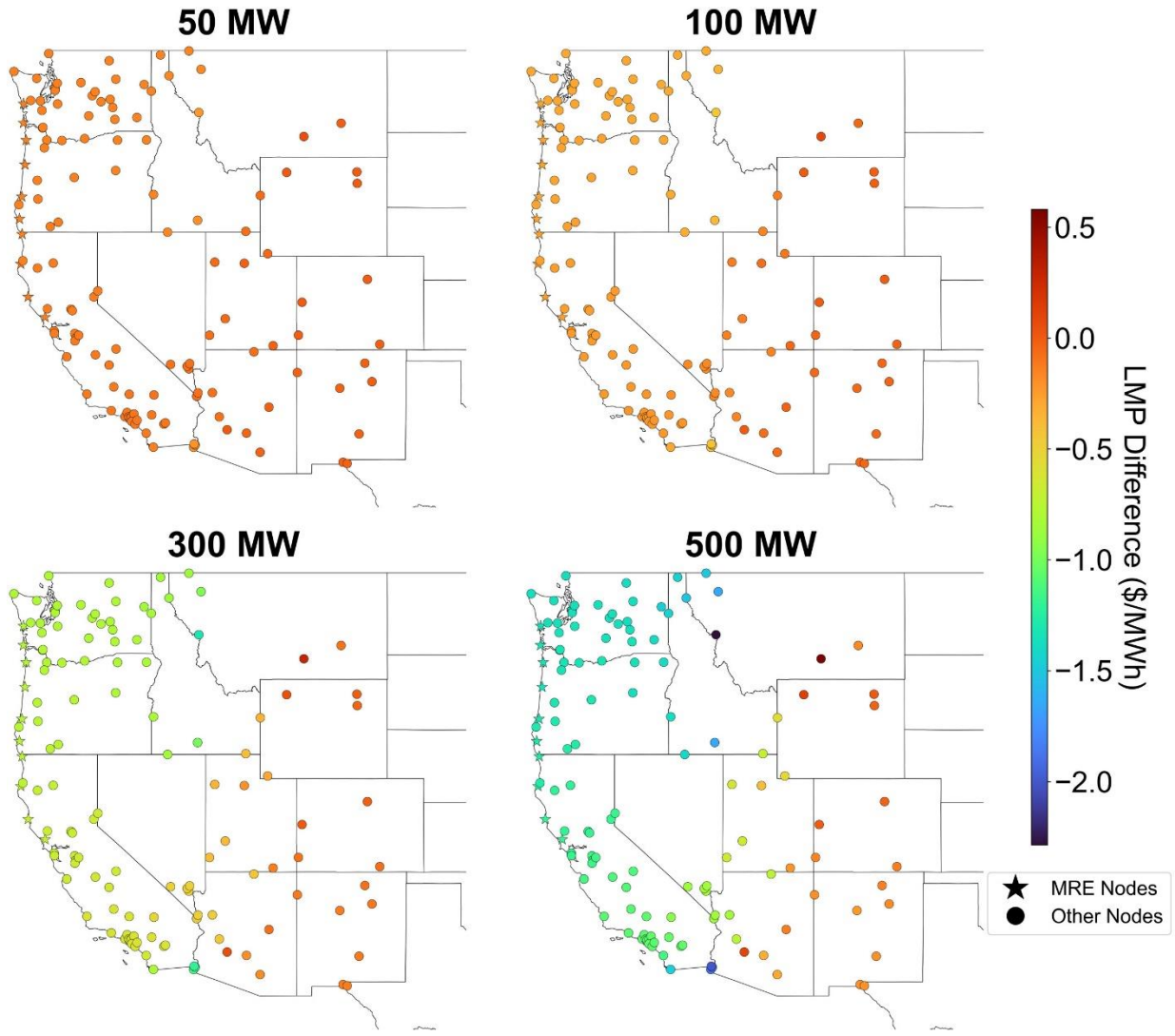

Figure 19: Average nodal LMP changes due to wave energy integration for four selected scenarios in 2019. LMP difference designates the change in LMPs between the baseline scenario (0 MW wave energy capacity) and each wave integration scenario. Negative values show LMP decrease due to wave energy integration. Color designates the magnitude of average LMP change at each node. MRE nodes are shown with stars whereas other nodes are shown with circles. In this figure, all transmission lines are scaled by ＋500 MW.

3.4.4. Impact of Wave Energy Integration Under Resilience Scenario: Wildfire Contingency Event

In this chapter, we analyzed the effect of including wave energy in the generation mix during a transmission line contingency (outage of major transmission lines) due to an artificial wildfire. Informed by wildfire statistics within the U.S. (Hoover & Hanson, 2021; National Interagency Fire Center, 2022), we assumed an artificial wildfire that extends spatially from

northern California to Oregon causing associated transmission line derating in the region. The choice of the event time (August 7th to August 14th, 2019) is guided by literature on identifying causative factors for wildfire inception events (NOAA, 2023), historical 2019 hourly dry bulb temperatures, relative humidity, and wind speed data from Montague Siskiyou Airport). We assumed that the wildfire-driven line contingency duration is 1 week. In order to study the impact of having wave resources in the generation mix during these aforementioned line outage scenarios, we considered installed capacities of 100 MW and 500 MW of wave generation to every wave energy generator node and compared the results with the baseline case, where no wave resource was available.

Nodal LMP effects of having wave power in the generation mix during the simulated transmission line contingency event are illustrated in Figure 20. When there is no wave power available, average LMPs in a majority of the nodes that are directly connected to transmission lines affected by the outage event spiked above 1000 $/MWh. This is because there was a supply shortfall in those nodes, which lead to unserved load events (reflected by high loss-of-load pricing). The price shock impact of the wildfire extends northwards up to some areas of Washington. However, with 500 MW wave power capacity at every wave energy generator node during the event, the nodal LMP spikes due to the wildfire event were observed to be alleviated to some extent.

It is crucial to track the hourly grid influences from MRE resources to comprehend the overall value of possible integration. Figure 21 visualizes the average LMPs in line outage nodes as well as the total unserved load for each scenario (0 MW i.e., baseline, 100 MW, and 500 MW of wave power capacity). Although the LMP depreciation benefits of having 100 MW wave power capacity are relatively lesser, integrating 500 MW wave capacity leads to significant LMP

reductions during the event. In line with this observation, 500 MW wave capacity integration was also observed to curb unserved load (i.e., loss of load events) in the 14 line outage nodes that are directly affected by the studied wildfire event.

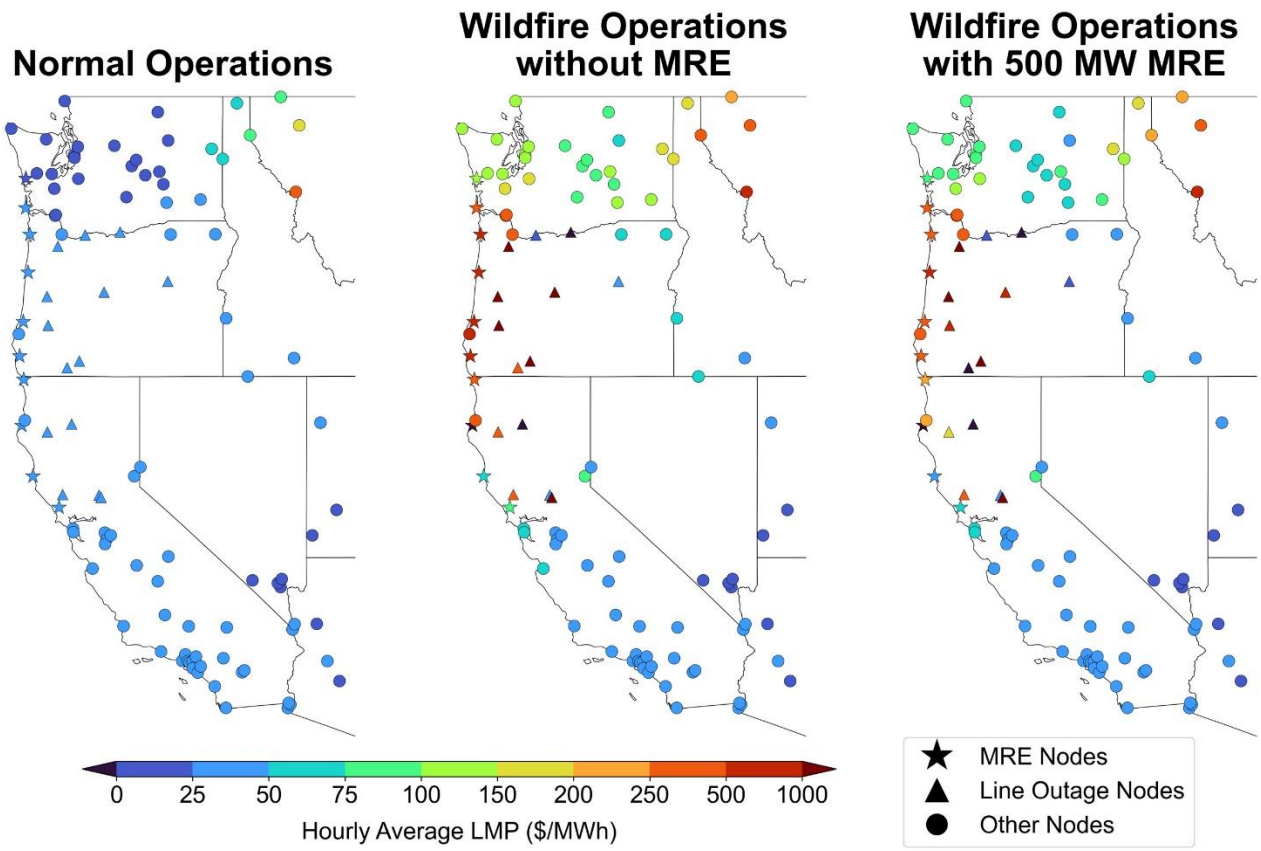

Figure 20: (Left) Nodal LMPs without the artificial wildfire; (center) nodal LMPs with the artificial wildfire but no wave power integration; (right) nodal LMPs with the artificial wildfire and 500 MW wave power integration to every MRE node. The nonlinear color bar designates the average LMPs during the week of the hypothetical event. MRE nodes are shown with stars, nodes connected to lines on outage are shown with triangles, and other nodes are shown with circles.

Table 6 provides summary statistics for the whole Western Interconnection under each scenario. The wildfire event increased average LMPs throughout the Western Interconnection by 177.4 $/MWh under baseline conditions (no wave power). Integrating 100 MW and 500 MW wave power to every MRE node (i.e., 1000 MW and 5000 MW wave power in total across the entire U.S. Western Interconnection) led average LMPs to drop by 7.64 and 41.56 $/MWh, respectively.

Wave power also reduces the price volatility by decreasing standard deviation, and maximum and minimum LMPs during the event. Even though 100 MW wave power integration does not change the minimum LMPs, increasing wave power capacity further to 500 MW reduces the minimum LMPs by more than 30 $/MWh. Lastly, the wildfire event (and subsequent transmission line outages) was observed to have increased the average hourly unserved load substantially. However, having 500 MW wave power in each MRE node could potentially alleviate 254.11 MW load loss on an hourly average basis, throughout the Western Interconnection.

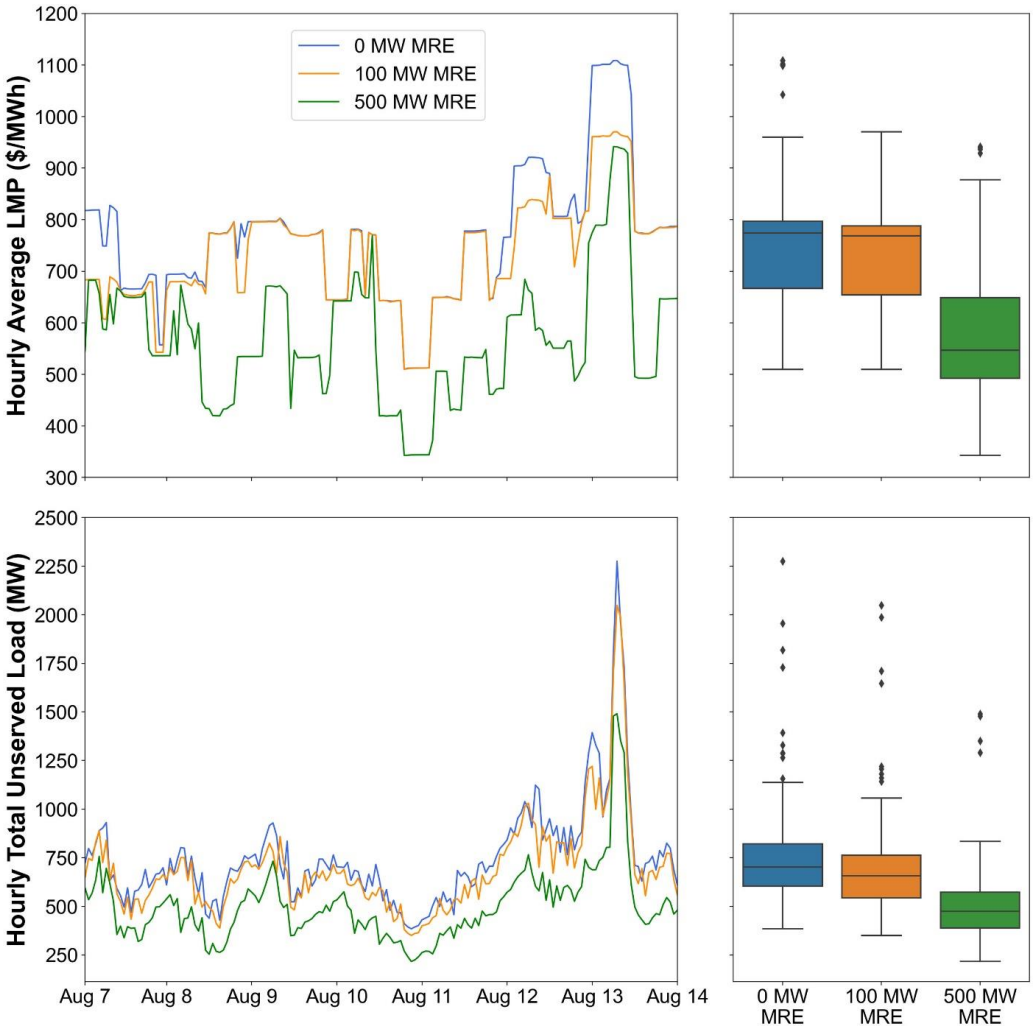

Figure 21: (Top left) Hourly average LMP time series in line outage nodes; (top right) distribution of hourly average LMPs in line outage nodes; (bottom left) hourly total unserved load time series in line outage nodes; (bottom right) distribution of hourly total unserved load in line outage nodes. These results are focusing on the week of the hypothetical wildfire event. Colors designate the three MRE integration scenarios (0 MW MRE (baseline), 100 MW MRE, and 500 MW MRE).

Table 6: Summary statistics for the whole Western Interconnection during the contingency event in 2019.

Scenario	Avg. LMP ($/MWh)	Std. Dev. of LMPs ($/MWh)	Max. LMP ($/MWh)	Min. LMP ($/MWh)	Avg. Hourly Unserved Load (MW)
No wildfire	30.73	7.40	51.75	23.25	2.36
No wave power + wildfire scenario	208.13	40.89	321.22	129.55	789.56
100 MW wave power + wildfire scenario	200.49	33.67	290.24	129.54	733.67
500 MW wave power + wildfire scenario	166.57	39.07	284.01	99.02	535.45

3.4.5. Impact of Wave Energy Integration During a Heat Wave Scenario: 2020 California Event

In this chapter, we investigate the impact of having different wave power capacities during the historical California heat wave (August 14th–August 19th, 2020). This event caused a considerable rise in LMPs throughout California due to higher electricity loads resulting from increased space cooling demands. Amidst this historical event, California Independent System Operator (CAISO) ordered rotation outages in California to preserve stability in bulk electricity grid operations (CAISO, 2021).

Figure 22 shows the nodal LMP effects of having wave power in the generation mix during the heat wave event. Integrating 100 MW wave power does not lead to a noticeable LMP drop. On the other hand, when the installed capacity of wave power at each MRE node increased to 500 MW, we can see the nodal LMPs decrease to some extent. However, LMP depreciation is only localized to northern California (up to the Bay Area) due to the lack of transmission capacity to transmit low-cost wave power to southern California. Therefore, we can infer that concurrent transmission expansion is required to take full advantage of wave power during an extreme weather event like a heat wave.

When compared to the line contingency event discussed in Chapter 3.4.4, the severity of LMP spikes and loss of load events during the 2020 California heat wave is lower (see Figure 23). Although 100 MW wave power capacity helped to reduce LMPs slightly, the positive impact of integrating 500 MW wave power is much more pronounced. During the 2020 California heat wave, integrating 100 MW and 500 MW wave power might have reduced the average hourly LMPs by 0.8 and 5.36 $/MWh. Wave power did not play a significant role in changing the minimum LMPs but 500 MW wave power could have alleviated maximum LMPs by 16.6 $/MWh. In addition, wave power help curb price volatility and increase reliability by decreasing the standard deviation of LMPs and total unserved load (see Table 7). However, a comparison of Figure 23 with Figure 21 reveals that the cost and reliability (i.e., LMP and loss of load) advantages of having wave energy through this heat wave are considerably lesser than the line contingency scenario in Chapter 3.4.4.

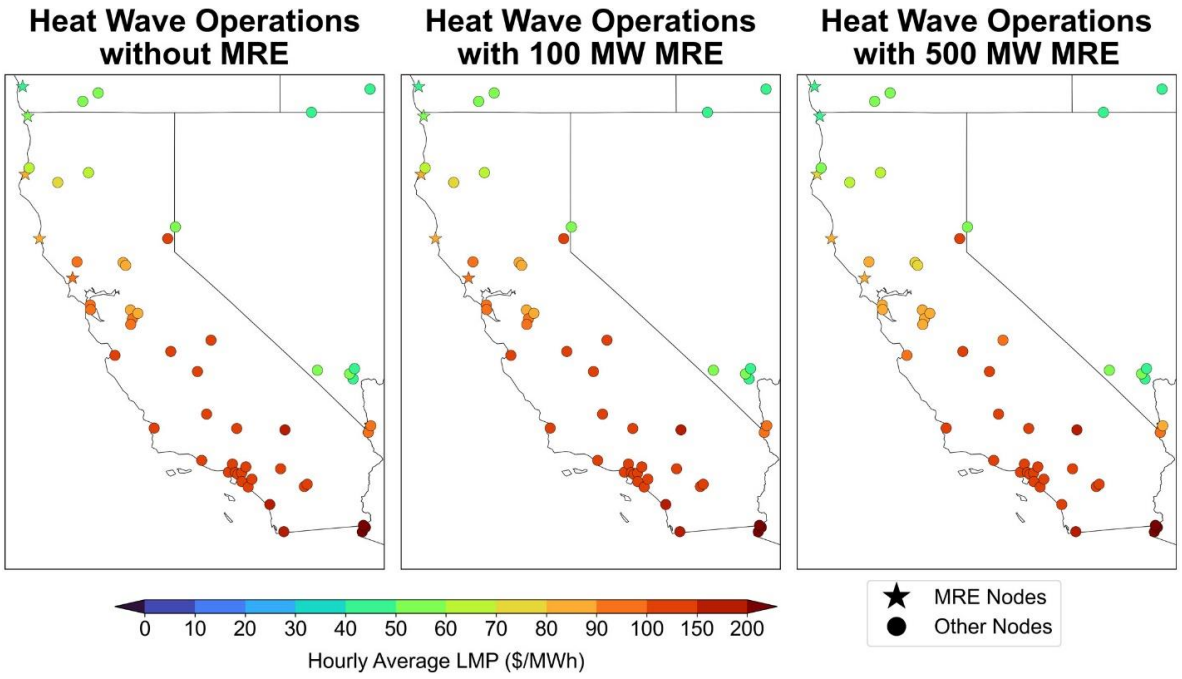

Figure 22: (Left) hourly average LMPs during the heat wave without wave power integration; (middle) hourly average LMPs during the heat wave with 100 MW wave power integration; (right) hourly average LMPs during the heat wave with 500 MW wave power integration.

Finally, the share of wave power in the generation mix in California during the historical heat wave is presented in Figure 24. Since wave power is more prominent during nighttime (Bhattacharya et al., 2021), its share in the generation mix is more observable during those periods. Nevertheless, wave power is present in the generation mix in varying amounts throughout the day. On a cumulative scale, during the heat wave event, 500 MW wave capacity installation in each MRE node constitutes nearly 1% of the total generation mix by replacing power generated from natural gas in California. The capacity of total wave power in California (2000 MW from 4 MRE nodes) corresponds to nearly 2.5% of the total installed capacity in California. Note that our analysis does not consider temperature-based deratings of thermal power plants. We believe that when integrated into the model, an additional temperature-based derating component in the operation of the thermal power plants would likely increase the benefit of wave power utilization during this heat wave (Dyreson et al., 2022). However, a detailed analysis of temperature-based deratings of thermal power plants is beyond the scope of this current work and is deferred to future work.

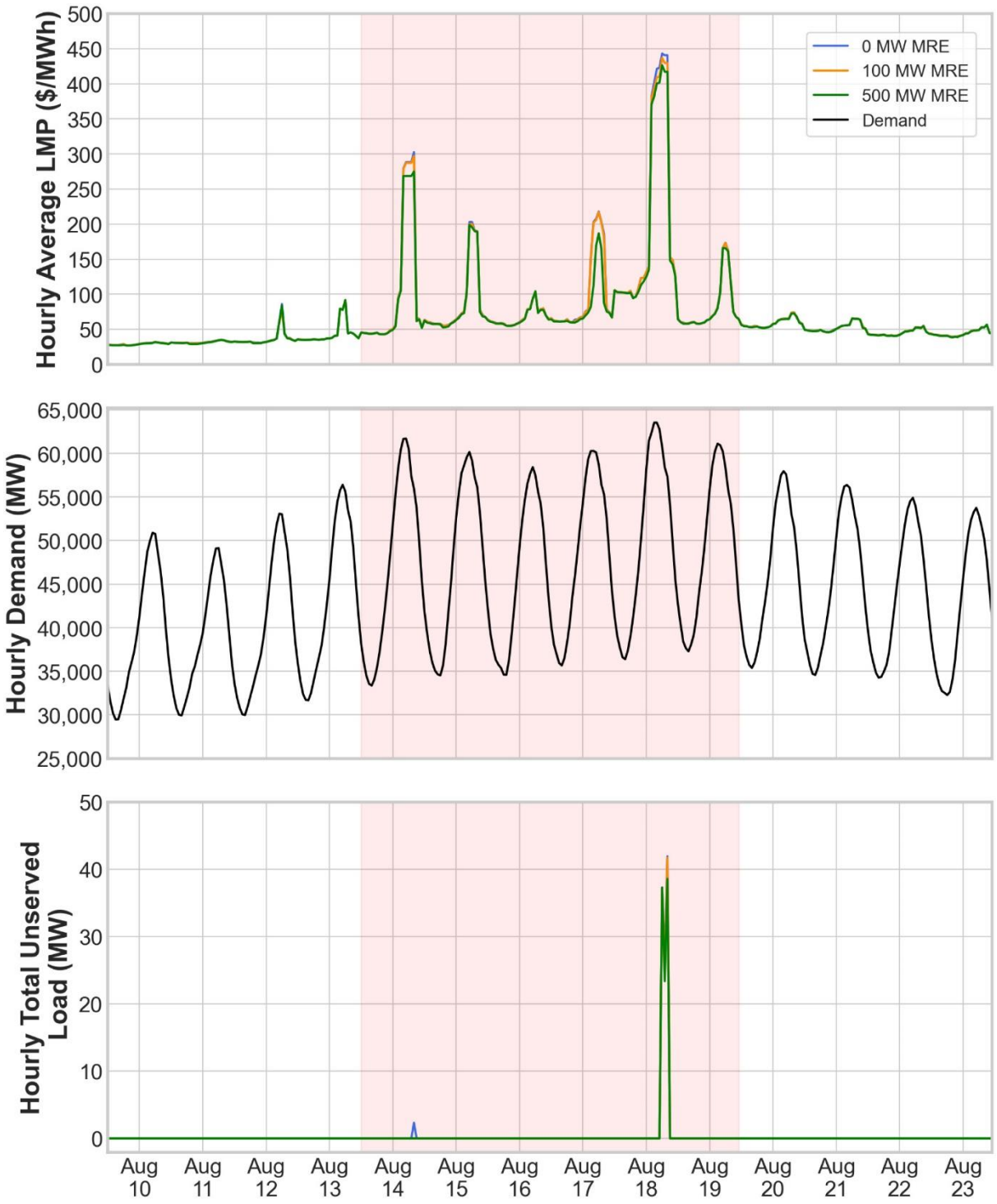

Figure 23: (Top) hourly average LMP time series in California; (middle) hourly electricity demand time series in California; (bottom) hourly total unserved load time series in California. The duration of the heat wave is highlighted in red. Colors designate the three MRE integration scenarios (0 MW MRE (baseline), 100 MW MRE, and 500 MW MRE).

Table 7: Summary statistics for California during the heat wave event in 2020.

Scenario	Avg. LMP ($/MWh)	Std. Dev. of LMPs ($/MWh)	Max. LMP ($/MWh)	Min. LMP ($/MWh)	Total Hourly Unserved Load (MW)
No wave power + heat wave scenario	106.91	90.39	443.21	42.94	107.78
100 MW wave power + heat wave scenario	106.11	88.64	437.13	42.93	103.77
500 MW wave power + heat wave scenario	101.55	84.19	426.61	42.90	99.16

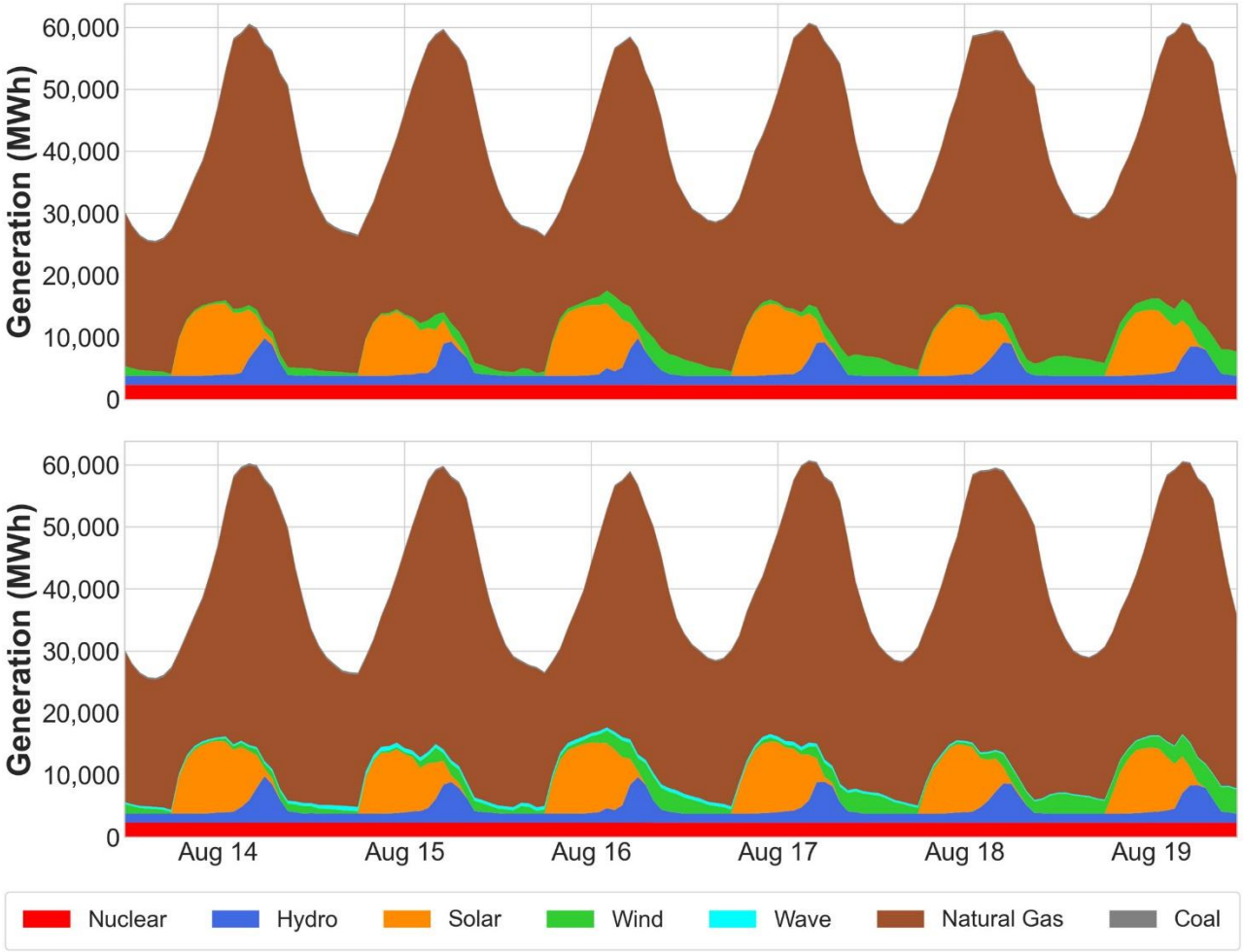

Figure 24: (Top) hourly generation mix in California during the heat wave without wave power integration; (bottom) hourly generation mix in California during the heat wave with 500 MW wave capacity integration.

3.5. Conclusion, Limitation and Future Directions

In this chapter, we performed a data-driven analysis to understand the impact of wave energy integration on power system operations for a bulk transmission grid. Specifically, a reduced topology network of the U.S. Western Interconnection was developed, to which wave generation was added at strategic points, to varying capacities. Our results indicated that beyond a threshold of approximately 100 MW of wave capacity in each of the MRE nodes, wave energy integration can bring down energy prices (LMPs), as well as reduce price volatility. Without widespread transmission infrastructure upgrades, the impact of wave generation is likely to remain geographically confined to the Pacific Northwest region (mainly Washington, Oregon, and northern parts of California). Our studies also indicate that concurrent transmission upgrades, along with wave energy integration are likely to aid a greater geographical spread of the benefits of wave energy integration. Finally, we studied the impact of wave generation during two resilience-driven events. In the first of these events, where we simulated a wildfire-driven transmission outage across a major transmission corridor, we observed that wave energy integration can enable price spike reduction by assuaging generation shortages, especially in nodes that are directly impacted by the outage events, and have sufficient transmission network connectivity to receive wave power benefits. In the second scenario, we studied the impacts of wave energy generation on grid operations during a heat wave event. The advantages of wave power were observed to be marginal in this case, likely due to wave being predominantly a winter peaking resource (while the heat wave happened in summer) and the impacted zone having limited connectivity to wave resources.

While several interesting operational insights were obtained through our studies, there are some limitations, and therefore, future research directions, which are discussed as follows. Firstly, this model assumes that the grid operator has perfect foresight and there are no forecast uncertainties (i.e., there are no errors in demand, solar, wind, and wave power forecasts). Moreover, we model only day-ahead market operations. Including real-time electricity markets with stochastic forecast errors would make the simulations more accurate; however, would steeply increase computation time and resource needs. Secondly, we consider one central operator for all balancing authorities within the selected model. In other words, one objective function represents coordination across all BAs en masse. Since the benefits of the wave energy-based generation resources are not shared equally among BAs, having different objective functions with an embedded economic investment model can help with analyzing the effects of wave energy resources in each individual BA. Finally, we assumed the same wave power capacity integrated into every wave generator (MRE) node. Deciding on different wave power capacities for each node by taking wave power density at each coastal node into consideration would increase the model's fidelity to the real-world decision-making process. Along with the aforementioned directions, future efforts will also probe similar research questions for other types of grids that have different demand patterns and resource availability (such as U.S. Eastern Interconnection) and other potential climate-driven resilience scenarios (such as winter storms).

3.6. Software and Data Availability

The model is open-source and publicly available. All codes of the model and data used are available under MIT free software license (Akdemir et al., 2023).

CHAPTER 4. BENEFITS OF COOPERATIVE TRANSMISSION EXPANSION PLANNING IN U.S. WESTERN INTERCONNECTION

4.1. Background

Keeping global warming under 1.5 °C or 2 °C entails reaching net-zero emissions by 2050 or 2070, respectively (IPCC, 2022). A global transformation of the energy sector is needed to decrease greenhouse gas (GHG) emissions and achieve these climate goals (Guler et al., 2021; Rodríguez-Sarasty et al., 2021). Increasing the share of variable renewable energy sources such as solar and wind is crucial for decarbonizing electricity grids (Golombek et al., 2022; Liu et al., 2019). A compounding challenge will be climate change itself, which could influence electricity demand, system reliability, electricity prices, and GHG emissions in bulk power systems (Hill et al., 2021; Su, Kern, Reed, et al., 2020; Wessel et al., 2022). For example, the intensity and frequency of extreme weather events are increasing due to climate change, and these kinds of events, like heat waves and hurricanes, strain electricity grids by damaging or reducing the efficiency of the power plants and infrastructure (Akdemir et al., 2022; Matko et al., 2016). Since grid operators are facing a dual challenge of decarbonizing and maintaining the reliability of power systems during extreme weather events (Akdemir et al., 2023), joint consideration of these two phenomena in power system modeling is important (Dyreson et al., 2022).

Substantial investment in high-voltage transmission expansion is now widely viewed as an imperative in deep decarbonization of the power grid via variable renewable energy sources (Golombek et al., 2022; Liu et al., 2019). Transmission expansion planning (TEP) is the process of deciding when and where new lines should be installed or the capacity of existing lines should be enhanced (Conejo et al., 2016; Gacitua et al., 2018; Hemmati et al., 2013). TEP exercises attempt to maximize the social welfare of power system operations while minimizing the cost of

long-term transmission investment plans (Kirschen & Strbac, 2018; Munoz et al., 2015). However, the academic representation of TEP process generally assumes an overly optimistic level of coordination between transmission planning entities, which might result in unrealistic plans or study outcomes (Kasina & Hobbs, 2020). Therefore, these kinds of studies might not convey the total value of coordination between transmission planning entities, which could result in individual plans that cost more but do not unlock the full power system reliability benefits (Peskoe, 2024).

Numerous studies in the power system literature have focused on TEP problems from different aspects (Al-Saba & El-Amin, 2002; Bahiense et al., 2001; Buygi et al., 2004; Cadini et al., 2010; Choi et al., 2007; Dyreson et al., 2022; Hobbs et al., 2016; Kasina & Hobbs, 2020; Li et al., 2022; Munoz et al., 2014; Ruiz & Conejo, 2015; Xiaotong et al., 2012). For instance, Ruiz et al. proposed an adaptive robust transmission optimization model to pick investment alternatives by minimizing total system costs for worst-case outcomes of uncertain parameters (Ruiz & Conejo, 2015), whereas Choi et al. considered different types of contingencies to solve TEP problem (Choi et al., 2007). In addition, Cadini et al. introduced two objectives of a TEP problem as reliability and cost, and used a multi-objective genetic algorithm to find a solution (Cadini et al., 2010). Al-Saba et al. tested artificial intelligence (AI) tools like neural networks and Tabu search in solving TEP problem (Al-Saba & El-Amin, 2002).

However, none of these studies quantifies the value of cooperation in interregional TEP during extreme weather events under future climate projections. There is a risk of understating the value of regional and interregional transmission investments if extreme and high-value conditions like heat waves are not sufficiently taken into consideration (Americans for a Clean Energy Grid, 2023; Lawrence Berkeley National Laboratory, 2022). For instance, balancing authorities (BAs) would have more opportunity to give/receive power support to each other during weather

extremes, if the transmission network is planned cooperatively while considering these kinds of high-value conditions. On the other hand, our hypothesis would be that widespread heat waves might undermine these collaboration benefits as more BAs would be under stress due to overutilization of generators to satisfy significant spikes in electricity demands.

In this study, we are investigating the operational impacts of cooperation between transmission planning entities, quantified in terms of economic and reliability benefits under future climate scenarios and during heat wave events. Our research questions are how cooperative transmission expansion planning might help the grid operations during heat waves and how those benefits might evolve with respect to the spatial scale of the event (local vs. widespread) under future climate projections.

We make use of two western United States (U.S.) heat wave events in 2019 (in June and August) as base cases of local and widespread heat wave examples. Furthermore, the same two heat waves are replayed 40 years into the future (i.e., in 2059) under a future climate scenario that utilizes representative concentration pathways (RCP) and shared socioeconomic pathways (SSP). Grid conditions under these scenarios are simulated with a customized Grid Operations (GO) modeling framework with a production cost model (PCM) component to assess the economic and reliability impacts of individual (i.e., only intraregional) vs. cooperative (i.e., both intraregional and interregional) TEP. In order to come up with representative conditions of the U.S. electricity grid in 2059, we utilize several supporting models including a transmission expansion model to optimize capacity additions to existing transmission lines, Total Electricity Loads Model (TELL) (McGrath et al., 2022) to predict hourly electricity loads in each region, Global Change Analysis Model (GCAM) (Binsted et al., 2022) to generate future generation capacity additions and fuel prices, Capacity Expansion Regional Feasibility Model (CERF) (C. Vernon et al., 2021) to site the

future generators to appropriate locations depending on numerous suitability layers, and Renewable Energy Potential Model (reV) to determine hourly solar and wind generation profiles for the future years.

4.2. Methods

In this chapter, we start with a brief explanation of GO modeling framework as well as its PCM component. Then, a description of the TEP model as well as the supporting models used in this study (i.e., GCAM, CERF, TELL, and reV) are presented.

4.2.1. Grid Operations (GO) Framework

Grid operations models are often customized to specific regions or applications due to higher computational intensity requirements (Oikonomou et al., 2022), and balancing model fidelity (i.e., accuracy) with computational burden (i.e., model runtime) has become a major challenge for power system researchers (Frysztacki et al., 2021). We utilize a customizable framework for balancing computational speed and fidelity in interconnection-wide PCMs called GO (Akdemir, Oikonomou, Kern, Voisin, Ssembatya, et al., 2024).

Open-source GO framework utilizes BA-level data and synthetic grid topologies (Birchfield et al., 2017; Electric Grid Test Case Repository, 2017a, 2017b, 2018) created by Texas A&M University (TAMU), and allows users to create simpler representations of three U.S. interconnections to find a balance between model fidelity and runtime. Although this model is available for three interconnections of the U.S., in this study, we utilize U.S. Western Interconnection as a test bed with a sub-model of GO called GO WEST. The geographical scope of this model includes the 28 BAs located in the U.S. states of Western Interconnection, which are California, Oregon, Washington, Arizona, Colorado, Idaho, Nevada, Wyoming, Utah, Montana, and New Mexico. This area serves electricity to 80 million customers (WECC, 2017) with a

nameplate capacity of more than 258,200 MW (WECC, 2018). GO WEST is a Python-based software including a PCM module that helps researchers customize the topology with respect to their research questions/needs and simulate grid operations within the resultant topology. It makes use of a 10,000-node synthetic representation of U.S. Western Interconnection (Birchfield et al., 2017; Electric Grid Test Case Repository, 2017a). Since running a model with this complexity would entail a significant amount of time and resources, GO WEST allows researchers to alter model complexity by creating a reduced network through four user-defined parameters, which are number of nodes, mathematical formulation, transmission line capacity scaling factor and hurdle rate scaling factor.

After selecting these four model parameters and creating a reduced order representation of Western Interconnection via a network reduction algorithm, GO WEST allocates datasets to each node in the network and simulates the hourly grid operations with an embedded PCM module. PCM module consists of a Python/Pyomo-based UC/ED type model that leverages LP or MILP formulations depending on the user's choice. This module can work with both open-source solvers (e.g., HiGHS) and commercial solvers (e.g., CPLEX, Gurobi). The objective function is minimizing the total operational cost of satisfying hourly electricity demand at each node subject to several constraints such as maximum generator capacities, ramp rates, and thermal capacities of transmission lines. PCM module utilizes the DC power flow approximation and considers Kirchhoff's voltage law (KVL) and Kirchhoff's current law (KCL) during the optimization step. The temporal resolution of the PCM is hourly and has a user-defined 24-hour planning horizon.

Decision variables of the model consist of on/off status (if MILP is used) and electricity generation from each generator, voltage angle at each node, power flow on each transmission line, and unserved energy (i.e., loss of load - LOL) at each node. We placed a hypothetical generator at

each node with an extremely high marginal cost of generation (2,000 $/MWh = value of lost load (VOLL) in California Independent System Operator (CAISO) (CAISO, 2022a)). These hypothetical generators are only triggered when there is an energy imbalance due to a lack of generation capacity and/or transmission congestion at that node. The power generated from these hypothetical generators illustrates the amount of lost load at that node. Model outputs include hourly generation schedule of each generator, hourly locational marginal price (LMP) at each node, hourly unserved energy at each node, hourly voltage angles at each node, and hourly power flow on each transmission line.

Schedule and dispatch decisions of thermal generators like natural gas rely on several factors such as fuel prices, heat rates, variable operation and maintenance (O&M cost), and technical generator constraints. GO framework considers nuclear power plants as a must-run resource except when there is a forced or planned generator outage. Alternatively, renewable generators such as wind and solar are modeled differently. For historical years, hourly generation for each BA from EIA-930 dataset (EIA, 2022b) is allocated to each node as a potential generation. For future years, reV model determines the hourly solar and wind profiles, which are multiplied by the capacity of solar and wind generators to come up with hourly potential generation. Then, PCM decides how much potential renewable generation to dispatch depending on the grid conditions. That means, even though the marginal cost of renewable generators is minimal, PCM might decide to curtail renewables if needed. Lastly, daily maximum, hourly maximum, and hourly minimum hydropower generation targets are created by utilizing EIA-923 dataset (EIA, 2022a) and downscaling based on USGS flows (Turner et al., 2022). These hydropower targets are fed into PCM and dispatched according to the grid conditions. For more detailed information about

GO framework and PCM component, please refer to (Akdemir, Oikonomou, Kern, Voisin, Ssembatya, et al., 2024).

4.2.2. Transmission Expansion Planning (TEP) Model

We developed a TEP model for this study to determine the thermal capacity additions to existing transmission lines. No new transmission lines are added to the system, leaving the reduced network topology preserved. Our TEP model is an LP model and can be solved with both open-source and commercial solvers. For both GO and TEP models, Gurobi is used as the solver in this paper.

The objective function of the TEP model is to minimize the total cost of the system which comprises the operational cost of satisfying electricity demand (i.e., generation cost), cost of loss of load (i.e., unserved energy), cost of power flow, and cost of new transmission capacity additions (i.e., capital/investment cost). The model formulation, including objective function and constraints, can be seen below.

Indices and Sets

$g = Generators$

$n = Nodes$

$l = Transmission\ lines$

$t = Demand\ periods\ [months\ of\ the\ year]$

$s(l) = Sending\ end\ node\ of\ transmission\ line\ l$

$r(l) = Receiving\ end\ node\ of\ transmission\ line\ l$

$g(n) = Generators\ located\ at\ node\ n$

Parameters

$\alpha_t = Duration\ of\ demand\ periods\ [hours]$

$F_{g,t} = Fuel\ price\ for\ generator\ g\ in\ demand\ period\ t\ [\$/MMBtu]$

$HR_g = Heat\ rate\ of\ generator\ g\ [MMBtu/MWh]$

$OM_g = Variable\ operation\ and\ maintenance\ cost\ of\ generator\ g\ [\$/MWh]$

$C = Cost\ of\ unserved\ energy\ [10000\ \$/MWh]$

$L_l = Length\ of\ transmission\ line\ l\ [miles]$

$K_l = Annualized\ investment\ cost\ for\ line\ b\ [\$/MW - mile]$

$U = Negligible\ cost\ of\ renewable\ generation\ and\ power\ flow\ on\ transmission\ lines\ [0.01\ \$/MWh]$

$GC_g = Maximum\ capacity\ of\ generator\ g\ [MW]$

$R_l = Reactance\ of\ transmission\ line\ l\ [ohms]$

$D_{n,t} = Demand\ at\ node\ n\ in\ demand\ period\ t\ [MWh]$

$ES_{n,t} = Maximum\ available\ solar\ generation\ at\ node\ n\ in\ demand\ period\ t\ [MWh]$

$EW_{n,t} = Maximum\ available\ wind\ generation\ at\ node\ n\ in\ demand\ period\ t\ [MWh]$

$EOF_{n,t} = Maximum\ available\ offshore\ wind\ generation\ at\ node\ n\ in\ demand\ period\ t\ [MWh]$

$EH_{n,t} = Maximum\ available\ hydro\ generation\ at\ node\ n\ in\ demand\ period\ t\ [MWh]$

$MH_{n,t} = Minimum\ required\ hydro\ generation\ at\ node\ n\ in\ demand\ period\ t\ [MWh]$

$EN_{n,t} = Maximum\ available\ nuclear\ generation\ at\ node\ n\ in\ demand\ period\ t\ [MWh]$

$I_l = Initial\ thermal\ capacity\ of\ transmission\ line\ l\ [MW]$

$TB = Yearly\ transmission\ investment\ budget\ [\$]$

Variables

$P_{g,t} = Power\ generation\ from\ thermal\ generator\ g\ in\ demand\ period\ t\ [MWh]$

$PV_{n,t} = Solar\ power\ generation\ at\ node\ n\ in\ demand\ period\ t\ [MWh]$

$W_{n,t} = Wind\ power\ generation\ at\ node\ n\ in\ demand\ period\ t\ [MWh]$

$OF_{n,t} = Offshore\ wind\ power\ generation\ at\ node\ n\ in\ demand\ period\ t\ [MWh]$

$HY_{n,t} = Hyropower\ generation\ at\ node\ n\ in\ demand\ period\ t\ [MWh]$

$S_{n,t} = Unserved\ energy\ at\ \ node\ n\ in\ demand\ period\ t\ [MWh]$

$TC_l = New\ thermal\ capacity\ of\ transmission\ line\ l\ [MW]$

$PF_{l,t} = Actual\ flow\ on\ transmission\ line\ l\ in\ demand\ period\ t\ [MWh]$

$DF_{l,t} = Dummy\ flow\ (absolute\ value\ of\ PF_{l,t})on\ transmission\ line\ l\ in\ demand\ period\ t\ [MWh]$

$\theta_{n,t} = Voltage\ angle\ at\ node\ n\ in\ demand\ period\ t\ [°]$

Objective Function

$$min\left(\sum_{t}\alpha_t\left[\sum_{g}P_{g,t}\left(F_{g,t}HR_g+OM_g\right)+\sum_{n}\left(S_{n,t}C+U(PV_{n,t}+W_{n,t}+OF_{n,t}+HY_{n,t})\right)+\sum_{l}DF_{l,t}U\right]+\sum_{l}(TC_l-I_l)L_lK_l\right) \quad (1)$$

Constraints

$$0 \le P_{g,t} \le GC_g \qquad (\forall g, \forall t) \quad (2)$$

$$0 \le PV_{n,t} \le ES_{n,t} \qquad (\forall n, \forall t) \quad (3)$$

$$0 \le W_{n,t} \le EW_{n,t} \qquad (\forall n, \forall t) \quad (4)$$

$$0 \le OF_{n,t} \le EOF_{n,t} \qquad (\forall n, \forall t) \quad (5)$$

$$MH_{n,t} \le HY_{n,t} \le EH_{n,t} \qquad (\forall n, \forall t) \quad (6)$$

$$\theta_{n,t} = 0 \quad (n: Reference\ bus, \forall t) \quad (7)$$

$$-180 \le \theta_{n,t} \le 180 \qquad (\forall n, \forall t) \quad (8)$$

$$PF_{l,t} = (\theta_{s(l),t} - \theta_{r(l),t})/R_l \qquad (\forall l, \forall t) \quad (9)$$

$$-TC_l \le PF_{l,t} \le TC_l \qquad (\forall l, \forall t) \quad (10)$$

$$-PF_{l,t} \le DF_{l,t} \le PF_{l,t} \qquad (\forall l, \forall t) \quad (11)$$

$$I_l \le TC_l \qquad (\forall l) \quad (12)$$

$$D_{n,t} = S_{n,t} + PV_{n,t} + W_{n,t} + OF_{n,t} + HY_{n,t} + EN_{n,t} + \sum_{g \in g(n)} P_{g,t} + \sum_{l \in r(l)=n} PF_{l,t} - \sum_{l \in s(l)=n} PF_{l,t} \qquad (\forall n, \forall t) \quad (13)$$

$$\sum_{l}(TC_l - I_l)L_lK_l \le TB \quad (14)$$

Constraint (2) designates the maximum and minimum capacity limit of generators whereas (3), (4), (5) and (6) designates the maximum and minimum generation from solar, wind, offshore wind and hydropower generators. Moreover, (7) and (8) define the voltage angle of the reference

bus and upper/lower limits of voltage angles, respectively. (9) calculates the power flow on transmission lines by utilizing DC power flow approximation (i.e., KVL). (10) restricts power flow to be smaller than thermal line capacity. Constraint (11) allows us to linearize the absolute value function and find the absolute value of flow variable (i.e., dummy flow). We created a dummy flow variable to prevent unserved energy from transmitting between nodes, which was observed in a 3-bus reference network. In order to preclude this behavior, a minor cost for transmitting electricity (0.01 $/MWh) is enforced. (12) ensures that optimized transmission line capacity should be higher than the initial (i.e., default) transmission line capacity. Furthermore, (13) illustrates the power balance (i.e., KCL) for each node. Lastly, (14) limits the transmission investments with a specific yearly budget.

For TEP decisions, we utilize 12-time steps representing the conditions of 12-months of the year. In this way, we prevent overinvestment in transmission lines by not assuming just a single highest-demand hour in a year. We assume that electricity demand is the highest total net hourly demand (i.e., demand-solar/wind generation) within Western Interconnection each month. In addition, we assumed nuclear as a must-run resource. On the other hand, TEP process assumes monthly average fuel prices for each generator and monthly hydropower generation during each month. Available solar and wind power values are gathered at the selected hour for the electricity demand each month. Lastly, we feed the model with the investment cost of new transmission capacity additions from (DeSantis et al., 2021), which considers length-dependent piecewise cost curves for AC and DC transmission lines.

4.2.3. Supporting Models

Here, we provide the details of the supporting models, which are GCAM, TELL, CERF, and reV.

4.2.3.1. Global Change Analysis Model (GCAM)

GCAM (Calvin et al., 2019) is a dynamic recursive, partial equilibrium model that captures supply and demand interactions within global energy, water, land, and emissions markets, driven by factors such as socioeconomic development, climate change, and technological advancement. GCAM delineates various economic scales by dividing the world into 32 geopolitical regions, 235 water basins, and 384 agro-ecological land use regions. In this study, we use GCAM-USA v5.3 (Binsted et al., 2022), which further enhances details by subdividing the U.S. into 51 state-level regions. The refined detail improves the representation of state-specific socioeconomic changes, multi-scale energy transformation processes, and final energy services for U.S. end-users. GCAM-USA seeks market equilibrium by balancing supply and demand in each market at a 5-year time step, with state-level markets connected to the global market for primary energy carriers and agriculture.

GCAM-USA provides a comprehensive representation of the energy system, covering various details of energy production, transformation, and consumption at both national and state levels. Additionally, GCAM-USA considers inter-state electricity trade, regionally distinct fuel prices, and detailed end-use sectors including industry, buildings, and transportation. GCAM-USA provides a detailed analysis of electric capacity, load profiles, dispatch strategies, and technology evolution at both state and electricity grid region levels (Binsted et al., 2022). The electric power sector model in GCAM-USA distinguishes between long-term capacity expansion decisions and short-term dispatching strategies to meet electricity demands at sub-annual intervals. Electric power capacity investment decisions are made across four investment segments, including baseload, intermediate, subpeak, and peak electricity. Capacity investment in each segment is estimated based on a non-linear logit function considering technological competition and levelized

cost, as well as existing stock and retirements. The total electricity capacity investment minimizes the probability of electricity shortages by ensuring adequate capacity meets electricity demands across dispatch segments, with a 15% reserve margin over peak annual electricity demand (Wise et al., 2019).

4.2.3.2. Total ELectricity Loads Model (TELL)

Hourly load profiles for each BA come from TELL model (McGrath et al., 2022; *TELL Documentation*, 2023). TELL is an open-source Python package that takes hourly population-weighted meteorology time series for each BA and predicts the hourly total electricity demand in response. TELL is a machine-learning-based model that trains a unique multilayered perceptron (MLP) model for each BA. The model was trained on historical total loads from 2016-2018 from the EIA-930 dataset (EIA, 2022b). In addition to the meteorological variables (temperature, humidity, shortwave radiation, longwave radiation, and surface wind speed), TELL also uses the time of day, day of the week, and federal holidays as predictive variables.

The unique meteorology forcing in this experiment is described in (Jones et al., 2022, 2023), which was processed to the county and then BA-scale as documented in (Burleyson, Thurber, et al., 2023b, 2023a). Loads grow over time in response to population and other socioeconomic drivers that are not captured by the TELL MLP models. To capture these effects, the raw output from the TELL MLP models is scaled so that TELL loads match the annual total loads for each state as simulated by the GCAM-USA model which does capture population and socioeconomic impacts on loads. Details of this coupling approach are provided in (McGrath et al., 2022).

4.2.3.3. Capacity Expansion Regional Feasibility Model (CERF)

CERF model (C. Vernon et al., 2021), is an open-source geospatial power plant siting model that downscales regional capacity expansion plans to evaluate the evolution of the power plant landscape over time. The model identifies feasible, location-specific sites for both renewable and non-renewable technologies. By integrating detailed geospatial suitability data with an economic algorithm, CERF selects optimal plant locations based on factors like grid interconnection costs and the locational marginal value of new generation. Considering dynamic factors such as protected lands, population density, existing infrastructure, and water availability, CERF serves as a form of "ground-truthing" to both ensure the viability of broader expansion planning models and depict the evolution of the power plant landscape under various climate, socioeconomic, technological, and policy scenarios.

CERF operates at a geospatial resolution of 1 km². Drawing on geospatially referenced suitability criteria (C. R. Vernon et al., 2023), CERF considers constraints common to all power plants, like avoiding protected areas, as well as technology-specific constraints, such as minimum mean annual streamflow for thermoelectric cooling water, solar irradiance, and wind speeds. The model combines these constraints to identify suitable 1 km² grid cells for each technology type. The economic algorithm then determines individual power plant locations through a competitive process, considering technology-specific costs for connecting to the nearest substation and gas pipeline (if necessary), along with the technology-specific value of new generation in that location based on locational marginal prices.

4.2.3.4. Renewable Energy Potential Model (reV)

reV is a tool for modeling a variety of aspects of renewable energy systems including generation, capacity, and economics (Buster et al., 2023; Maclaurin et al., 2021). For the

simulation of renewable generation, reV uses models that are part of the System Advisor Model (SAM) (*System Advisor Model*, 2023). Specifically, for wind generation the model is called windpower (Freeman et al., 2014) and for solar generation the model is called pvwatts (Dobos, 2014).

reV requires several meteorological variables as inputs. For wind, the variables include temperature, pressure, wind direction, and wind speed at the hub height of the turbine. For solar, these include temperature, solar irradiance, pressure, and wind speed all at or near the surface. These variables were derived from the Thermodynamic Global Warming (TGW) dataset, a dynamically downscaled meteorological dataset available at $1/8^{th}$ degree over the continental US (Jones et al., 2023). Several preprocessing steps were required to produce all the necessary wind and solar input variables from the raw meteorological data. For example, the wind data needs to be vertically interpolated to the required hub heights, and the solar irradiance needs to be broken into its component pieces of global horizontal, diffuse normal, and direct normal irradiance. Full details of the meteorological data preprocessing are described in (Campbell et al., 2024).

4.3. Experimental Design

In this chapter, we describe our experimental design, including the different modeling scenarios used to quantify differences between the costs and benefits of individual, intermediate, and cooperative TEP to withstand future heat waves (see Table 8).

Table 8: Experimental setup showing the scenario parameters and scenario names.

Year	Climate Change Scenario	Transmission Expansion Type	Heat Wave Scale
2019	Historical	Default Line Limits (Base)	Local
			Widespread
		Individual TEP	Local
			Widespread
		Intermediate TEP	Local
			Widespread
		Cooperative TEP	Local
			Widespread
2059	RCP4.5 Hotter_SSP3	Individual TEP	Local
			Widespread
		Intermediate TEP	Local
			Widespread
		Cooperative TEP	Local
			Widespread

We selected two heat waves between 2015 and 2019 by analyzing the 2-meter temperatures and electricity demands between 1980-2019 for Western Interconnection BAs (Burleyson, Khan, et al., 2023; Burleyson, Thurber, et al., 2023a, 2023b; Jones et al., 2022). While selecting the heat waves, we calculated three different metrics: hourly BA temperature anomalies with respect to average temperature between 1980-2014, hourly Western Interconnection temperature anomalies (by calculating BA area weighted temperature anomalies) with respect to average temperature between 1980-2014 to assess the geographical coverage of the heat waves and hourly cooling degree days (CDD) for each BA to assess the severity of the heat waves. We have analyzed these metrics to make sure the selected heat waves have led to extreme temperatures for at least 3 consecutive days. Furthermore, we made sure that the hourly demands during widespread heat wave are higher than hourly demands during local heat wave. Considering all of these together, we selected one local and one widespread heat wave. The peak temperatures as well as demand profiles throughout these heat waves are shown in Figure 25. The selected local heat wave occurred

between June 9-11, 2019 (National Weather Service, 2019), and the widespread heat wave occurred between August 4-6, 2019 (NASA, 2019).

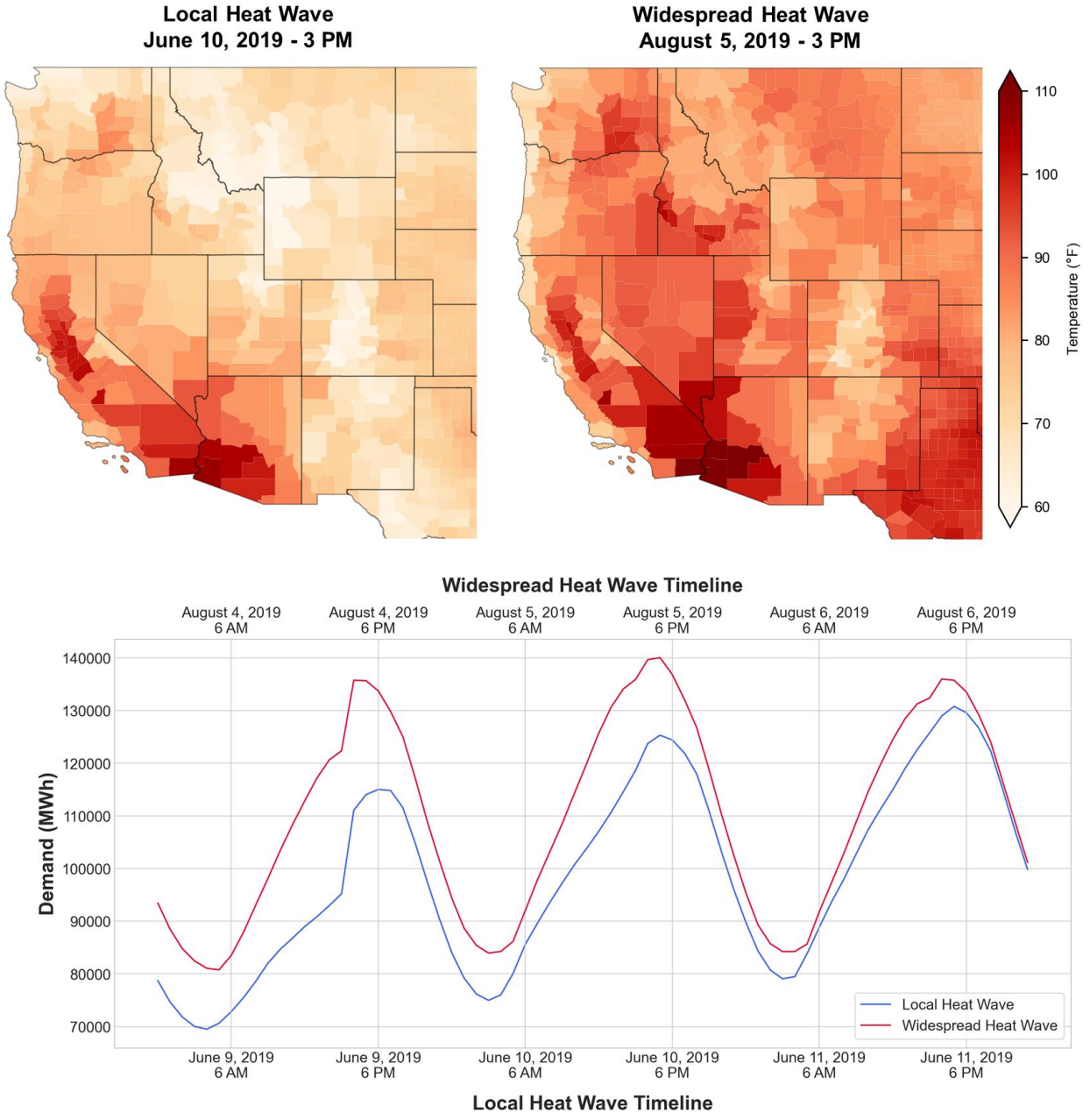

Figure 25: (Top left) Peak hourly temperature distribution during local heat wave; (top right) peak hourly temperature distribution during widespread heat wave; (bottom) total electricity demand time series during both heat waves for the Western Interconnection.

Using the GO framework, we selected a PCM version with 125 nodes, an LP formulation, +500 MW transmission line limit scaling factor, and a -100% hurdle rate scaling factor, since these parameters gave the best results in terms of matching historical LMPs and generation mix throughout Western Interconnection in the original GO parameter sweep experiment (Akdemir, Oikonomou, Kern, Voisin, Ssembatya, et al., 2024). Utilized GO WEST topology including 125 nodes and three transmission planning regions (TPRs) in the Western Interconnection (California Independent System Operator (CAISO), WestConnect, and NorthernGrid (FERC, 2021)) are shown in Figure 26.

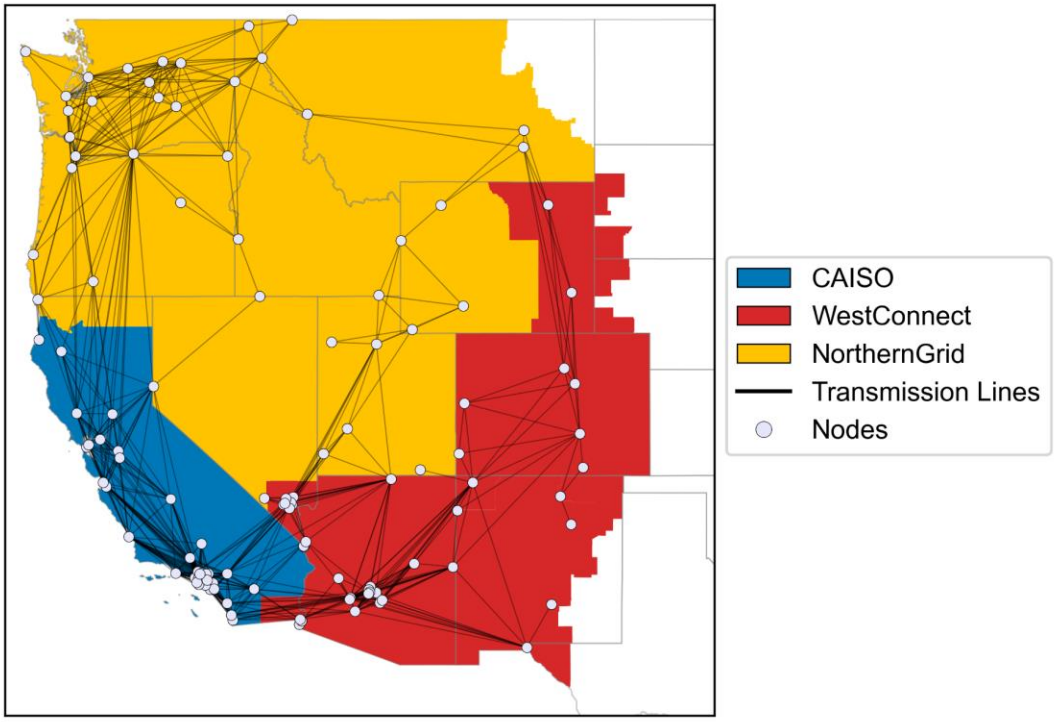

Figure 26: 125 nodes topology of GO WEST and TPRs in the Western Interconnection.

For the historical runs (i.e., heat waves in 2019), we use the 2015 power system infrastructure (i.e., generators and transmission lines) and fuel prices, but 2019 demand and solar/wind values. In the historical base case, we have used current transmission line capacities

(i.e., default 2015 values from GO framework) and simulated the grid operations under these conditions.

In order to model the cooperative TEP scenario, we ran the TEP model for each candidate transmission line to minimize the cost of grid operations and capital costs of transmission capacity additions throughout Western Interconnection. With the new transmission line capacities, we simulated historical cooperative TEP scenario. For the intermediate TEP scenario, we applied a +200% penalty (i.e., increased cost of building transmission capacity) to the lines crossing boundaries of TPRs. In this way, TEP model is discouraged (but not prohibited) from increasing transmission line capacities of the lines between any two TPRs (which resemble institutional hurdles). For individual TEP scenario, we enforced an extreme interregional transmission line investment cost penalty to prohibit increasing transmission line capacities between any two TPRs completely.

The reason for selecting +200% cost penalty for intermediate TEP scenario is that it provides a middle point for interregional transmission expansion. We did a sensitivity analysis on selecting different interregional cost penalties on transmission line buildouts (see Figure 45, Figure 46, Figure 47, Figure 48 and Figure 49 in Appendix B). When investments are analyzed between 2015 and 2020, 33.58% of all transmission investments are interregional in cooperative TEP scenario (i.e., 0% interregional cost penalty). On the other hand, 0% of all transmission investments are interregional in individual TEP scenario. When we enforce +200% penalty, the share of interregional transmission expansion is 15.68%, which is close to the middle point between 0% and 33.58% interregional investment shares from individual and cooperative TEP scenarios, respectively.

For future runs (i.e., heat waves in 2059), we assume the 2055 power system infrastructure (i.e., generators and transmission lines) and fuel prices, but 2059 demand and solar/wind values. We selected a climate change projection that represents a plausible future of U.S Western Interconnection: RCP4.5Hotter_SSP3. The origin of this scenario is TGW datasets (Jones et al., 2022) and projections of hourly meteorology by BA based on TGW datasets (Burleyson, Thurber, et al., 2023a). For more information about how TGW data is created, please refer to (Jones et al., 2023).

We run the models in an iterative fashion (i.e., GCAM-GO-CERF-TEP iteration) to create 2055 power system infrastructure. This iterative simulation process is an effort to mimic the actual decision-making on generator investments by considering the grid conditions (e.g., nodal LMPs) 5-years into the future and determining where to site new generators accordingly. Electricity demand and wind/solar generation profiles are modeled with TELL and reV, respectively. GCAM is key in providing generation capacity expansion, new generator costs, and fuel prices at state scale. CERF sites the new generators coming from GCAM in each state by considering various suitability layers.

Since transmission infrastructure will have changed by 2055, we make use of TEP model to come up with individual, intermediate, and cooperative transmission line capacities at every 5-year time step. No future TEP case (i.e., keeping transmission capacities constant by 2055) is out of scope of this paper and not considered because it would not be realistic as significant transmission investments are expected for the future due to decarbonization efforts (Kasam-Griffith et al., 2020; Konstantelos & Strbac, 2018; Sepulveda et al., 2018; Strbac et al., 2014).

For the future individual, intermediate, and cooperative TEP scenarios, we run the TEP model for each candidate transmission line to minimize the cost of grid operations and capital costs

of transmission capacity additions, similar to the historical runs explained above. In this study, future individual, intermediate, and cooperative TEP approaches persist throughout the experiment (up until 2055) and do not affect each other. Therefore, there are three independent branches to represent individual vs. intermediate vs. cooperative TEP scenarios.

In order to provide equal grounds for each TEP scenario, a yearly transmission investment budget is enforced as a constraint in TEP model. Between 2015-2020, transmission budget is determined as $4 billion/year, informed by historical investments within Western Interconnection (EIA, 2014; Pfeifenberger & Tsoukalis, 2021). This budget is raised by 20% (i.e., to $4.8 billion/year) and by 50% (i.e., to $6 billion/year) between 2020-2030 and 2030-2055, respectively to prevent underinvestment or overinvestment problems. Transmission budget outlooks are gathered from the base electrification case in (Weiss et al., 2019). Figure 27 provides an overall representation of the experimental setup.

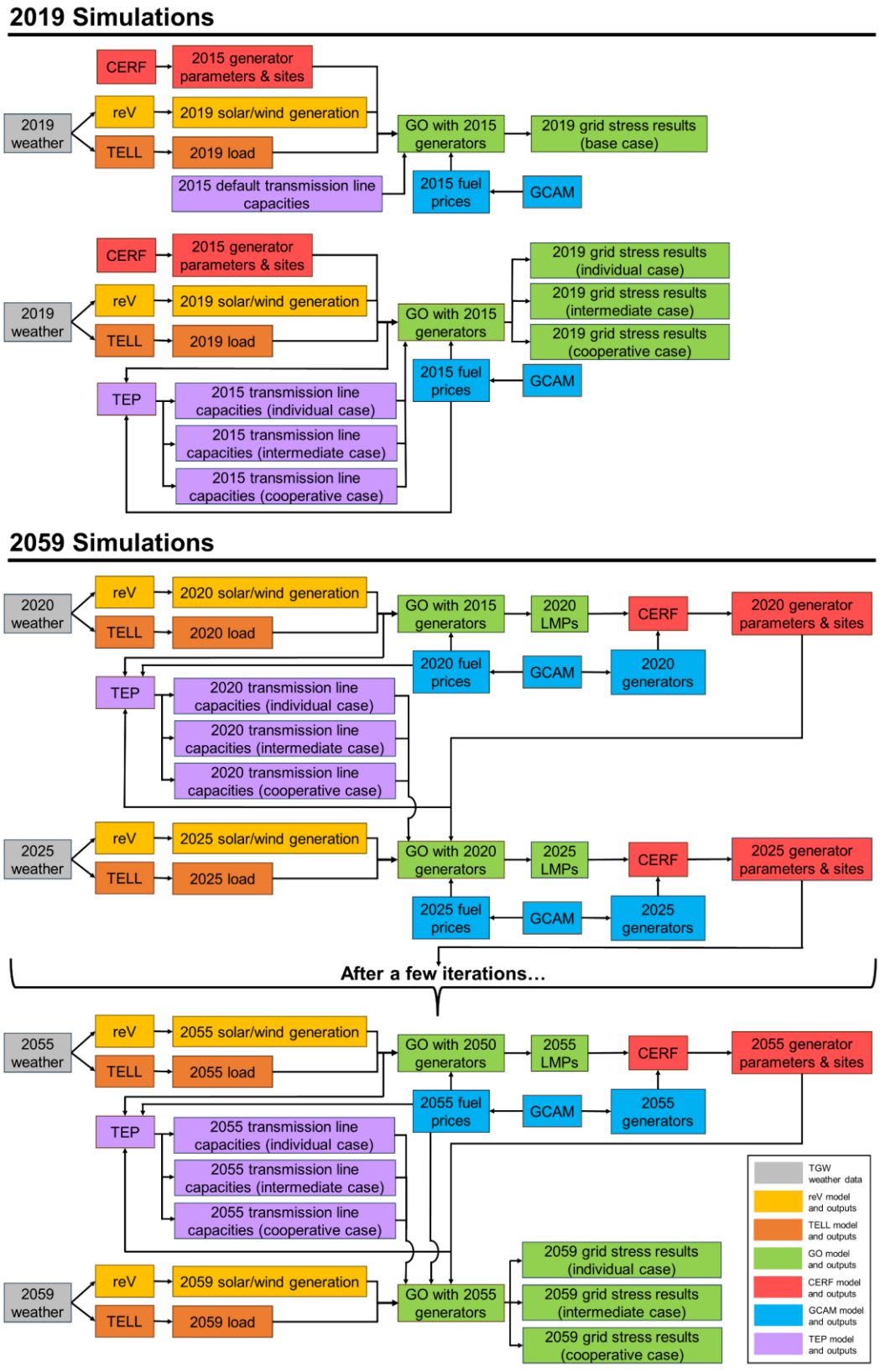

Figure 27: Flowchart of the experimental setup to simulate grid stress during 2019-2059 heat waves.

4.4. Results and Discussion

In this chapter, yearly and heat wave-specific results for 2019 are discussed first. Then, how Western Interconnection evolved under RCP4.5Hotter_SSP3 scenario is outlined. Lastly, more in-depth results on the LMPs, unserved energy, generation mix, and power flow for the whole year and during heat waves are presented for 2059.

All hourly average LMPs reported in this chapter are demand-weighted so that nodes with higher demand contribute to regional (i.e., hub) LMPs more. Moreover, although no TEP is required for 2019, we included 2019 in our analysis to show how historical grid operations could have been affected and to lay the foundation for 2059 results, which is our main focus.

4.4.1. General Results for 2019

LMPs and unserved energy are two useful metrics to understand the impact of different TEP approaches on the electricity grid. In Table 9 and Figure 28, some statistics, and distributions of LMP and unserved energy in 2019 are presented. Any type of transmission expansion in 2019 seems beneficial, especially for WestConnect. However, the impact of individual TEP on CAISO LMPs is negligible compared to base case. In general, LMPs are reduced mostly with cooperative TEP, followed by intermediate TEP and individual TEP cases. Compared to base case, throughout Western Interconnection, average LMPs are reduced by 45.31, 41.34, and 40.52 $/MWh under cooperative, intermediate, and individual TEP cases, respectively.

Furthermore, cooperative TEP benefits CAISO the most in terms of LMP reduction. In comparison to individual TEP, the marginal LMP benefit of cooperative TEP is 11.33, 0.03, and 0.36 $/MWh for CAISO, WestConnect, and NorthernGrid, respectively. Lastly, any type of TEP zeroes out the LOL to demand ratio in 2019.

Table 9: LMP and unserved energy statistics for the whole Western Interconnection and individual TPRs in 2019

Region	Scenario	Average LMP ($/MWh)	Annual LOL to Demand Ratio (%)
Western Interconnection	Base	94.55	0.35
	Cooperative	49.24	0
	Intermediate	53.21	0
	Individual	54.03	0
CAISO	Base	61.77	0
	Cooperative	50.29	0
	Intermediate	56.49	0
	Individual	61.62	0
WestConnect	Base	196.27	1.32
	Cooperative	45.38	0
	Intermediate	46.81	0
	Individual	45.41	0
NorthernGrid	Base	53.99	0
	Cooperative	51.03	0
	Intermediate	54.21	0
	Individual	51.39	0

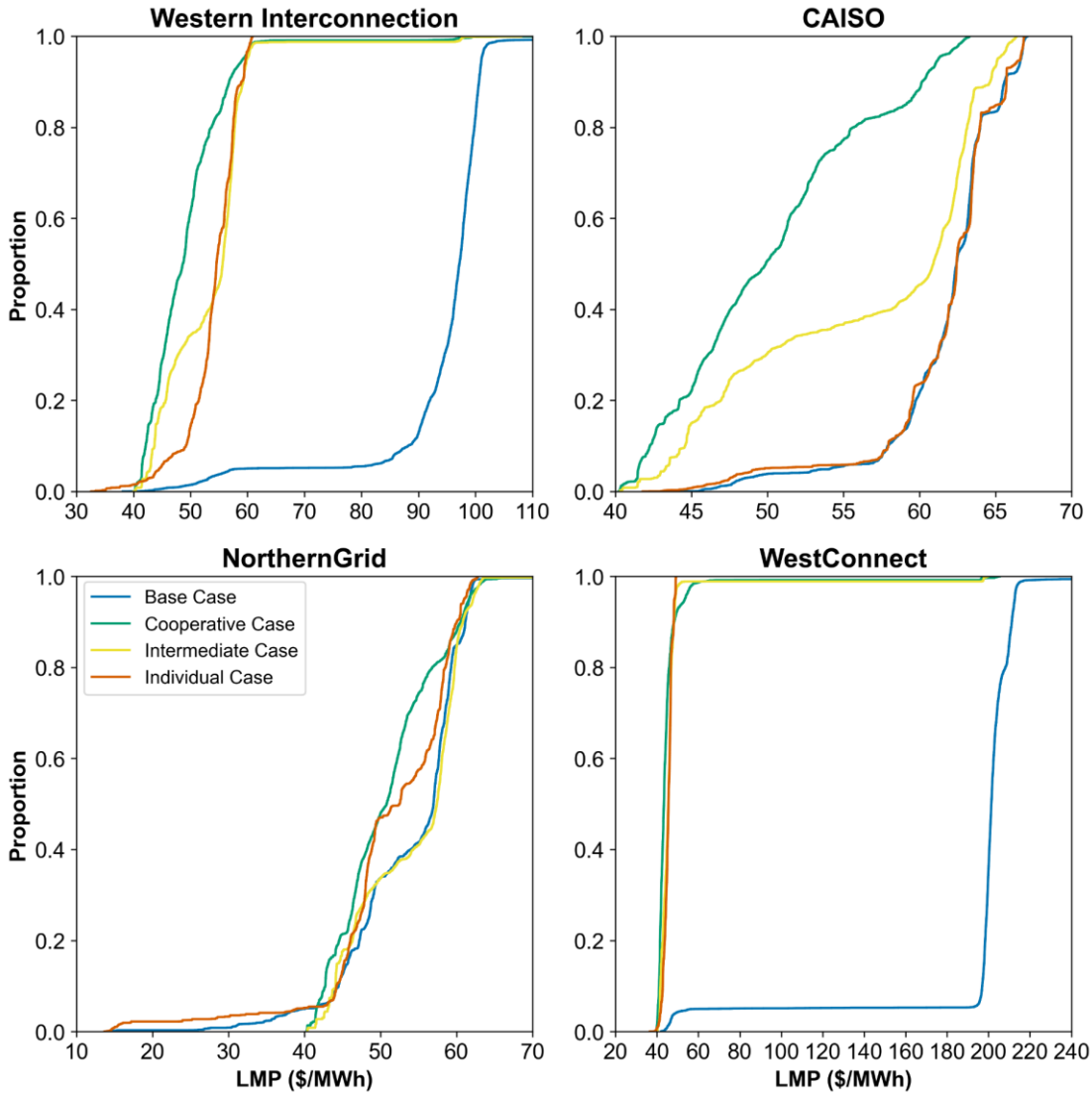

Figure 28: Hourly average LMP distributions for the whole Western Interconnection and individual TPRs in 2019.

In terms of generation mix, there are no significant changes under different TEP scenarios. More cooperative TEP approaches lead to lower utilization of coal and higher utilization of natural gas generators, but this is mostly due to increased connectivity and locational fuel price differences. On the other hand, more individualized TEP approaches cause CAISO to utilize its local generators more, limiting the amount of power imports from NorthernGrid and WestConnect (see Figure 29).

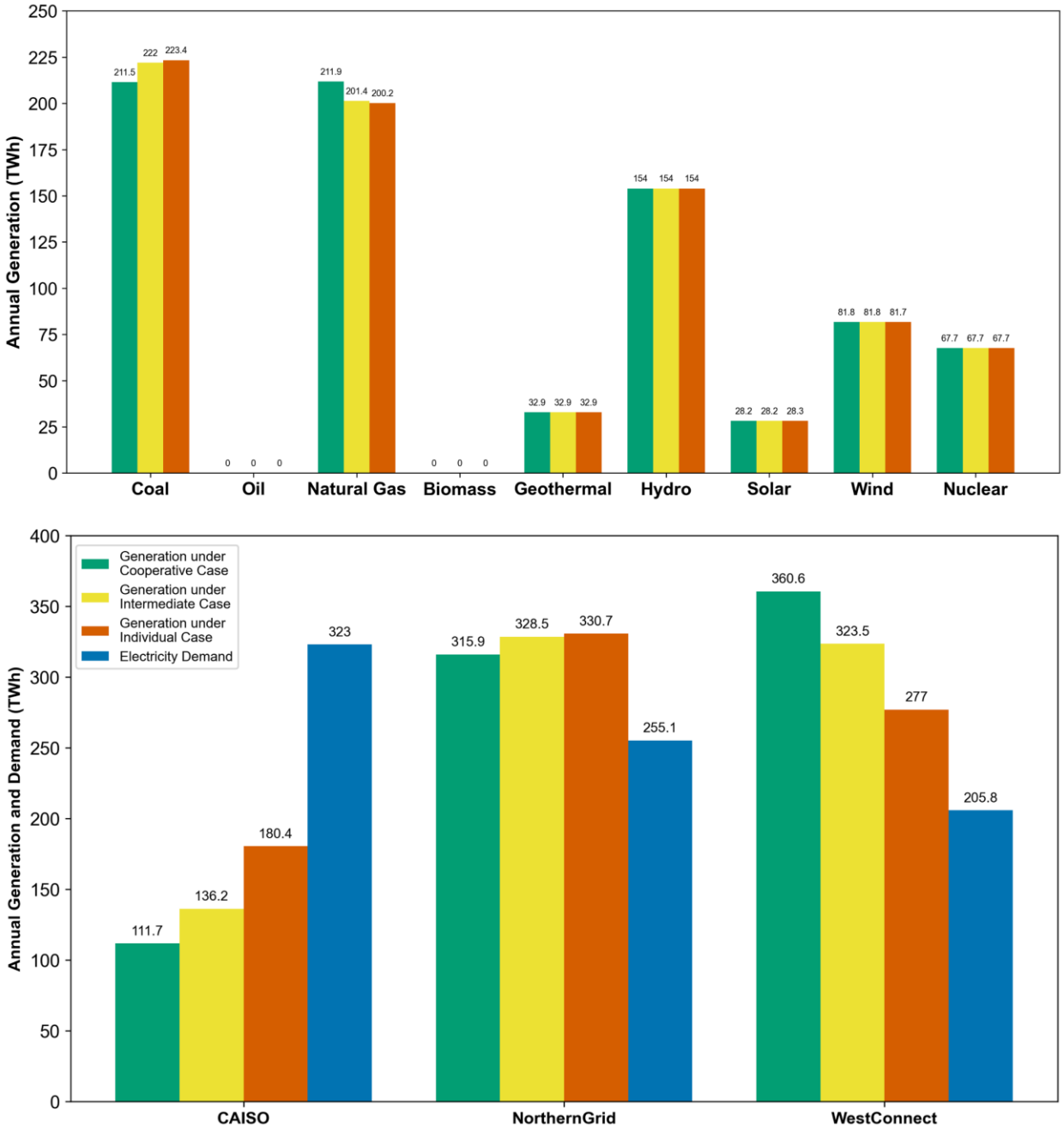

Figure 29: (Top) Total annual generation by type in Western Interconnection in 2019; (bottom) total annual generation and demand in three TPRs in 2019. Colors designate the three TEP scenarios and electricity demand.

4.4.2. Heat Wave Results for 2019

Every TEP scenario helped reduce the LMPs and zeroed out unserved energy during 2019 local heat wave. However, the extent of benefits changes among different scenarios. Throughout local heat wave, average LMPs were 79.83, 49.8, 51.69, and 52.39 $/MWh for base case,

cooperative TEP, intermediate TEP, and individual TEP, respectively. On the other hand, during 2019 widespread heat wave, average LMPs were 108.19, 59.09, 61.38, and 56.73 $/MWh for base case, cooperative TEP, intermediate TEP, and individual TEP, respectively. In addition, minor unserved energy events persist in cooperative and intermediate TEP whereas zeroed out in individual case (see Figure 30). These results suggest that though cooperative TEP is the most advantageous approach both annually and during local heat wave, the positive impacts of cooperative TEP are undermined by widespread heat waves.

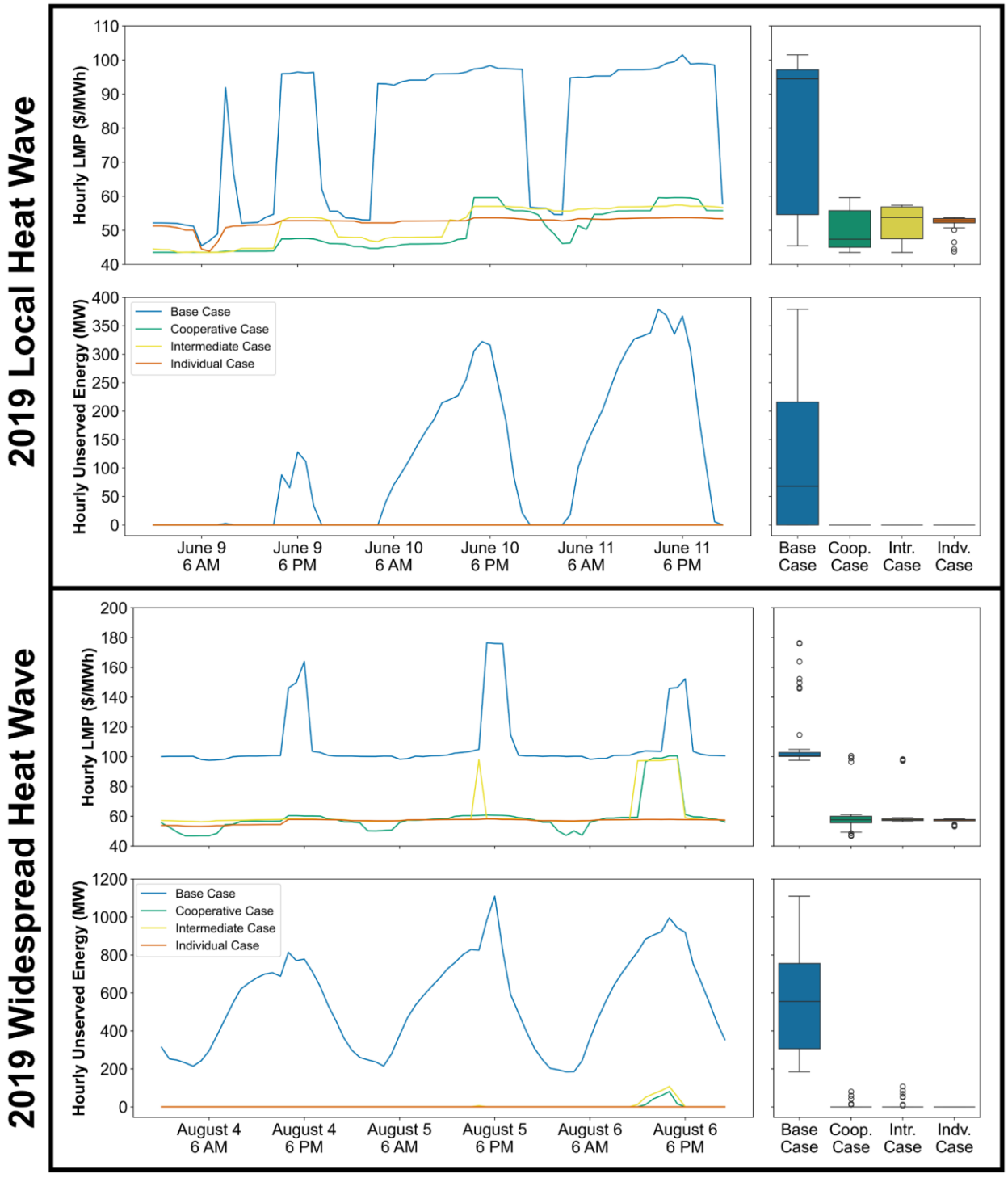

Figure 30: Time series and distribution of hourly average LMPs and total unserved energy in Western Interconnection during 2019 local and widespread heat waves.

4.4.3. Grid Transformation between 2015 and 2055

The transmission network in 2055 varies substantially depending on TEP scenarios, even though all three have the same annual investment budget (Figure 31). This divergence stems from distinct interregional transmission line investment cost penalties, which lead to better utilization of budget in cooperative TEP than intermediate TEP and individual TEP. The inability to strengthen interregional transmission lines in individual TEP caused budget leftover to some degree. In that sense, higher transmission capacity additions are observed in cooperative TEP than in individual TEP, just because cooperative TEP allows planners to build high-value interregional lines that can alleviate congestion on some regional lines.

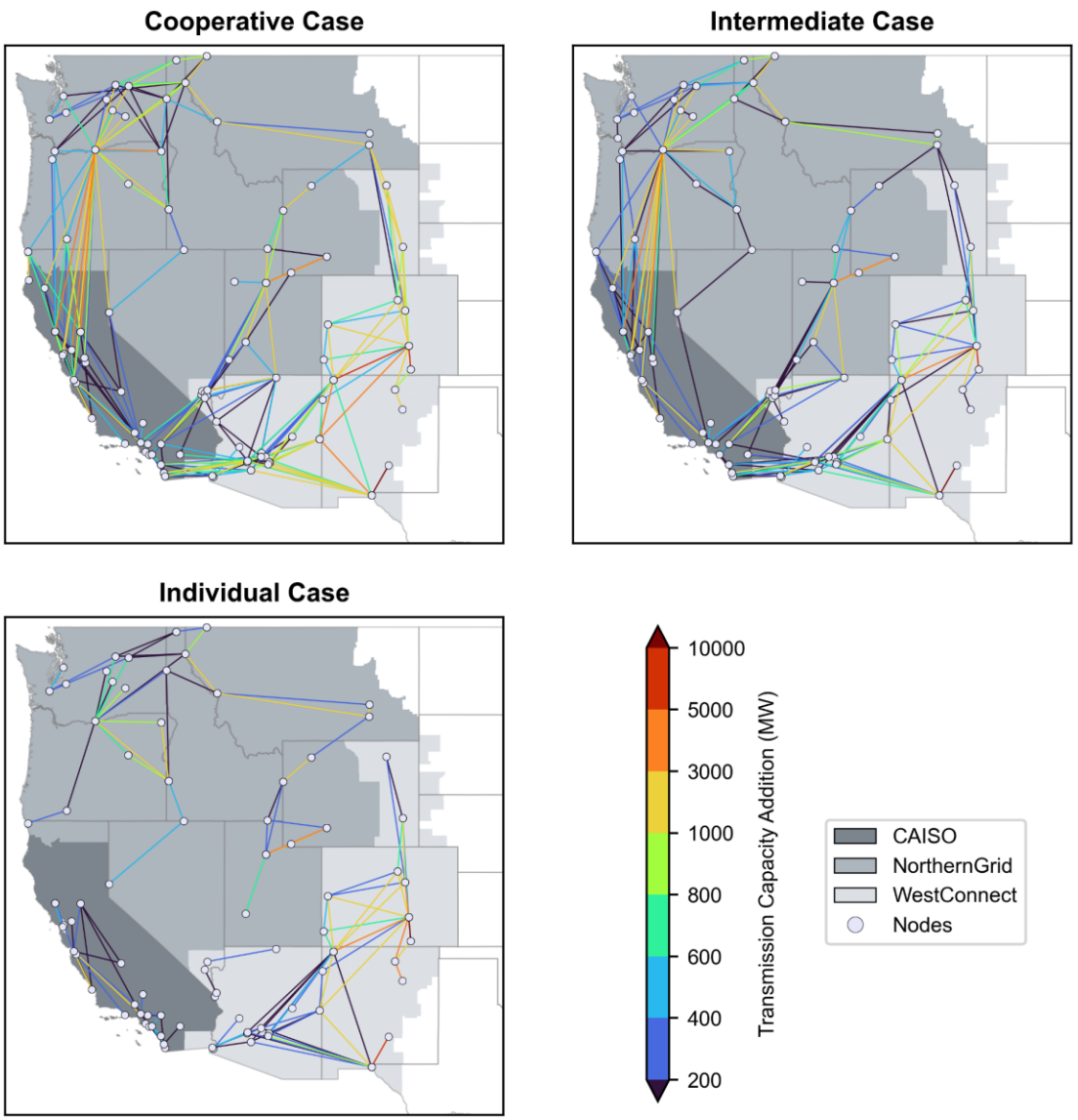

Figure 31: Transmission investment paths under cooperative, intermediate, and individual TEP scenarios. The colorbar represents the additional transmission capacity investment at each existing line.

Generator mix evolution originates from GCAM and CERF models as explained previously. Compared to 2015, there is abundant installed solar and wind capacity in 2055. Furthermore, all coal and oil capacity is retired and natural gas and nuclear capacity are reduced under RCP4.5Hotter_SSP3 scenario. Like in 2015, solar and hydropower generators are mostly

located in CAISO and NorthernGrid (i.e., Pacific Northwest), respectively. Moreover, most of the new wind generators are installed in WestConnect (see Figure 32).

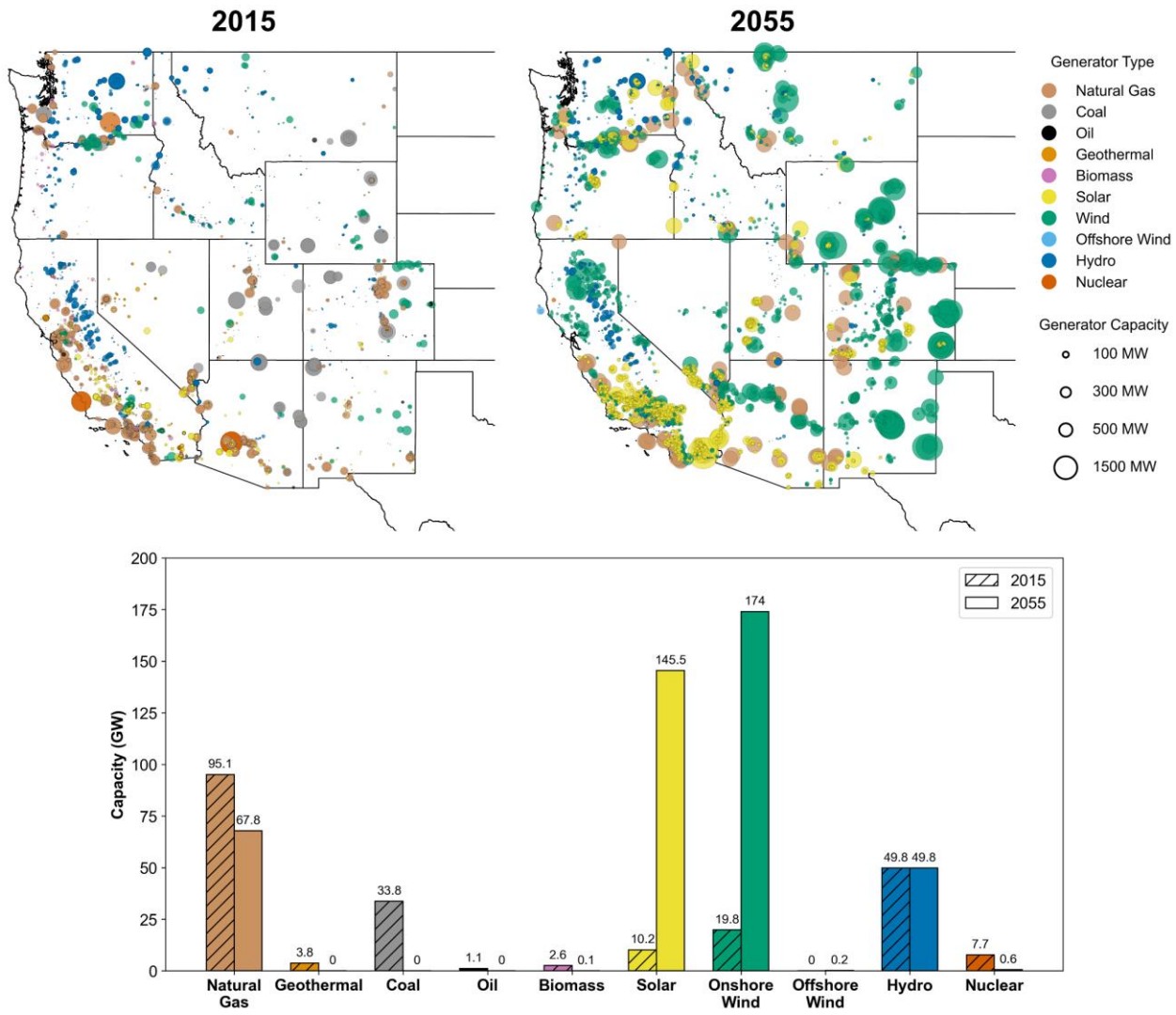

Figure 32: (Top) Individual generator locations and capacity by type in 2015 and 2055; (bottom) total generator capacity by type in 2015 and 2055.

4.4.4. General Results for 2059

When yearly LMPs and unserved energy are evaluated in 2059, we see that the lowest average LMPs are observed in cooperative TEP in the whole Western Interconnection and three TPRs. In addition, CAISO seems to take the most advantage of cooperative TEP among all TPRs. Contrasted with individual TEP, cooperative TEP leads to 244.37, 582.17, 5.95, and 8.98 $/MWh

average LMP drop in Western Interconnection, CAISO, WestConnect, NorthernGrid, respectively. Also, cooperative TEP mitigates electricity outages (i.e., unserved energy) throughout the whole interconnection in general, and primarily in CAISO. The potential benefits of cooperation in transmission expansion are much smaller in WestConnect and NorthernGrid in terms of LMP reduction and improvements (see Table 10 and Figure 33).

Table 10: LMP and unserved energy statistics for the whole Western Interconnection and individual TPRs in 2059

Region	**Scenario**	**Average LMP ($/MWh)**	**Annual LOL to Demand Ratio (%)**
Western Interconnection	Cooperative	135.82	0.15
	Intermediate	178.44	0.28
	Individual	380.19	3.06
CAISO	Cooperative	142.31	0.21
	Intermediate	193.18	0.27
	Individual	724.48	6.98
WestConnect	Cooperative	112.18	0.11
	Intermediate	125.53	0.26
	Individual	118.13	0.04
NorthernGrid	Cooperative	146.67	0.11
	Intermediate	202.49	0.32
	Individual	155.65	0.01

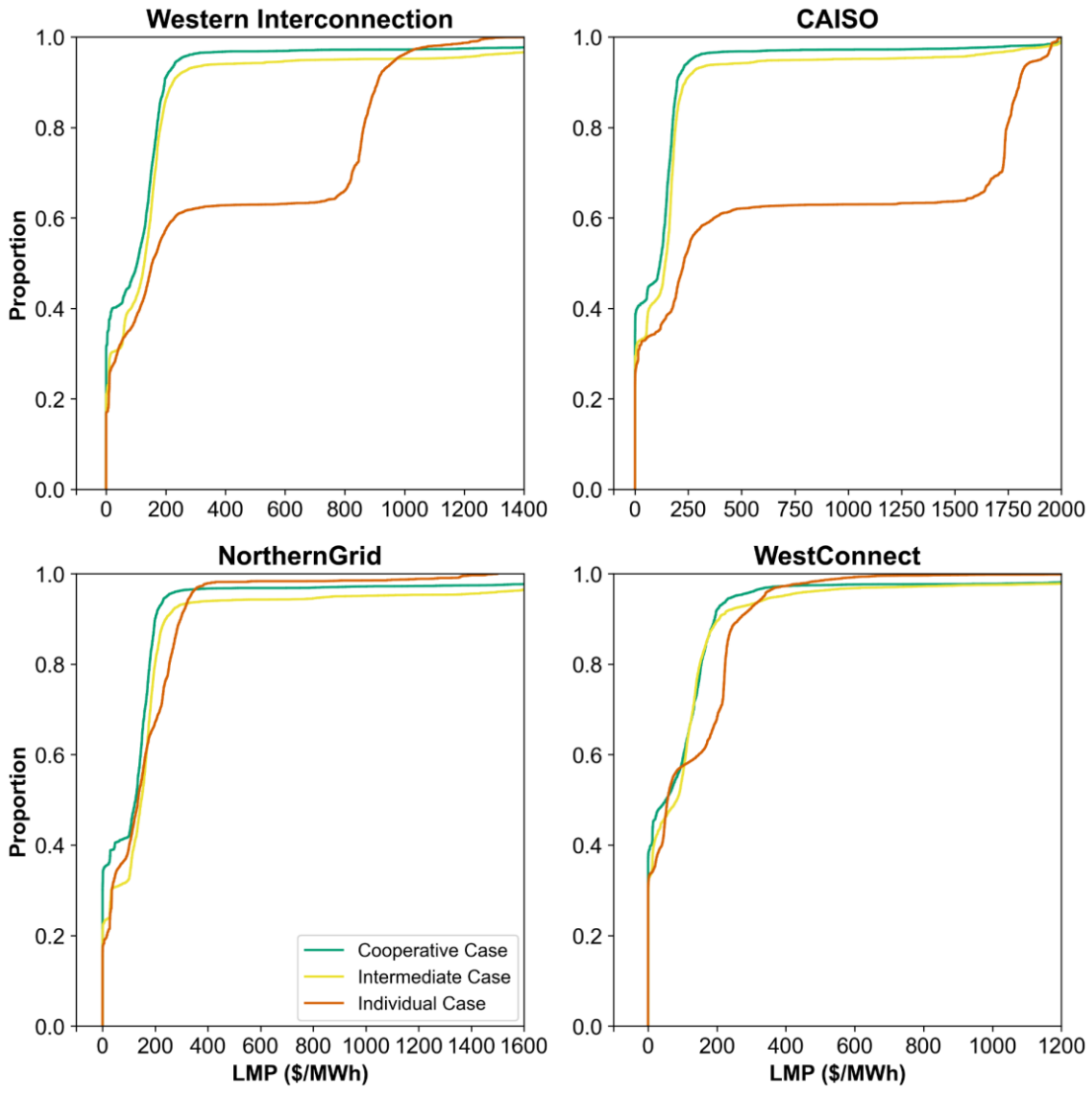

Figure 33: Hourly average LMP distributions for the whole Western Interconnection and individual TPRs in 2059.

Other than LMP and outage reduction, cooperative TEP induces lower electricity generation from fossil fuel sources like natural gas and higher generation from renewable sources like wind (see Figure 34). Higher utilization of wind power is mainly because CAISO can import more wind power from WestConnect (for separate generation mixes of three TPRs, see Figure 50, Figure 51, Figure 52, Figure 53, Figure 54, and Figure 55 in Appendix B). In this sense, a more cooperative TEP approach might aid in lowering electricity-related GHG emissions to achieve climate goals. For instance, total renewable curtailments are 23.9%, 27.7%, and 30.9% under

cooperative, intermediate, and individual TEP scenarios. Thus, cooperatively planning transmission investment supports minimizing renewable curtailments, which in turn draw down LMPs and GHG emissions.

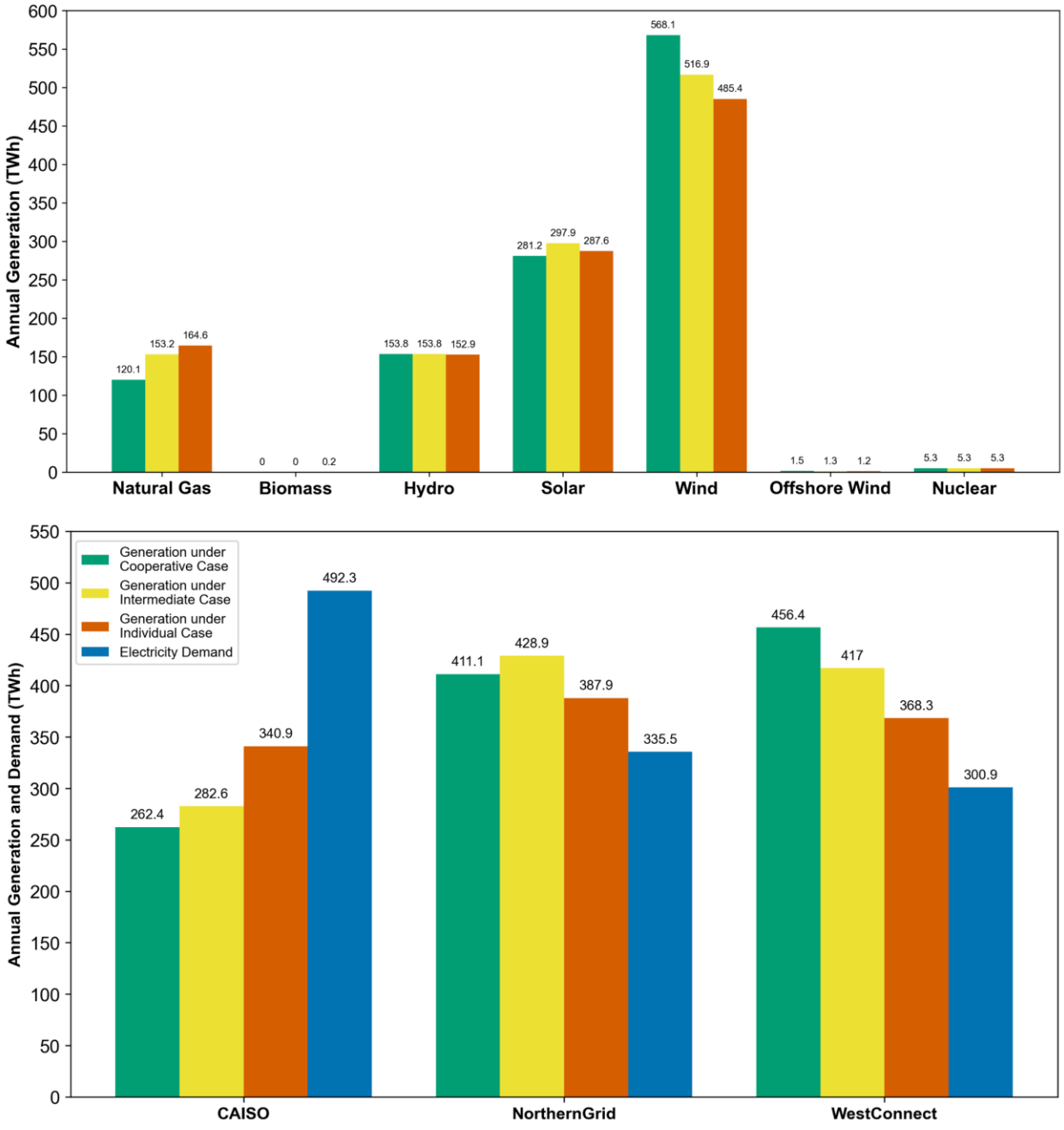

Figure 34: (Top) Total annual generation by type in Western Interconnection in 2059; (bottom) total annual generation and demand in three TPRs in 2059. Colors designate the three TEP scenarios and electricity demand.

4.4.5. Heat Wave Results for 2059

The negative impacts of the same local and widespread heat waves are more noticeable in 2059 than in 2019. Since the variable renewable energy sources dominate the power supply of the electricity grid in 2059, the grid becomes more volatile in terms of LMPs and unserved energy in the absence of electricity storage. Average interconnection-wide LMPs during 2059 local heat wave are 231.72, 300.76, and 459.26 $/MWh under cooperative, intermediate, and individual TEP scenarios, respectively. Moreover, we see significantly lower average outages in cooperative TEP (214.66 MW), followed by intermediate TEP (739.23 MW) and individual TEP scenario (10527.72 MW).

On the other hand, throughout 2059 widespread heat waves, average LMPs are 942.62, 954.07, and 671.42 $/MWh under cooperative, intermediate, and individual TEP scenarios, respectively. Even though the lowest average LMPs are observed in individual TEP scenario, median LMPs under cooperative TEP are lower (see Figure 35). Furthermore, the lowest average unserved energy is observed under cooperative TEP (4690.92 MW), in comparison to intermediate TEP (6078.53 MW) and individual TEP (13512.89 MW).

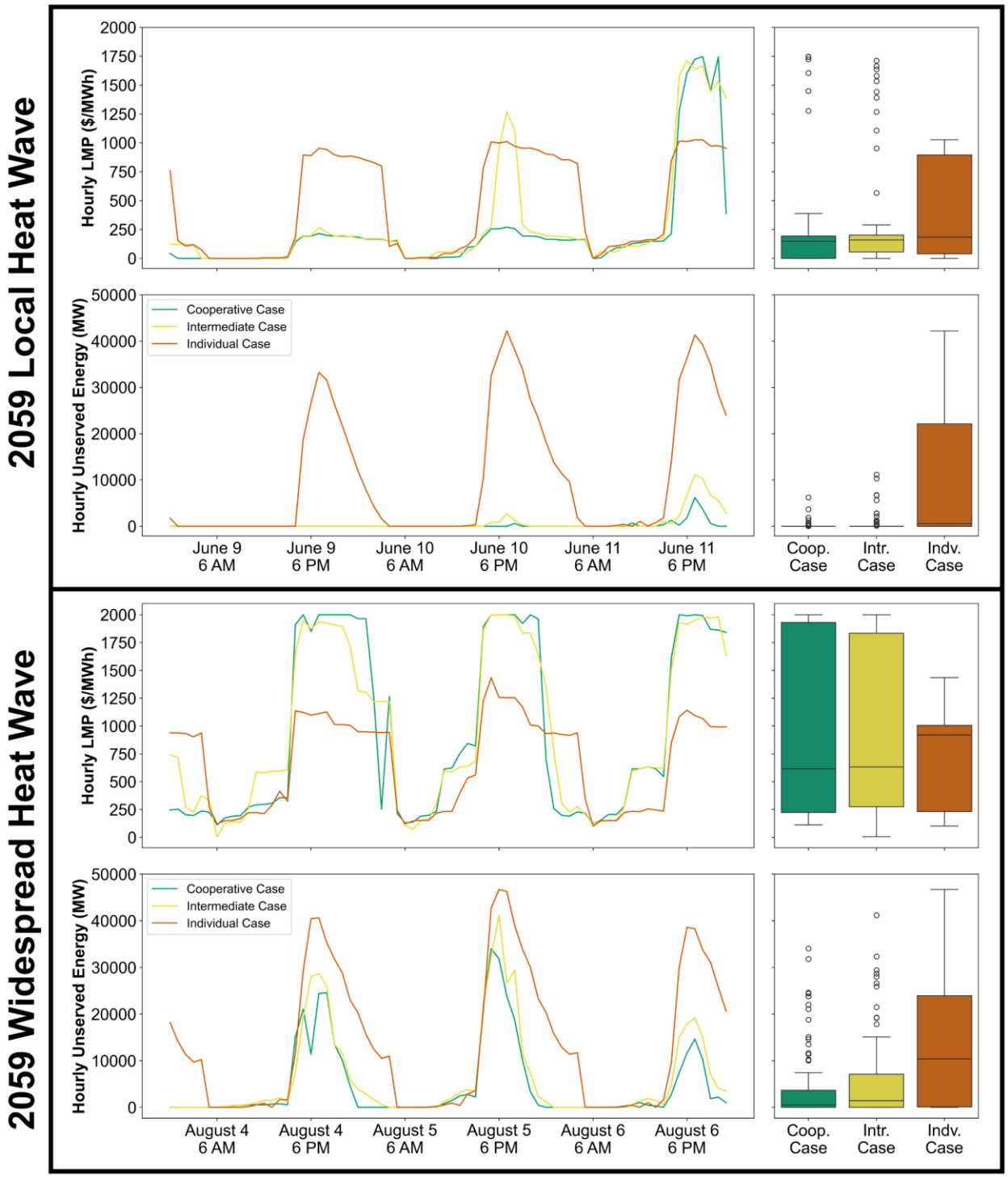

Figure 35: Time series and distribution of hourly average LMPs and total unserved energy in Western Interconnection during 2059 local and widespread heat waves.

When LMP results are investigated spatially, we see the average nodal LMPs escalate noticeably from local heat wave to widespread heat wave (Figure 36). Under both heat waves, individual planning seems more favorable for NorthernGrid and WestConnect nodes whereas cooperative planning is desperately needed for CAISO. However, even with cooperative TEP, LMPs in CAISO nodes are still too high just because of the lower availability of imports from NorthernGrid and WestConnect (see Figure 37).

The fact that CAISO reaps the most benefits of cooperative TEP can be explained by the generation mix and power exchange characteristics. As can be seen in Figure 8, CAISO has significant solar power penetration in 2059, which makes it prone to importing electricity from the other two TPRs. Since GO model does not have a representation of electricity storage for now, imports occur especially in late evening hours when available solar generation is minimal. CAISO imports a significant amount of electricity from other two TPRs throughout the year. During both heat waves, energy imports to CAISO are higher than yearly average but the other two TPRs are able to transmit less electricity during widespread heat wave than local heat wave (which affected only CAISO and southwest) due to higher grid stress. Power imports to CAISO follow the net demand trend (i.e., the famous "duck curve" (EIA, 2023)) throughout the day but the power deficit increases as we go from annual to local and widespread heat waves. There is significant renewable curtailment on an average day, but the curtailment decreases during local heat waves and nearly becomes zero during widespread heat wave due to very high demands. As CAISO can import less electricity during those less curtailment times, power deficiency peaks, and potential benefit of cooperative TEP significantly drops. We can conclude that cooperative TEP is helpful on average, but the marginal LMP benefit of cooperative TEP significantly decreases as we go from annual to local to widespread heat wave timeframes (see Figure 37).

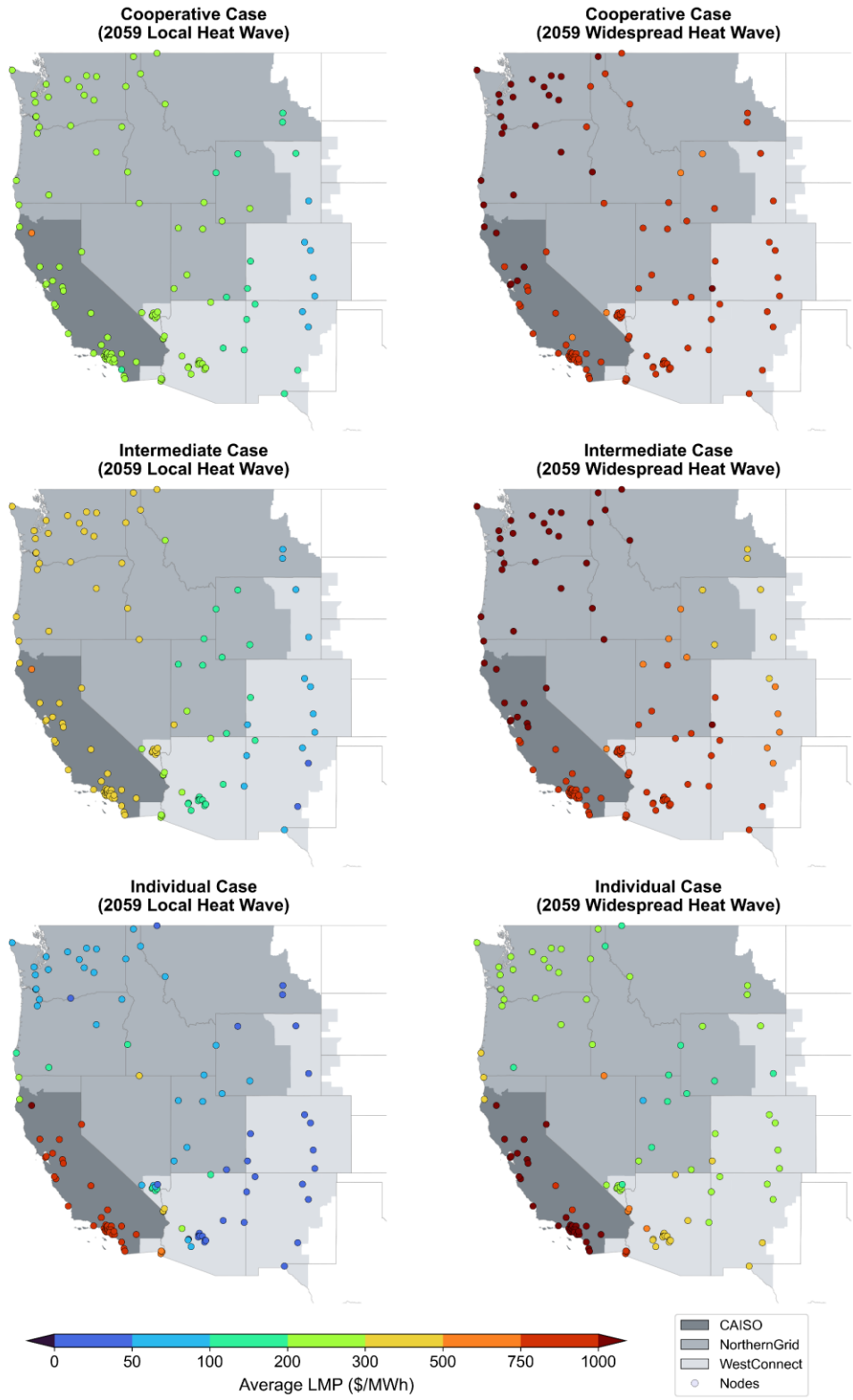

Figure 36: Map of nodal LMPs during local and widespread heat waves under different scenarios in 2059. Colors designate the hourly average LMPs throughout the heat waves.

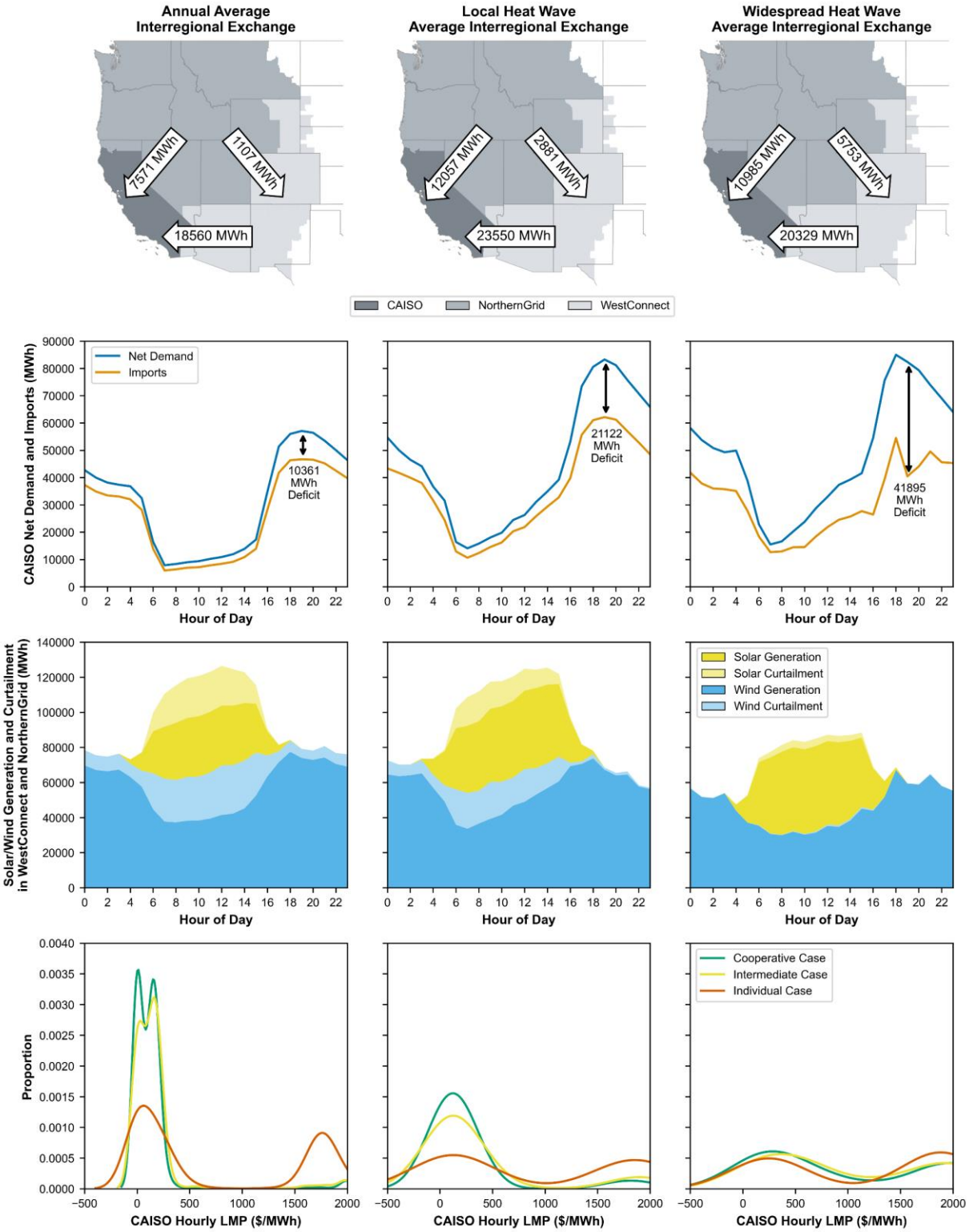

Figure 37: (Top row) Average interregional power exchanges between TPRs; (second row) hour of day profile of net demand (i.e. demand-solar/wind generation) and imports in CAISO; (third row) hour of day profile solar/wind generation/curtailment in WestConnect and NorthernGrid; (bottom row) kernel density distribution of LMPs in CAISO under three TEP cases. The left, middle, and right columns illustrate yearly, local heat wave and widespread heat wave results, respectively.

4.5. Limitations and Future Work

Though this study offers useful insights on different transmission planning approaches, it comes with some limitations that are also directions for future work. Firstly, GO model has perfect foresight, meaning that it models only day-ahead electricity market operations with no forecast errors. Incorporating real-time market with demand/renewable forecast errors would enhance the scope of questions that can be answered. Moreover, there is no electricity storage representation in GO and TEP models. Integrating energy storage investment decisions and operations into the modeling chain can provide further insight into the value of interregional cooperation. This point would also require increasing the number of investment decision periods represented in TEP model. Lastly, GO model assumes only a central operator with one objective function for the whole interconnection. Finding a way to mimic a cost-minimizing approach within each BA/TPR might be helpful in simulating individual decision-making within these zones.

4.6. Conclusion

Electricity grids are under serious transformation due to decarbonization and electrification efforts. A significant amount of new transmission line investments is anticipated to connect new generators like solar and wind power. However, there are some institutional and economic obstacles in front of building long interregional transmission lines. In this paper, we examine the impact of cooperation while making transmission expansion plans. We utilized 2019 as a base year and selected two heat waves of different spatial scales (local vs. widespread). Then, we replayed the same heatwaves in 2059 with a future representation of Western Interconnection (i.e. generators, fuel prices demand, etc.) under RCP4.5Hotter_SSP3 climate/socioeconomic scenario. We developed and used a transmission expansion planning (TEP) model to try different transmission planning approaches including a full cooperation scenario (i.e., cooperative TEP),

intermediate cooperation scenario (i.e., intermediate TEP), and no cooperation scenario (i.e., individual TEP) by imposing a varied investment cost of interregional transmission lines between three transmission planning regions in Western Interconnection.

The results suggest that cooperative TEP yields the best results in terms of LMPs and unserved energy (i.e., outage). From a yearly perspective, the lowest hourly average LMPs are observed under cooperative TEP compared to intermediate TEP and individual TEP for the whole interconnection and three regions. Moreover, Cooperative TEP helps substantially with minimizing unserved energy and decreasing greenhouse gas emissions through decreasing reliance on natural gas while reducing renewable energy curtailment and increasing wind power utilization. When results are analyzed specifically for local and widespread heat waves, we see that cooperative TEP turned out to be advantageous during local heat wave. However, since all zones are under stress to meet extreme demand due to increased cooling needs, the marginal benefit of cooperative TEP becomes very small during widespread heat waves. Although similar trends are observed in both years, the overall distinction between cooperative vs. individual TEP is more apparent in 2059. Furthermore, cooperative TEP turned out to be most favorable for CAISO as a significant amount of solar installation caused the region to import a substantial amount of electricity (mostly from wind power) from other regions to balance supply and demand, especially during late evening hours when available solar power is very minimal. Building on top of this experiment, more detailed probabilistic assessments can be used to allocate the cost of interregional lines depending on the prospective regional benefits. All in all, cooperation during transmission expansion planning is extremely useful in terms of reducing LMPs and increasing reliability by minimizing outages during future extreme weather events. Since wider-scale extreme weather events like widespread heat waves can undermine the potential benefits of cooperation to

some extent, strategic storage investments are essential. Consequently, robust optimization techniques that consider high-value periods like heat waves should be used while making decisions about the capacity and location of energy storage solutions, which would enable full utilization of the investment.

4.7. Software and Data Availability

The model is open-source and publicly available. All codes of the model and data used are available under MIT free software license (Akdemir, Kern, Oikonomou, & Voisin, 2024; Akdemir, Oikonomou, Kern, Voisin, Mongird, et al., 2024). All model outputs utilized in this study are available under Creative Commons Attribution 4.0 International license (Akdemir, Mongird, Kern, Oikonomou, et al., 2024a). Also, a meta-repository with the workflow and visualization scripts for the whole experiment is available under BSD 2-Clause license (Akdemir, Mongird, Kern, Oikonomou, et al., 2024b).

REFERENCES

Akdemir, K. Z., Kern, J. D., & Lamontagne, J. (2022). Assessing risks for New England's wholesale electricity market from wind power losses during extreme winter storms. *Energy*, *251*, 123886. https://doi.org/10.1016/j.energy.2022.123886

Akdemir, K. Z., Kern, J., Oikonomou, K., & Voisin, N. (2024). *keremakdemir/Transmission_Expansion_Planner: TEP v1.0.0* (v1.0.0) [Computer software]. https://doi.org/10.5281/ZENODO.11003185

Akdemir, K. Z., Konstantinos, O., Kern, J. D., & Bhattacharya, S. (2023). *GO WEST MRE Impacts*. https://github.com/keremakdemir/GO_WEST_MRE_Impacts/tree/Selective_line_scaling

Akdemir, K. Z., Mongird, K., Kern, J., Oikonomou, K., Voisin, N., Burleyson, C., Rice, J., Zhao, M., Bracken, C., & Vernon, C. (2024a). *Cooperative Transmission Expansion Planning Experiment Data and Results* [dataset]. MSD-LIVE. https://doi.org/10.57931/2338087

Akdemir, K. Z., Mongird, K., Kern, J., Oikonomou, K., Voisin, N., Burleyson, C., Rice, J., Zhao, M., Bracken, C., & Vernon, C. (2024b, April 25). *Akdemir-etal_2024_applied_energy*. https://github.com/IMMM-SFA/akdemir-etal_2024_applied_energy

Akdemir, K. Z., Oikonomou, K., Kern, J. D., & Voisin, N. (2023a). *IM3 GO WEST Parameter Search Dataset* [dataset]. MSD-LIVE. https://doi.org/10.57931/1923267

Akdemir, K. Z., Oikonomou, K., Kern, J. D., Voisin, N., Ssembatya, H., & Qian, J. (2024). An open-source framework for balancing computational speed and fidelity in production cost models. *Environmental Research: Energy*, *1*(1), 015003. https://doi.org/10.1088/2753-3751/ad1751

Akdemir, K. Z., Oikonomou, K., Kern, J., & Voisin, N. (2023b). *GO-WEST v1.0.0* (v1.0.0) [Computer software]. Zenodo. https://doi.org/10.5281/ZENODO.10067714

Akdemir, K. Z., Oikonomou, K., Kern, J., Voisin, N., Mongird, K., Burleyson, C., Rice, J., Vernon, C., Zhao, M., & Bracken, C. (2024). *GO-WEST v1.1.0* (v1.1.0) [Computer software]. https://doi.org/10.5281/ZENODO.11003229

Akdemir, K. Z., Robertson, B., Oikonomou, K., Kern, J., Voisin, N., Hanif, S., & Bhattacharya, S. (2023). Opportunities for wave energy in bulk power system operations. *Applied Energy*, 121845. https://doi.org/10.1016/j.apenergy.2023.121845

Al-Saba, T., & El-Amin, I. (2002). The application of artificial intelligent tools to the transmission expansion problem. *Electric Power Systems Research*, *62*(2), 117–126. https://doi.org/10.1016/S0378-7796(02)00037-8

Americans for a Clean Energy Grid. (2023). *Transmission Planning and Development Regional Report Card*. https://www.cleanenergygrid.org/wp-content/uploads/2023/06/ACEG_Transmission_Planning_and_Development_Report_Card.pdf

Antenucci, A., Crespo del Granado, P., Gjorgiev, B., & Sansavini, G. (2019). Can models for long-term decarbonization policies guarantee security of power supply? A perspective from gas and power sector coupling. *Energy Strategy Reviews*, *26*, 100410. https://doi.org/10.1016/j.esr.2019.100410

Arabzadeh, V., Mikkola, J., Jasiūnas, J., & Lund, P. D. (2020). Deep decarbonization of urban energy systems through renewable energy and sector-coupling flexibility strategies. *Journal of Environmental Management*, *260*, 110090. https://doi.org/10.1016/j.jenvman.2020.110090

Armstrong, S., Cotilla-Sanchez, E., & Kovaltchouk, T. (2015). Assessing the Impact of the Grid-Connected Pacific Marine Energy Center Wave Farm. *IEEE Journal of Emerging and Selected Topics in Power Electronics*, *3*(4), 1011–1020. https://doi.org/10.1109/JESTPE.2015.2429577

Bahiense, L., Oliveira, G. C., Pereira, M., & Granville, S. (2001). A mixed integer disjunctive model for transmission network expansion. *IEEE Transactions on Power Systems*, *16*(3), 560–565. https://doi.org/10.1109/59.932295

Barstow, S., Mørk, G., Mollison, D., & Cruz, J. (2008). The Wave Energy Resource. In J. Cruz (Ed.), *Ocean Wave Energy* (pp. 93–132). Springer Berlin Heidelberg. https://doi.org/10.1007/978-3-540-74895-3_4

Behboodi, S., Chassin, D. P., Djilali, N., & Crawford, C. (2017). Interconnection-wide hour-ahead scheduling in the presence of intermittent renewables and demand response: A surplus maximizing approach. *Applied Energy*, *189*, 336–351. https://doi.org/10.1016/j.apenergy.2016.12.052

Bhattacharya, S., Pennock, S., Robertson, B., Hanif, S., Alam, M. J. E., Bhatnagar, D., Preziuso, D., & O'Neil, R. (2021). Timing value of marine renewable energy resources for potential grid applications. *Applied Energy*, *299*, 117281. https://doi.org/10.1016/j.apenergy.2021.117281

Biener, W., & Garcia Rosas, K. R. (2020). Grid reduction for energy system analysis. *Electric Power Systems Research*, *185*, 106349. https://doi.org/10.1016/j.epsr.2020.106349

Binsted, M., Iyer, G., Patel, P., Graham, N. T., Ou, Y., Khan, Z., Kholod, N., Narayan, K., Hejazi, M., Kim, S., Calvin, K., & Wise, M. (2022). GCAM-USA v5.3_water_dispatch: Integrated modeling of subnational US energy, water, and land systems within a global

framework. *Geoscientific Model Development*, *15*(6), 2533–2559. https://doi.org/10.5194/gmd-15-2533-2022

Birchfield, A. B., Xu, T., Gegner, K. M., Shetye, K. S., & Overbye, T. J. (2017). Grid Structural Characteristics as Validation Criteria for Synthetic Networks. *IEEE Transactions on Power Systems*, *32*(4), 3258–3265. https://doi.org/10.1109/TPWRS.2016.2616385

Bistline, J. E. T. (2021). The importance of temporal resolution in modeling deep decarbonization of the electric power sector. *Environmental Research Letters*, *16*(8), 084005. https://doi.org/10.1088/1748-9326/ac10df

Booij, N., Holthuijsen, L. H., & Ris, R. C. (1997). The "Swan" Wave Model for Shallow Water. *Coastal Engineering 1996*, 668–676. https://doi.org/10.1061/9780784402429.053

Brouwer, A. S., van den Broek, M., Zappa, W., Turkenburg, W. C., & Faaij, A. (2016). Least-cost options for integrating intermittent renewables in low-carbon power systems. *Applied Energy*, *161*, 48–74. https://doi.org/10.1016/j.apenergy.2015.09.090

Brown, T., Hörsch, J., & Schlachtberger, D. (2018). PyPSA: Python for Power System Analysis. *Journal of Open Research Software*, *6*(1), 4. https://doi.org/10.5334/jors.188

Burleyson, C., Khan, Z., Kulshresta, M., Voisin, N., & Rice, J. (2023). *Hourly Electricity Demand Projections for Eight Combined Climate and Socioeconomic Scenarios* [dataset]. MultiSector Dynamics - Living, Intuitive, Value-adding, Environment. https://doi.org/10.57931/2228460

Burleyson, C., Thurber, T., & Vernon, C. (2023a). *Projections of Hourly Meteorology by Balancing Authority Based on the IM3/HyperFACETS Thermodynamic Global Warming (TGW) Simulations* [dataset]. MultiSector Dynamics - Living, Intuitive, Value-adding, Environment. https://doi.org/10.57931/1960530

Burleyson, C., Thurber, T., & Vernon, C. (2023b). *Projections of Hourly Meteorology by County Based on the IM3/HyperFACETS Thermodynamic Global Warming (TGW) Simulations* [dataset]. MultiSector Dynamics - Living, Intuitive, Value-adding, Environment. https://doi.org/10.57931/1960548

Buster, G., Rossol, M., Pinchuk, P., Benton, B. N., Spencer, R., Bannister, M., & Williams, T. (2023). *NREL/reV: reV 0.8.0* (v0.8.0) [Computer software]. [object Object]. https://doi.org/10.5281/ZENODO.8247528

Buygi, M. O., Balzer, G., Shanechi, H. M., & Shahidehpour, M. (2004). Market-Based Transmission Expansion Planning. *IEEE Transactions on Power Systems*, *19*(4), 2060–2067. https://doi.org/10.1109/TPWRS.2004.836252

Cadini, F., Zio, E., & Petrescu, C. A. (2010). Optimal expansion of an existing electrical power transmission network by multi-objective genetic algorithms. *Reliability Engineering & System Safety*, *95*(3), 173–181. https://doi.org/10.1016/j.ress.2009.09.007

CAISO. (2021). *Final Root Cause Analysis: Mid-August 2020 Extreme Heat Wave*.

CAISO. (2022a). *Annual Report on Market Issues & Performance*.

CAISO. (2022b). *California ISO OASIS*. http://oasis.caiso.com/mrioasis/logon.do

Calvin, K., Dasgupta, D., Krinner, G., Mukherji, A., Thorne, P. W., Trisos, C., Romero, J., Aldunce, P., Barrett, K., Blanco, G., Cheung, W. W. L., Connors, S., Denton, F., Diongue-Niang, A., Dodman, D., Garschagen, M., Geden, O., Hayward, B., Jones, C., … Péan, C. (2023). *IPCC, 2023: Climate Change 2023: Synthesis Report. Contribution of Working Groups I, II and III to the Sixth Assessment Report of the Intergovernmental Panel on Climate Change [Core Writing Team, H. Lee and J. Romero (eds.)]. IPCC,*

Geneva, Switzerland. (First). Intergovernmental Panel on Climate Change (IPCC). https://doi.org/10.59327/IPCC/AR6-9789291691647

Calvin, K., Patel, P., Clarke, L., Asrar, G., Bond-Lamberty, B., Cui, R. Y., Di Vittorio, A., Dorheim, K., Edmonds, J., Hartin, C., Hejazi, M., Horowitz, R., Iyer, G., Kyle, P., Kim, S., Link, R., McJeon, H., Smith, S. J., Snyder, A., … Wise, M. (2019). GCAM v5.1: Representing the linkages between energy, water, land, climate, and economic systems. *Geoscientific Model Development*, *12*(2), 677–698. https://doi.org/10.5194/gmd-12-677-2019

Campbell, A., Bracken, C., Underwood, S., & Voisin, N. (2024). A Multi-Decadal Hourly Coincident Wind and Solar Power Production Dataset for the Contiguous US. *Under Review in Scientific Data*.

Choi, J., Mount, T. D., & Thomas, R. J. (2007). Transmission Expansion Planning Using Contingency Criteria. *IEEE Transactions on Power Systems*, *22*(4), 2249–2261. https://doi.org/10.1109/TPWRS.2007.908478

Cohen, S. M., Dyreson, A., Turner, S., Tidwell, V., Voisin, N., & Miara, A. (2022). A multi-model framework for assessing long- and short-term climate influences on the electric grid. *Applied Energy*, *317*, 119193. https://doi.org/10.1016/j.apenergy.2022.119193

Conejo, A. J., Baringo Morales, L., Kazempour, S. J., & Siddiqui, A. S. (2016). *Investment in Electricity Generation and Transmission*. Springer International Publishing. https://doi.org/10.1007/978-3-319-29501-5

Daraeepour, A., Patino-Echeverri, D., & Conejo, A. J. (2019). Economic and environmental implications of different approaches to hedge against wind production uncertainty in two-

settlement electricity markets: A PJM case study. *Energy Economics*, *80*, 336–354. https://doi.org/10.1016/j.eneco.2019.01.015

Dario Jaramillo, R., & Garces, A. (2015). Wave energy: Modeling and Analysis of Power Grid Integration. *IEEE Latin America Transactions*, *13*(12), 3863–3872. https://doi.org/10.1109/TLA.2015.7404920

Deane, J. P., Drayton, G., & Ó Gallachóir, B. P. (2014). The impact of sub-hourly modelling in power systems with significant levels of renewable generation. *Applied Energy*, *113*, 152–158. https://doi.org/10.1016/j.apenergy.2013.07.027

Department of Energy. (2015). *Chapter 4: Advancing Clean Electric Power Technologies* (Quadrennial Technology Review: An Assessment of Energy Technologies and Research Opportunities). https://www.energy.gov/sites/prod/files/2017/03/f34/qtr-2015-chapter4.pdf

DeSantis, D., James, B. D., Houchins, C., Saur, G., & Lyubovsky, M. (2021). Cost of long-distance energy transmission by different carriers. *iScience*, *24*(12), 103495. https://doi.org/10.1016/j.isci.2021.103495

Dobos, A. (2014). *PVWatts Version 5 Manual* (NREL/TP-6A20-62641, 1158421; p. NREL/TP-6A20-62641, 1158421). https://doi.org/10.2172/1158421

Dranka, G. G., Ferreira, P., & Vaz, A. I. F. (2021). A review of co-optimization approaches for operational and planning problems in the energy sector. *Applied Energy*, *304*, 117703. https://doi.org/10.1016/j.apenergy.2021.117703

Dyreson, A., Devineni, N., Turner, S. W. D., De Silva M, T., Miara, A., Voisin, N., Cohen, S., & Macknick, J. (2022). The Role of Regional Connections in Planning for Future Power

System Operations Under Climate Extremes. *Earth's Future*, *10*(6). https://doi.org/10.1029/2021EF002554

EIA. (2014, September 3). *Electricity transmission investments vary by region*. https://www.eia.gov/todayinenergy/detail.php?id=17811

EIA. (2019). *Pacific Northwest sees highest daily natural gas spot prices in the U.S. since 2014*. https://www.eia.gov/todayinenergy/detail.php?id=38932

EIA. (2022a). *Form EIA-923 detailed data with previous form data (EIA-906/920)*. https://www.eia.gov/electricity/data/eia923/

EIA. (2022b). *Hourly Electric Grid Monitor*. https://www.eia.gov/electricity/gridmonitor/dashboard/electric_overview/US48/US48

EIA. (2022c). *Wholesale Electricity and Natural Gas Market Data*. https://www.eia.gov/electricity/wholesale/

EIA. (2023, June 21). *As solar capacity grows, duck curves are getting deeper in California*. https://www.eia.gov/todayinenergy/detail.php?id=56880

Electric Grid Test Case Repository. (2017a). *ACTIVSg10k: 10000-bus synthetic grid on footprint of western United States*. https://electricgrids.engr.tamu.edu/electric-grid-test-cases/activsg10k/

Electric Grid Test Case Repository. (2017b). *ACTIVSg2000: 2000-bus synthetic grid on footprint of Texas*. https://electricgrids.engr.tamu.edu/electric-grid-test-cases/activsg2000/

Electric Grid Test Case Repository. (2018). *ACTIVSg70k: 70,000 bus synthetic grid on footprint of eastern United States*. https://electricgrids.engr.tamu.edu/electric-grid-test-cases/activsg70k/

Electric Grid Test Case Repository. (2022). *Texas A&M University Electric Grid Datasets*. Texas A&M University. https://electricgrids.engr.tamu.edu/

Exascale Computing Project. (2023). *EXASGD*. https://www.exascaleproject.org/research-project/exasgd/

Exposito, A. G., Ramos, J. L. M., & Santos, J. R. (2004). Slack Bus Selection to Minimize the System Power Imbalance in Load-Flow Studies. *IEEE Transactions on Power Systems*, *19*(2), 987–995. https://doi.org/10.1109/TPWRS.2004.825871

Fairley, I., Lewis, M., Robertson, B., Hemer, M., Masters, I., Horrillo-Caraballo, J., Karunarathna, H., & Reeve, D. (2020a). *Global wave resource classification and application to marine energy deployments* [Other]. pico. https://doi.org/10.5194/egusphere-egu2020-8135

Fairley, I., Lewis, M., Robertson, B., Hemer, M., Masters, I., Horrillo-Caraballo, J., Karunarathna, H., & Reeve, D. E. (2020b). A classification system for global wave energy resources based on multivariate clustering. *Applied Energy*, *262*, 114515. https://doi.org/10.1016/j.apenergy.2020.114515

Fairley, I., Smith, H. C. M., Robertson, B., Abusara, M., & Masters, I. (2017). Spatio-temporal variation in wave power and implications for electricity supply. *Renewable Energy*, *114*, 154–165. https://doi.org/10.1016/j.renene.2017.03.075

FERC. (2021, November 9). *Regions Map Printable Version Order No. 1000*. https://www.ferc.gov/media/regions-map-printable-version-order-no-1000

Freeman, J., Jorgenson, J., Gilman, P., & Ferguson, T. (2014). *Reference Manual for the System Advisor Model's Wind Power Performance Model* (NREL/TP-6A20-60570, 1150800; p. NREL/TP-6A20-60570, 1150800). https://doi.org/10.2172/1150800

Frysztacki, M. M., Hörsch, J., Hagenmeyer, V., & Brown, T. (2021). The strong effect of network resolution on electricity system models with high shares of wind and solar. *Applied Energy*, *291*, 116726. https://doi.org/10.1016/j.apenergy.2021.116726

Gacitua, L., Gallegos, P., Henriquez-Auba, R., Lorca, Á., Negrete-Pincetic, M., Olivares, D., Valenzuela, A., & Wenzel, G. (2018). A comprehensive review on expansion planning: Models and tools for energy policy analysis. *Renewable and Sustainable Energy Reviews*, *98*, 346–360. https://doi.org/10.1016/j.rser.2018.08.043

Galván, A., Haas, J., Moreno-Leiva, S., Osorio-Aravena, J. C., Nowak, W., Palma-Benke, R., & Breyer, C. (2022). Exporting sunshine: Planning South America's electricity transition with green hydrogen. *Applied Energy*, *325*, 119569. https://doi.org/10.1016/j.apenergy.2022.119569

Golombek, R., Lind, A., Ringkjøb, H.-K., & Seljom, P. (2022). The role of transmission and energy storage in European decarbonization towards 2050. *Energy*, *239*, 122159. https://doi.org/10.1016/j.energy.2021.122159

Göteman, M., Giassi, M., Engström, J., & Isberg, J. (2020). Advances and Challenges in Wave Energy Park Optimization—A Review. *Frontiers in Energy Research*, *8*, 26. https://doi.org/10.3389/fenrg.2020.00026

Guler, B., Çelebi, E., & Nathwani, J. (2021). Cost-effective decarbonization through investment in transmission interconnectors as part of regional energy hubs (REH). *The Electricity Journal*, *34*(3), 106924. https://doi.org/10.1016/j.tej.2021.106924

Halamay, D. A., Brekken, T. K. A., Simmons, A., & McArthur, S. (2011). Reserve Requirement Impacts of Large-Scale Integration of Wind, Solar, and Ocean Wave Power Generation.

IEEE Transactions on Sustainable Energy, *2*(3), 321–328. https://doi.org/10.1109/TSTE.2011.2114902

Hamid, I., Alam, M. S., Kanwal, A., Jena, P. K., Murshed, M., & Alam, R. (2022). Decarbonization pathways: The roles of foreign direct investments, governance, democracy, economic growth, and renewable energy transition. *Environmental Science and Pollution Research*, *29*(33), 49816–49831. https://doi.org/10.1007/s11356-022-18935-3

Hamilton, W. T., Husted, M. A., Newman, A. M., Braun, R. J., & Wagner, M. J. (2020). Dispatch optimization of concentrating solar power with utility-scale photovoltaics. *Optimization and Engineering*, *21*(1), 335–369. https://doi.org/10.1007/s11081-019-09449-y

Hemmati, R., Hooshmand, R.-A., & Khodabakhshian, A. (2013). State-of-the-art of transmission expansion planning: Comprehensive review. *Renewable and Sustainable Energy Reviews*, *23*, 312–319. https://doi.org/10.1016/j.rser.2013.03.015

Hill, J., Kern, J., Rupp, D. E., Voisin, N., & Characklis, G. (2021). The Effects of Climate Change on Interregional Electricity Market Dynamics on the U.S. West Coast. *Earth's Future*, *9*(12). https://doi.org/10.1029/2021EF002400

Hobbs, B. F., Kasina, S., Xu, Q., Park, S. W., Ouyang, J., Ho, J. L., & Donohoo-Vallett, P. E. (2016). What is the Benefit of Including Uncertainty in Transmission Planning? A WECC Case Study. *2016 49th Hawaii International Conference on System Sciences (HICSS)*, 2364–2371. https://doi.org/10.1109/HICSS.2016.295

Homeland Infrastructure Foundation-Level Data. (2022a). *Control Areas*. https://hifld-geoplatform.opendata.arcgis.com/datasets/geoplatform::control-areas/explore?location=39.644053%2C-112.615515%2C4.91

Homeland Infrastructure Foundation-Level Data. (2022b). *Electric Retail Service Territories*. https://hifld-geoplatform.opendata.arcgis.com/datasets/geoplatform::electric-retail-service-territories-2/explore?location=38.884462%2C-114.257812%2C5.75

Hoover, K., & Hanson, L. A. (2021). *Wildfire Statistics*. https://apps.dtic.mil/sti/pdfs/AD1143321.pdf

Ibanez, E., Magee, T., Clement, M., Brinkman, G., Milligan, M., & Zagona, E. (2014). Enhancing hydropower modeling in variable generation integration studies. *Energy*, *74*, 518–528. https://doi.org/10.1016/j.energy.2014.07.017

Iglesias, G., López, M., Carballo, R., Castro, A., Fraguela, J. A., & Frigaard, P. (2009). Wave energy potential in Galicia (NW Spain). *Renewable Energy*, *34*(11), 2323–2333. https://doi.org/10.1016/j.renene.2009.03.030

IPCC. (2022). *Global Warming of 1.5°C: IPCC Special Report on Impacts of Global Warming of 1.5°C above Pre-industrial Levels in Context of Strengthening Response to Climate Change, Sustainable Development, and Efforts to Eradicate Poverty* (1st ed.). Cambridge University Press. https://doi.org/10.1017/9781009157940

Jacobson, P. T., Hagerman, G., & Scott, G. (2011). *Mapping and Assessment of the United States Ocean Wave Energy Resource* (DOE/GO/18173-1, 1060943; p. DOE/GO/18173-1, 1060943). https://doi.org/10.2172/1060943

Jiang, Z., Tong, N., Liu, Y., Xue, Y., & Tarditi, A. G. (2020). Enhanced dynamic equivalent identification method of large-scale power systems using multiple events. *Electric Power Systems Research*, *189*, 106569. https://doi.org/10.1016/j.epsr.2020.106569

Jin, S., Zheng, S., & Greaves, D. (2022). On the scalability of wave energy converters. *Ocean Engineering*, *243*, 110212. https://doi.org/10.1016/j.oceaneng.2021.110212

Johnson, B., & Cotilla-Sanchez, E. (2020). Estimating the impact of ocean wave energy on power system reliability with a well-being approach. *IET Renewable Power Generation*, *14*(4), 608–615. https://doi.org/10.1049/iet-rpg.2019.0567

Jones, A. D., Rastogi, D., Vahmani, P., Stansfield, A. M., Reed, K. A., Thurber, T., Ullrich, P. A., & Rice, J. S. (2023). Continental United States climate projections based on thermodynamic modification of historical weather. *Scientific Data*, *10*(1), 664. https://doi.org/10.1038/s41597-023-02485-5

Jones, A. D., Rastogi, D., Vahmani, P., Stansfield, A., Reed, K., Thurber, T., Ullrich, P., & Rice, J. S. (2022). *IM3/HyperFACETS Thermodynamic Global Warming (TGW) Simulation Datasets* [dataset]. MultiSector Dynamics - Living, Intuitive, Value-adding, Environment. https://doi.org/10.57931/1885756

Jorgenson, J., Denholm, P., & Mai, T. (2018). Analyzing storage for wind integration in a transmission-constrained power system. *Applied Energy*, *228*, 122–129. https://doi.org/10.1016/j.apenergy.2018.06.046

Kasam-Griffith, A., Turkmani, N., Wolf, M., Peluso, N., & Green, T. (2020). Transmission transition: Modernizing U.S. transmission planning to support decarbonization. *MIT Science Policy Review*, *1*, 87–91. https://doi.org/10.38105/spr.udjlliebw0

Kasina, S., & Hobbs, B. F. (2020). The value of cooperation in interregional transmission planning: A noncooperative equilibrium model approach. *European Journal of Operational Research*, *285*(2), 740–752. https://doi.org/10.1016/j.ejor.2020.02.018

Kirschen, D. S., & Strbac, G. (2018). *Fundamentals of Power System Economics*. John Wiley & Sons, Inc. https://www.wiley.com/en-us/Fundamentals+of+Power+System+Economics%2C+2nd+Edition-p-9781119213253

Konstantelos, I., & Strbac, G. (2018). The role of storage in transmission investment deferral and management of future planning uncertainty. In A. F. Zobaa, P. F. Ribeiro, S. H. Aleem, & S. N. Afifi (Eds.), *Energy Storage at Different Voltage Levels: Technology, integration, and market aspects* (pp. 113–145). Institution of Engineering and Technology. https://doi.org/10.1049/PBPO111E_ch5

Krishnan, V., Ho, J., Hobbs, B. F., Liu, A. L., McCalley, J. D., Shahidehpour, M., & Zheng, Q. P. (2016). Co-optimization of electricity transmission and generation resources for planning and policy analysis: Review of concepts and modeling approaches. *Energy Systems*, *7*(2), 297–332. https://doi.org/10.1007/s12667-015-0158-4

Kundur, P. S., & Malik, O. P. (2022). *Power System Stability and Control*. McGraw Hill. https://www.mhprofessional.com/power-system-stability-and-control-second-edition-9781260473544-usa

Lane, J. L., Smart, S., Schmeda-Lopez, D., Hoegh-Guldberg, O., Garnett, A., Greig, C., & McFarland, E. (2016). Understanding constraints to the transformation rate of global energy infrastructure. *WIREs Energy and Environment*, *5*(1), 33–48. https://doi.org/10.1002/wene.177

Lara, J. D., Lee, J. T., Callaway, D. S., & Hodge, B.-M. (2020). Computational experiment design for operations model simulation. *Electric Power Systems Research*, *189*, 106680. https://doi.org/10.1016/j.epsr.2020.106680

LaRocca, S., Johansson, J., Hassel, H., & Guikema, S. (2015). Topological Performance Measures as Surrogates for Physical Flow Models for Risk and Vulnerability Analysis for Electric Power Systems. *Risk Analysis*, *35*(4), 608–623. https://doi.org/10.1111/risa.12281

Lavidas, G., & Blok, K. (2021). Shifting wave energy perceptions: The case for wave energy converter (WEC) feasibility at milder resources. *Renewable Energy*, *170*, 1143–1155. https://doi.org/10.1016/j.renene.2021.02.041

Lawrence Berkeley National Laboratory. (2022). *Empirical Estimates of Transmission Value using Locational Marginal Prices*. https://emp.lbl.gov/publications/empirical-estimates-transmission

Lehmann, M., Karimpour, F., Goudey, C. A., Jacobson, P. T., & Alam, M.-R. (2017). Ocean wave energy in the United States: Current status and future perspectives. *Renewable and Sustainable Energy Reviews*, *74*, 1300–1313. https://doi.org/10.1016/j.rser.2016.11.101

Li, C., Conejo, A. J., Liu, P., Omell, B. P., Siirola, J. D., & Grossmann, I. E. (2022). Mixed-integer linear programming models and algorithms for generation and transmission expansion planning of power systems. *European Journal of Operational Research*, *297*(3), 1071–1082. https://doi.org/10.1016/j.ejor.2021.06.024

Liu, H., Brown, T., Andresen, G. B., Schlachtberger, D. P., & Greiner, M. (2019). The role of hydro power, storage and transmission in the decarbonization of the Chinese power system. *Applied Energy*, *239*, 1308–1321. https://doi.org/10.1016/j.apenergy.2019.02.009

Maclaurin, G., Grue, N., Lopez, A., Heimiller, D., Rossol, M., Buster, G., & Williams, T. (2021). *The Renewable Energy Potential (reV) Model: A Geospatial Platform for Technical Potential and Supply Curve Modeling* (NREL/TP--6A20-73067, 1563140, MainId:13369; p. NREL/TP--6A20-73067, 1563140, MainId:13369). https://doi.org/10.2172/1563140

Mai, T., Steinberg, D., Logan, J., Bielen, D., Eurek, K., & McMillan, C. (2018). An Electrified Future: Initial Scenarios and Future Research for U.S. Energy and Electricity Systems. *IEEE Power and Energy Magazine*, *16*(4), 34–47. https://doi.org/10.1109/MPE.2018.2820445

Matko, M., Golobič, M., & Kontič, B. (2016). Integration of extreme weather event risk assessment into spatial planning of electric power infrastructure. *Urbani Izziv*, *27*(1), 95–112. https://doi.org/10.5379/urbani-izziv-en-2016-27-01-001

Matthew, C., & Spataru, C. (2021). Scottish Islands Interconnections: Modelling the Impacts on the UK Electricity Network of Geographically Diverse Wind and Marine Energy. *Energies*, *14*(11), 3175. https://doi.org/10.3390/en14113175

McGrath, C. R., Burleyson, C. D., Khan, Z., Rahman, A., Thurber, T., Vernon, C. R., Voisin, N., & Rice, J. S. (2022). tell: A Python package to model future total electricity loads in the United States. *Journal of Open Source Software*, *7*(79), 4472. https://doi.org/10.21105/joss.04472

Mideksa, T. K., & Kallbekken, S. (2010). The impact of climate change on the electricity market: A review. *Energy Policy*, *38*(7), 3579–3585. https://doi.org/10.1016/j.enpol.2010.02.035

Moazzen, I., Robertson, B., Wild, P., Rowe, A., & Buckham, B. (2016). Impacts of large-scale wave integration into a transmission-constrained grid. *Renewable Energy*, *88*, 408–417. https://doi.org/10.1016/j.renene.2015.11.049

Munoz, F. D., Hobbs, B. F., Ho, J. L., & Kasina, S. (2014). An Engineering-Economic Approach to Transmission Planning Under Market and Regulatory Uncertainties: WECC Case Study. *IEEE Transactions on Power Systems*, *29*(1), 307–317. https://doi.org/10.1109/TPWRS.2013.2279654

Munoz, F. D., Watson, J.-P., & Hobbs, B. F. (2015). Optimizing Your Options: Extracting the Full Economic Value of Transmission When Planning Under Uncertainty. *The Electricity Journal*, *28*(5), 26–38. https://doi.org/10.1016/j.tej.2015.05.002

NASA. (2019). *American and European Heatwaves During Summer 2019*. https://gmao.gsfc.nasa.gov/research/science_snapshots/2019/Am_Euro_heatwaves-2019.php

NASA. (2023, September 27). *Vital Signs of the Planet*. https://climate.nasa.gov/

National Interagency Fire Center. (2022). *InterAgency Fire Perimeter History All Years View*. https://data-nifc.opendata.arcgis.com/datasets/nifc::interagencyfireperimeterhistory-all-years-view/explore?location=41.667952%2C-122.217971%2C8.72

National Weather Service. (2019). *Historic Heat Wave for Bay Area*. https://www.weather.gov/mtr/HeatWave_6_9-11_2019

NERC. (2022). *Generating Availability Data System (GADS)*. https://www.nerc.com/pa/RAPA/gads/Pages/GeneratingAvailabilityDataSystem-(GADS).aspx

NOAA. (2023). *Local Climatological Data Station Details: MONTAGUE SISKIYOU AIRPORT, CA US*. https://www.ncdc.noaa.gov/cdo-web/datasets/LCD/stations/WBAN:24259/detail

NREL. (2021). *Marine Energy Atlas*. https://maps.nrel.gov/marine-energy-atlas

NREL. (2022). *Sienna*. https://www.nrel.gov/analysis/sienna.html

Nsanzineza, R., O'Connell, M., Brinkman, G., & Milford, J. B. (2017). Emissions implications of downscaled electricity generation scenarios for the western United States. *Energy Policy, 109*, 601–608. https://doi.org/10.1016/j.enpol.2017.07.051

O'Connell, Voisin, N., Macknick, & Fu. (2019). Sensitivity of Western U.S. power system dynamics to droughts compounded with fuel price variability. *Applied Energy*, *247*, 745–754. https://doi.org/10.1016/j.apenergy.2019.01.156

Oh, H. (2010). A New Network Reduction Methodology for Power System Planning Studies. *IEEE Transactions on Power Systems*, *25*(2), 677–684. https://doi.org/10.1109/TPWRS.2009.2036183

Oikonomou, K., Tarroja, B., Kern, J., & Voisin, N. (2022). Core process representation in power system operational models: Gaps, challenges, and opportunities for multisector dynamics research. *Energy*, *238*, 122049. https://doi.org/10.1016/j.energy.2021.122049

O'Neill, R. P., Krall, E. A., Hedman, K. W., & Oren, S. S. (2013). A model and approach to the challenge posed by optimal power systems planning. *Mathematical Programming*, *140*(2), 239–266. https://doi.org/10.1007/s10107-013-0695-3

OpenStreetMap Foundation. (2023). *OpenStreetMap*. https://www.openstreetmap.org/

Panteli, M., & Mancarella, P. (2015). Influence of extreme weather and climate change on the resilience of power systems: Impacts and possible mitigation strategies. *Electric Power Systems Research*, *127*, 259–270. https://doi.org/10.1016/j.epsr.2015.06.012

Pennock, S., Coles, D., Angeloudis, A., Bhattacharya, S., & Jeffrey, H. (2022). Temporal complementarity of marine renewables with wind and solar generation: Implications for GB system benefits. *Applied Energy*, *319*, 119276. https://doi.org/10.1016/j.apenergy.2022.119276

Peskoe, A. (2024, February 22). *Profiteering Hampers U.S. Grid Expansion: Private utility companies are blocking new interregional transmission lines*. IEEE Spectrum. https://spectrum.ieee.org/transmission-expansion

Pfeifenberger, J., & Tsoukalis, J. (2021, June 1). *Transmission Investment Needs and Challenges*. https://www.brattle.com/wp-content/uploads/2021/10/Transmission-Investment-Needs-and-Challenges.pdf

Pleßmann, G., & Blechinger, P. (2017). How to meet EU GHG emission reduction targets? A model based decarbonization pathway for Europe's electricity supply system until 2050. *Energy Strategy Reviews*, *15*, 19–32. https://doi.org/10.1016/j.esr.2016.11.003

Rasool, S., Muttaqi, K. M., & Sutanto, D. (2020). Modelling of a wave-to-wire system for a wave farm and its response analysis against power quality and grid codes. *Renewable Energy*, *162*, 2041–2055. https://doi.org/10.1016/j.renene.2020.10.035

Reikard, G., Robertson, B., & Bidlot, J.-R. (2015). Combining wave energy with wind and solar: Short-term forecasting. *Renewable Energy*, *81*, 442–456. https://doi.org/10.1016/j.renene.2015.03.032

Reikard, G., Robertson, B., & Bidlot, J.-R. (2017). Wave energy worldwide: Simulating wave farms, forecasting, and calculating reserves. *International Journal of Marine Energy*, *17*, 156–185. https://doi.org/10.1016/j.ijome.2017.01.004

Robertson, B., Bailey, H., Leary, M., & Buckham, B. (2021). A methodology for architecture agnostic and time flexible representations of wave energy converter performance. *Applied Energy*, *287*, 116588. https://doi.org/10.1016/j.apenergy.2021.116588

Robertson, B., Bekker, J., & Buckham, B. (2020). Renewable integration for remote communities: Comparative allowable cost analyses for hydro, solar and wave energy. *Applied Energy*, *264*, 114677. https://doi.org/10.1016/j.apenergy.2020.114677

Robertson, B., Dunkle, G., Gadasi, J., Garcia-Medina, G., & Yang, Z. (2021). Holistic marine energy resource assessments: A wave and offshore wind perspective of metocean conditions. *Renewable Energy*, *170*, 286–301. https://doi.org/10.1016/j.renene.2021.01.136

Rodríguez-Sarasty, J. A., Debia, S., & Pineau, P.-O. (2021). Deep decarbonization in Northeastern North America: The value of electricity market integration and hydropower. *Energy Policy*, *152*, 112210. https://doi.org/10.1016/j.enpol.2021.112210

Ruiz, C., & Conejo, A. J. (2015). Robust transmission expansion planning. *European Journal of Operational Research*, *242*(2), 390–401. https://doi.org/10.1016/j.ejor.2014.10.030

Said, H. A., & Ringwood, J. V. (2021). Grid integration aspects of wave energy—Overview and perspectives. *IET Renewable Power Generation*, *15*(14), 3045–3064. https://doi.org/10.1049/rpg2.12179

Samaan, N., Milligan, M., Hunsaker, M., & Guo, T. (2015). Three-stage production cost modeling approach for evaluating the benefits of intra-hour scheduling between balancing authorities. *2015 IEEE Power & Energy Society General Meeting*, 1–5. https://doi.org/10.1109/PESGM.2015.7286647

Schyska, B. U., Kies, A., Schlott, M., Von Bremen, L., & Medjroubi, W. (2021). The sensitivity of power system expansion models. *Joule*, *5*(10), 2606–2624. https://doi.org/10.1016/j.joule.2021.07.017

Sepulveda, N. A., Jenkins, J. D., de Sisternes, F. J., & Lester, R. K. (2018). The Role of Firm Low-Carbon Electricity Resources in Deep Decarbonization of Power Generation. *Joule*, *2*(11), 2403–2420. https://doi.org/10.1016/j.joule.2018.08.006

Shawhan, D. L., Taber, J. T., Shi, D., Zimmerman, R. D., Yan, J., Marquet, C. M., Qi, Y., Mao, B., Schuler, R. E., Schulze, W. D., & Tylavsky, D. (2014). Does a detailed model of the electricity grid matter? Estimating the impacts of the Regional Greenhouse Gas Initiative. *Resource and Energy Economics*, *36*(1), 191–207. https://doi.org/10.1016/j.reseneeco.2013.11.015

Shi, D., Shawhan, D. L., Li, N., Tylavsky, D. J., Taber, J. T., Zimmerman, R. D., & Schulze, W. D. (2012). Optimal generation investment planning: Pt. 1: Network equivalents. *2012 North American Power Symposium (NAPS)*, 1–6. https://doi.org/10.1109/NAPS.2012.6336375

Soudan, B. (2019). Community-scale baseload generation from marine energy. *Energy*, *189*, 116134. https://doi.org/10.1016/j.energy.2019.116134

Strbac, G., Pollitt, M., Konstantinidis, C. V., Konstantelos, I., Moreno, R., Newbery, D., & Green, R. (2014). Electricity transmission arrangements in Great Britain: Time for change? *Energy Policy*, *73*, 298–311. https://doi.org/10.1016/j.enpol.2014.06.014

Su, Y., Kern, J. D., Denaro, S., Hill, J., Reed, P., Sun, Y., Cohen, J., & Characklis, G. W. (2020). An open source model for quantifying risks in bulk electric power systems from spatially

and temporally correlated hydrometeorological processes. *Environmental Modelling & Software, 126,* 104667. https://doi.org/10.1016/j.envsoft.2020.104667

Su, Y., Kern, J. D., Reed, P. M., & Characklis, G. W. (2020). Compound hydrometeorological extremes across multiple timescales drive volatility in California electricity market prices and emissions. *Applied Energy*, *276*, 115541. https://doi.org/10.1016/j.apenergy.2020.115541

Svendsen, H. G. (2015). Grid Model Reduction for Large Scale Renewable Energy Integration Analyses. *Energy Procedia*, *80*, 349–356. https://doi.org/10.1016/j.egypro.2015.11.439

System Advisor Model (Version 2023.12.17). (2023). [Computer software]. https://github.com/NREL/SAM

Tapia, T., Lorca, Á., Olivares, D., Negrete-Pincetic, M., & Lamadrid L, A. J. (2021). A robust decision-support method based on optimization and simulation for wildfire resilience in highly renewable power systems. *European Journal of Operational Research*, *294*(2), 723–733. https://doi.org/10.1016/j.ejor.2021.02.008

TELL documentation (v1.0.0). (2023). [Computer software]. https://immm-sfa.github.io/tell/

Turner, S. W. D., Voisin, N., & Nelson, K. (2022). Revised monthly energy generation estimates for 1,500 hydroelectric power plants in the United States. *Scientific Data*, *9*(1), 675. https://doi.org/10.1038/s41597-022-01748-x

Turner, S. W. D., Voisin, N., Oikonomou, K., & Bracken, C. (2023). *HydroWIRES B1: Monthly and Weekly Hydropower Constraints Based on Disaggregated EIA-923 Data* (v1.1.1) [dataset]. Zenodo. https://doi.org/10.5281/ZENODO.8212757

United Nations. (2023). *Causes and Effects of Climate Change*. https://www.un.org/en/climatechange/science/causes-effects-climate-change

van Vliet, M. T. H., Wiberg, D., Leduc, S., & Riahi, K. (2016). Power-generation system vulnerability and adaptation to changes in climate and water resources. *Nature Climate Change*, *6*(4), 375–380. https://doi.org/10.1038/nclimate2903

Vargas, C. A., Caracciolo, L., & Ball, P. J. (2022). Geothermal energy as a means to decarbonize the energy mix of megacities. *Communications Earth & Environment*, *3*(1), 66. https://doi.org/10.1038/s43247-022-00386-w

Vernon, C. R., Mongird, K., Nelson, K. D., & Rice, J. S. (2023). Harmonized geospatial data to support infrastructure siting feasibility planning for energy system transitions. *Scientific Data*, *10*(1), 786. https://doi.org/10.1038/s41597-023-02694-y

Vernon, C., Rice, J., Zuljevic, N., Mongird, K., Nelson, K., Iyer, G., Voisin, N., & Binsted, M. (2021). cerf: A Python package to evaluate the feasibility and costs of power plant siting for alternative futures. *Journal of Open Source Software*, *6*(65), 3601. https://doi.org/10.21105/joss.03601

Voisin, N., Kintner-Meyer, M., Skaggs, R., Nguyen, T., Wu, D., Dirks, J., Xie, Y., & Hejazi, M. (2016). Vulnerability of the US western electric grid to hydro-climatological conditions: How bad can it get? *Energy*, *115*, 1–12. https://doi.org/10.1016/j.energy.2016.08.059

Voisin, N., Kintner-Meyer, M., Wu, D., Skaggs, R., Fu, T., Zhou, T., Nguyen, T., & Kraucunas, I. (2018). Opportunities for Joint Water–Energy Management: Sensitivity of the 2010 Western U.S. Electricity Grid Operations to Climate Oscillations. *Bulletin of the American Meteorological Society*, *99*(2), 299–312. https://doi.org/10.1175/BAMS-D-16-0253.1

Ward, J. B. (1949). Equivalent Circuits for Power-Flow Studies. *Transactions of the American Institute of Electrical Engineers*, *68*(1), 373–382. https://doi.org/10.1109/T-AIEE.1949.5059947

WECC. (2017). *The Western Interconnection*. https://www.wecc.org/epubs/StateOfTheInterconnection/Pages/The-Western-Interconnection.aspx

WECC. (2018). *Resource Portfolio*. https://www.wecc.org/epubs/StateOfTheInterconnection/Pages/Resource-Portfolio.aspx

WECC. (2021). *2030 ADS PCM Release Notes*. https://www.wecc.org/Reliability/2030ADS_PCM_ReleaseNotes_GV-V2.3_6-9-2021.pdf

Weiss, J., Hagerty, J. M., & Castañer, M. (2019). *The Coming Electrification of the North American Economy, Why We Need a Robust Transmission Grid*. The Brattle Group. https://wiresgroup.com/wp-content/uploads/2020/05/2019-03-06-Brattle-Group-The-Coming-Electrification-of-the-NA-Economy.pdf

Wessel, J., Kern, J. D., Voisin, N., Oikonomou, K., & Haas, J. (2022). Technology Pathways Could Help Drive the U.S. West Coast Grid's Exposure to Hydrometeorological Uncertainty. *Earth's Future*, *10*(1). https://doi.org/10.1029/2021EF002187

Wise, M., Patel, P., Khan, Z., Kim, S. H., Hejazi, M., & Iyer, G. (2019). Representing power sector detail and flexibility in a multi-sector model. *Energy Strategy Reviews*, *26*, 100411. https://doi.org/10.1016/j.esr.2019.100411

Xiaotong, L., Yimei, L., Xiaoli, Z., & Ming, Z. (2012). Generation and Transmission Expansion Planning Based on Game Theory in Power Engineering. *Systems Engineering Procedia*, *4*, 79–86. https://doi.org/10.1016/j.sepro.2011.11.052

Xu, X., Robertson, B., & Buckham, B. (2020). A techno-economic approach to wave energy resource assessment and development site identification. *Applied Energy*, *260*, 114317. https://doi.org/10.1016/j.apenergy.2019.114317

Yang, Z., García-Medina, G., Wu, W.-C., & Wang, T. (2020). Characteristics and variability of the nearshore wave resource on the U.S. West Coast. *Energy*, *203*, 117818. https://doi.org/10.1016/j.energy.2020.117818

Zanocco, C., Stelmach, G., Giordono, L., Flora, J., & Boudet, H. (2023). Poor Air Quality during Wildfires Related to Support for Public Safety Power Shutoffs. *Society & Natural Resources*, *36*(9), 1045–1059. https://doi.org/10.1080/08941920.2022.2041138

Zheng, C. (2021). Dynamic self-adjusting classification for global wave energy resources under different requirements. *Energy*, *236*, 121525. https://doi.org/10.1016/j.energy.2021.121525

Zhu, Y., & Tylavsky, D. (2018). An Optimization-Based DC-Network Reduction Method. *IEEE Transactions on Power Systems*, *33*(3), 2509–2517. https://doi.org/10.1109/TPWRS.2017.2745492

APPENDICES

Appendix A: UC/ED Modeling Approach

Here, a detailed explanation of the UC/ED model is presented. UC/ED inputs, objective function, and constraints are further clarified.

A.1. UC/ED Inputs

There are numerous inputs fed to the UC/ED model including generator parameters, generator outage time series, must-run generation, hydropower targets, fuel prices, load, solar and wind generation time series, transmission line parameters, and hurdle rates between balancing authorities (BAs).

A.1.1. Generator Parameters

Five types of generators are used in GO WEST, which are natural gas, coal, hydropower, solar, and wind. Generator information is gathered from TAMU synthetic grid datasets (Birchfield et al., 2017; Electric Grid Test Case Repository, 2017a). Generator names, locations (connection to specific node), types, maximum capacities in MW, minimum capacities in MW, heat rates in MMBtu/MWh, no load cost in U.S. dollar ($), variable operation and maintenance costs in $/MWh, start-up cost in $, ramp rate in MW, minimum up and down times in hours are fed into the model for each generator. In addition, one loss-of-load variable with infinite capacity for a marginal cost of 2,000 $/MWh is added to each node to prevent model from crashing due to the inability to meet demand. These variables are only used as a last resort.

A.1.2. Generator Outage Modeling

Hourly generator outage time series information is gathered from NERC Generating Availability Data System (GADS) for 2019, 2020, and 2021 (NERC, 2022). When listing outage data, NERC does not give information about the specific generator names or locations but groups them with respect to their installed capacity. There are 36 capacity categories for coal, natural gas,

and nuclear power plants. For every hour, GO WEST checks these outage time series and categories, and filters the specific generators for each capacity category. Generator power outage amount (reported in MW) is allocated equally to the generators that fall into the same capacity category. In this sense, available capacity of generators changes each hour depending on the outage status.

A.1.3. Solar, Wind, and Must-run Generation

Solar and wind generation is modeled through historical solar and wind generation time series. Historical solar and wind generation for each BA is collected from EIA-930 dataset (EIA, 2022b) for 2019, 2020, and 2021. Available hourly solar and wind generation for each node is fed into the model and, GO WEST dispatches or curtails solar and wind according to the system conditions. As solar and wind generators have a negligible marginal cost in the objective function (0.01 $/MWh), those resources are most likely to be used fully. On the other hand, the model has the ability to curtail them if needed.

For simplicity, nuclear generators are regarded as must-run generators and assumed to be run all the time. Nuclear output changes only if there is a nuclear generator outage in GADS dataset.

A.1.4. Hydropower Generation

Annual hydropower generation are collected from EIA-923 dataset (EIA, 2022a) for 2019, 2020, and 2021 and further disaggregated into weekly energy target at individual power plants based on observed weekly flow release and storage conditions (Turner et al., 2023). From weekly data, hourly minimum, hourly maximum, and daily allowed total generation is calculated and fed into the model. GO WEST schedules and dispatches hydropower resources depending on the minimum and maximum allowed hourly generation and daily total generation.

A.1.5. Fuel Prices

Daily natural gas (NG) prices are collected from CAISO OASIS (CAISO, 2022b) for 2019 and 2020 and 2021. However, there is only NG information for 8 out of 28 BAs. NG prices for the remaining 20 BAs are estimated according to geographical proximity. For those 20 BAs, an inverse distance coefficient matrix is created by using distances to each of those 8 BAs. The summation of 8 BA's distance coefficients is 1 for each of those 20 BAs. Daily NG prices in each 8 BAs are multiplied with their respective inverse distance coefficients and then summed to create daily NG price time series for those 20 BAs with no listed data. By utilizing this approach, BAs that are closer to the unknown BAs have a greater impact on the estimated NG price for those 20 BAs. In order to make sure there is no bias in the estimated NG prices, monthly average of estimated prices is compared with monthly reported NG prices in EIA-923 (EIA, 2022a). If there is any difference between estimated monthly and EIA reported monthly NG prices, daily NG prices are adjusted according to the difference. In this way, monthly average of our NG price estimations exactly matches EIA-923 to correct any bias. Daily NG prices are fed into GO WEST model.

Monthly coal prices for each BA are gathered from EIA-923 dataset (EIA, 2022a) for 2019, 2020, and 2021. The same coal price is assumed for each day in respective months. Daily coal prices are fed into GO WEST model.

A.1.6. Electricity Load, Transmission Line Parameters, and Hurdle Rates

Hourly electricity load for each BA is drawn from EIA-930 dataset (EIA, 2022b) for 2019, 2020, and 2021. After cleaning and removing any outliers from the data, it is fed to GO WEST model. In addition, thermal limit in MW and reactance of each transmission line are calculated in network reduction algorithm and fed into the model. Lastly, hurdle rates for each connected BA pair are gathered from WECC 2030 Anchor Data Set (WECC, 2021) and used in the model.

A.2. Objective Function

GO WEST's objective function tries to minimize the total cost of meeting electricity demand for every hour in the operating horizon. In this sense, the model considers the total operational costs in U.S. Western Interconnection, not costs at individual nodes or BAs. Nevertheless, power balance constraint is satisfied in every node. Formulation of objective function for the mixed-integer linear programming (MILP) version is presented below:

$$Objective\ Function$$

$$= \sum_{t=1}^{T} \sum_{j}^{J} \sum_{z}^{Z} (Fuel\ Costs_{t,j,z} + Variable\ O\&M\ Costs_{t,j,z} + No\ Load\ Costs_{t,j,z}$$

$$+ Start\ Costs_{t,j,z})$$

$$+ \sum_{t=1}^{T} \sum_{s}^{S} \sum_{k}^{K} Power\ Flow\ Costs_{t,s,k} + \sum_{t=1}^{T} \sum_{z}^{Z} Unserved\ Energy\ Costs_{t,z}$$

Where,

$t \in$ operating horizon $\{1 \dots T\}$

$z \in set\ Z\ of\ nodes\ \{node1, node2 \dots node\ n\}$

$j \in set\ J\ of\ generators\ \{coal1, coal2, gas1, gas2 \dots J\}$

$s \in set\ S\ of\ nodes\ \{node1, node2 \dots node\ n\}$

$k \in set\ K\ of\ nodes\ \{node1, node2 \dots node\ n\}$

Individual elements of the objective function are detailed below:

$$Fuel\ Costs_{t,j,z} = PW_{j,z,t} \times (FP_{z,t} \times HR_{j,z})$$

$$Variable\ O\&M\ Costs_{t,j,z} = PW_{j,z,t} \times VC_{j,z}$$

$$No\ Load\ Costs_{t,j,z} = ON_{j,z,t} \times NL_{j,z}$$

$$Start\ Costs_{t,j,z} = SWITCH_{j,z,t} \times SC_{j,z}$$

$$Power\ Flow\ Costs_{t,s,k} = FLOW_{s,k,t} \times Hurdle_{s,k}$$

$$Unserved\ Energy\ Costs_{t,z} = UEPen \times LOLV_{t,z}$$

Where,

$PW_{j,z,t}$ = power produced in generator j in node z in hour t (MWh)

$FP_{z,t}$ = fuel price in node z in hour t (USD/MMBtu)

$HR_{j,z}$ = heat rate of generator j in node z (MMBtu/MWh)

$VC_{j,z}$ = variable O&M cost for generator j in node z (USD/MWh)

$ON_{j,z,t}$ = binary; 1 if generator j in node z is on in hour t; 0 otherwise

$NL_{j,z}$ = no-load cost for generator j in node z (USD)

$SWITCH_{j,z,t}$ = binary; 1 if generator j in node z starts in hour t; 0 otherwise

$SC_{j,z}$ = startup cost of generator j in node z (USD)

$FLOW_{s,k,t}$ = power flow from node s to node k in hour t (MWh)

$Hurdle_{s,k}$ = hurdle rate on power flows from node s to node k (USD/MWh)

$UEPen$ = unserved energy penalty (2000 USD/MWh)

$LOLV_{t,z}$ = loss of load (unserved energy amount) in node z in hour t (MWh)

A.3. Constraints

GO WEST's objective function is bounded by numerous constraints related to generator parameters, power balance, and power flow between each connected node. For instance, there are constraints to make sure that power generation from each generator is between minimum and maximum allowed capacities. Moreover, two constraints prevent any violation of minimum up and minimum down time of the generators. There are also constraints on ramp rates of generators and thermal limits of transmission lines between each connected node. Finally, an power balance constraint (representing Kirchhoff's Current Law) allows us to ensure that sum of power generated

in a node and power flow from other nodes to that node equals to sum of electricity demand and power flow from that node to other nodes. Power balance constraint is presented below:

$$\sum_{z}^{Z}(\sum_{j=1}^{J} PW_{j,z,t} + \sum_{s=1}^{S} FLOW_{s,z,t}) = \sum_{z}^{Z}(Demand_{z,t} + \sum_{k=1}^{K} FLOW_{z,k,t}) \quad \forall t$$

Where,

$FLOW_{s,z,t} =$ power flow from zone s to zone z in hour t (MW)

$FLOW_{z,k,t} =$ power flow from zone z to zone k in hour t (MW)

$Demand_{z,t} =$ electricity demand in zone z in hour t (MW)

Appendix B: Supplementary Figures

GO can also track a particular model's ability to replicate the distribution of LMPs. Figure 38 compares the distributions of historical and simulated daily LMPs from the best-performing model version in 2019. This version shows an ability to capture the distribution, average, and standard deviation of LMPs in all five pricing hubs.

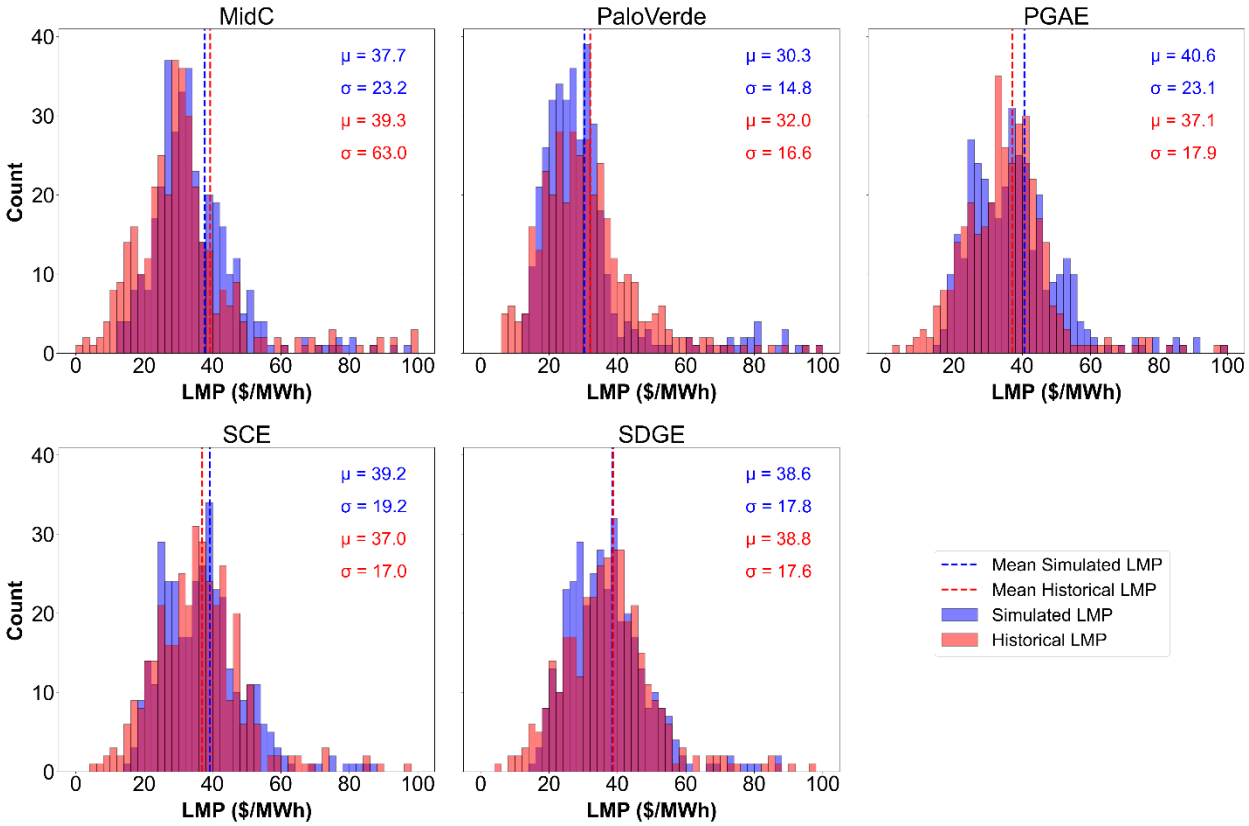

Figure 38: Distribution of historical and simulated daily LMPs for each pricing hub. Results are from the best-performing model version in 2019.

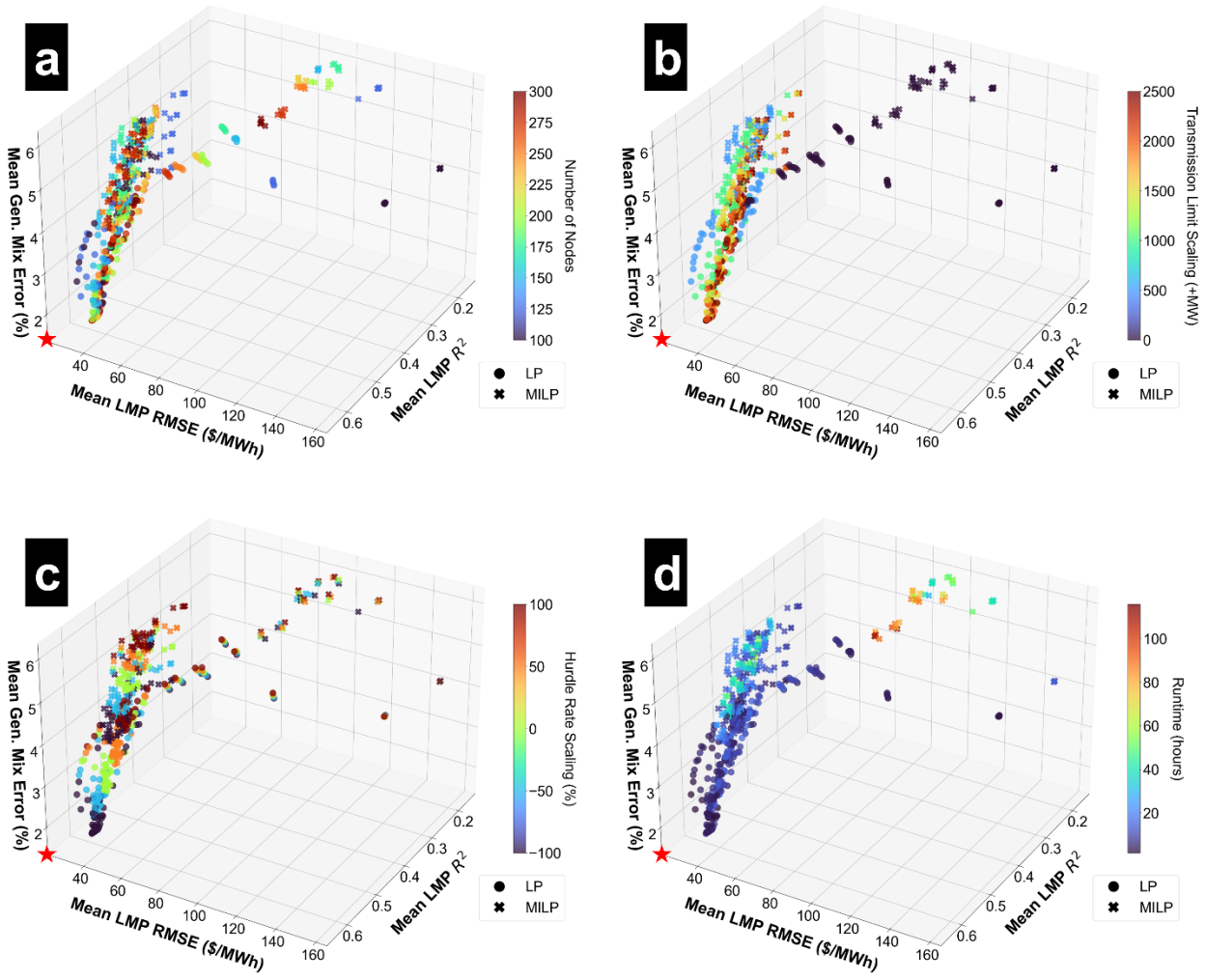

Figure 39: 3D model performance plots showing the tradeoff between three model selection metrics and (a) number of nodes, (b) transmission limit scaling factors, (c) hurdle rate scaling factors, and (d) runtimes in 2020. Each point represents one model version out of 540. Circles represent LP versions whereas crosses represent MILP versions. Red stars show the best possible solution on these figures.

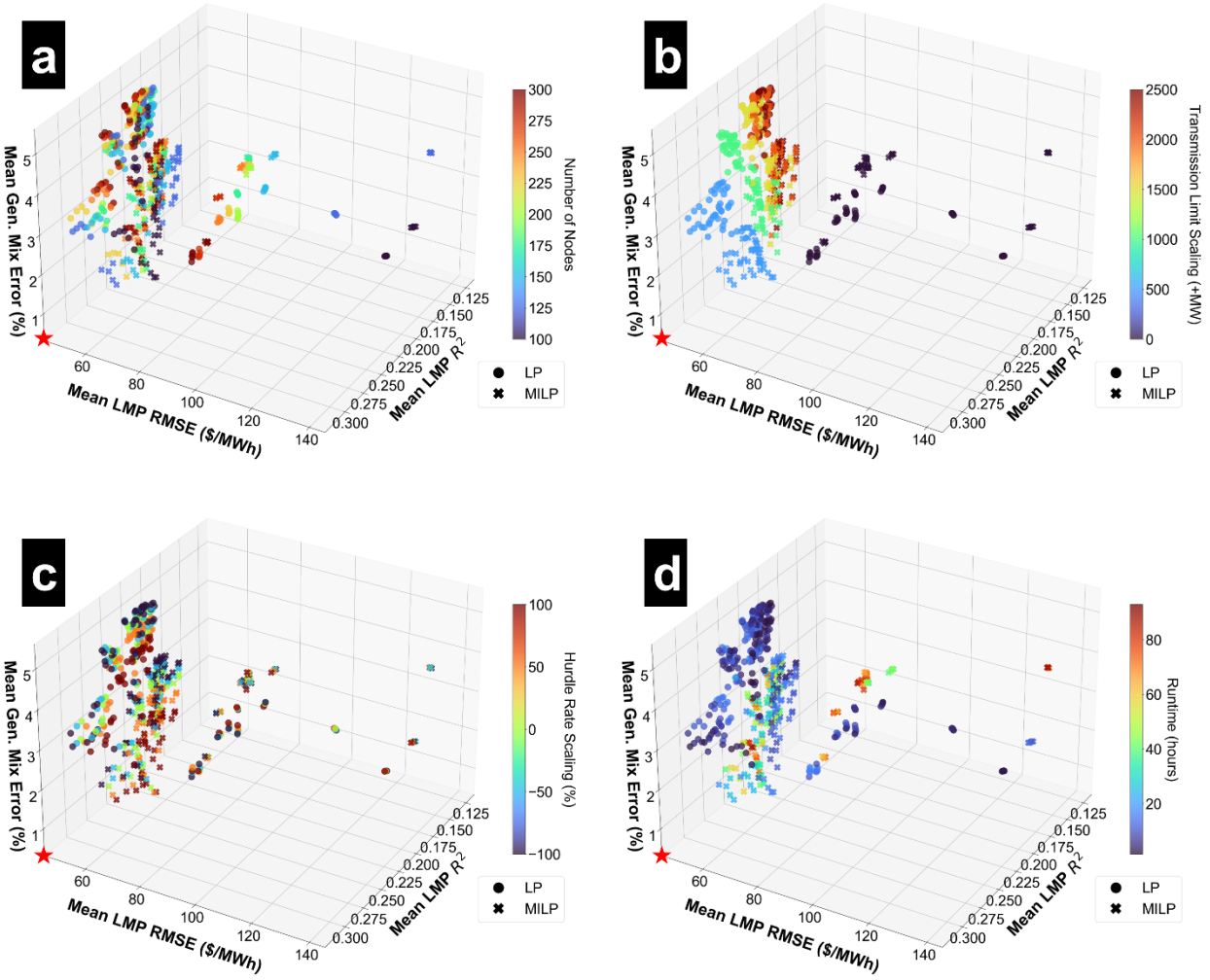

Figure 40: 3D model performance plots showing the tradeoff between three model selection metrics and (a) number of nodes, (b) transmission limit scaling factors, (c) hurdle rate scaling factors, and (d) runtimes in 2021. Each point represents one model version out of 540. Circles represent LP versions whereas crosses represent MILP versions. Red stars show the best possible solution on these figures.

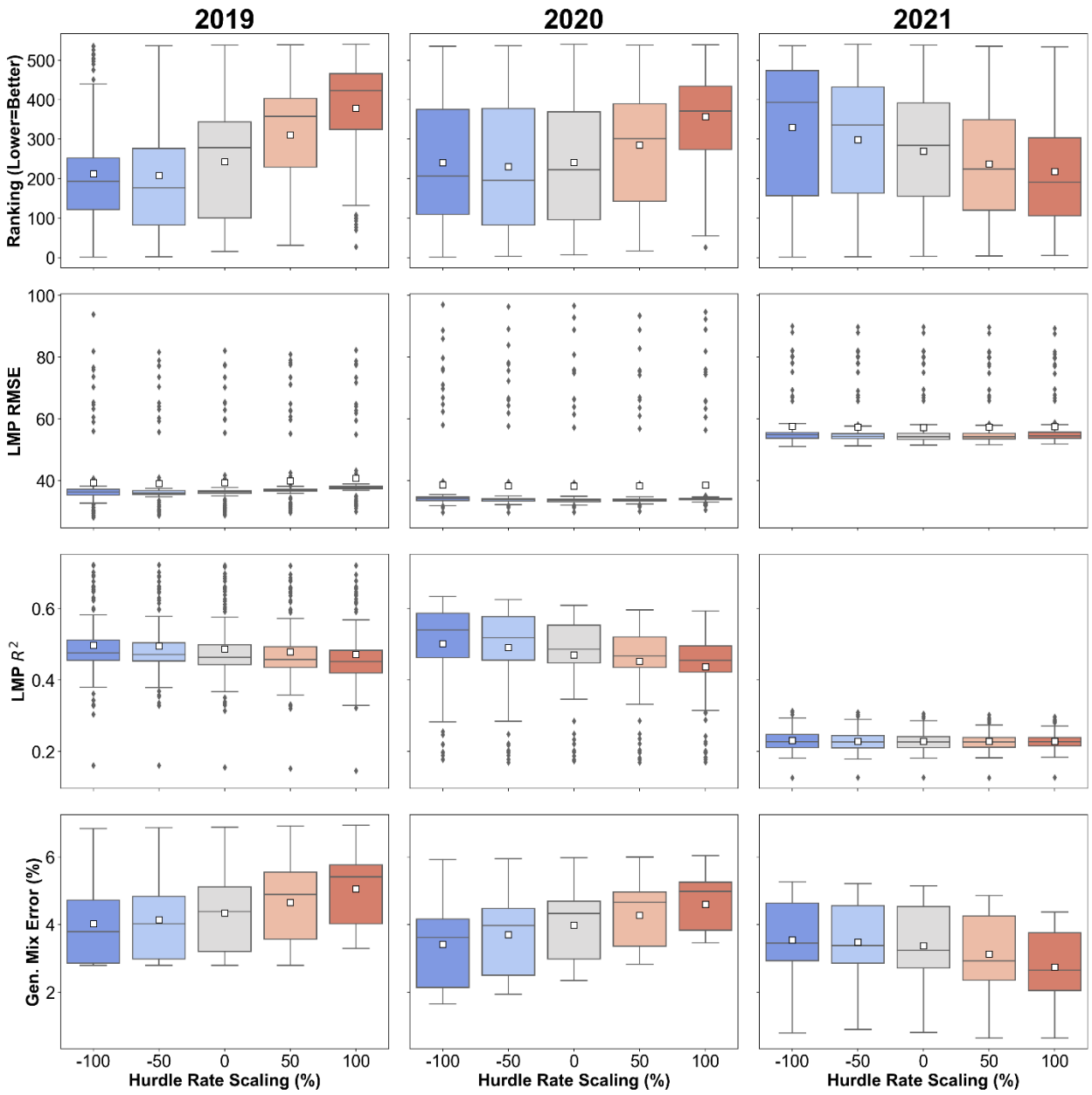

Figure 41: Effect of changing hurdle rate scaling on model rankings as well as three model selection metrics

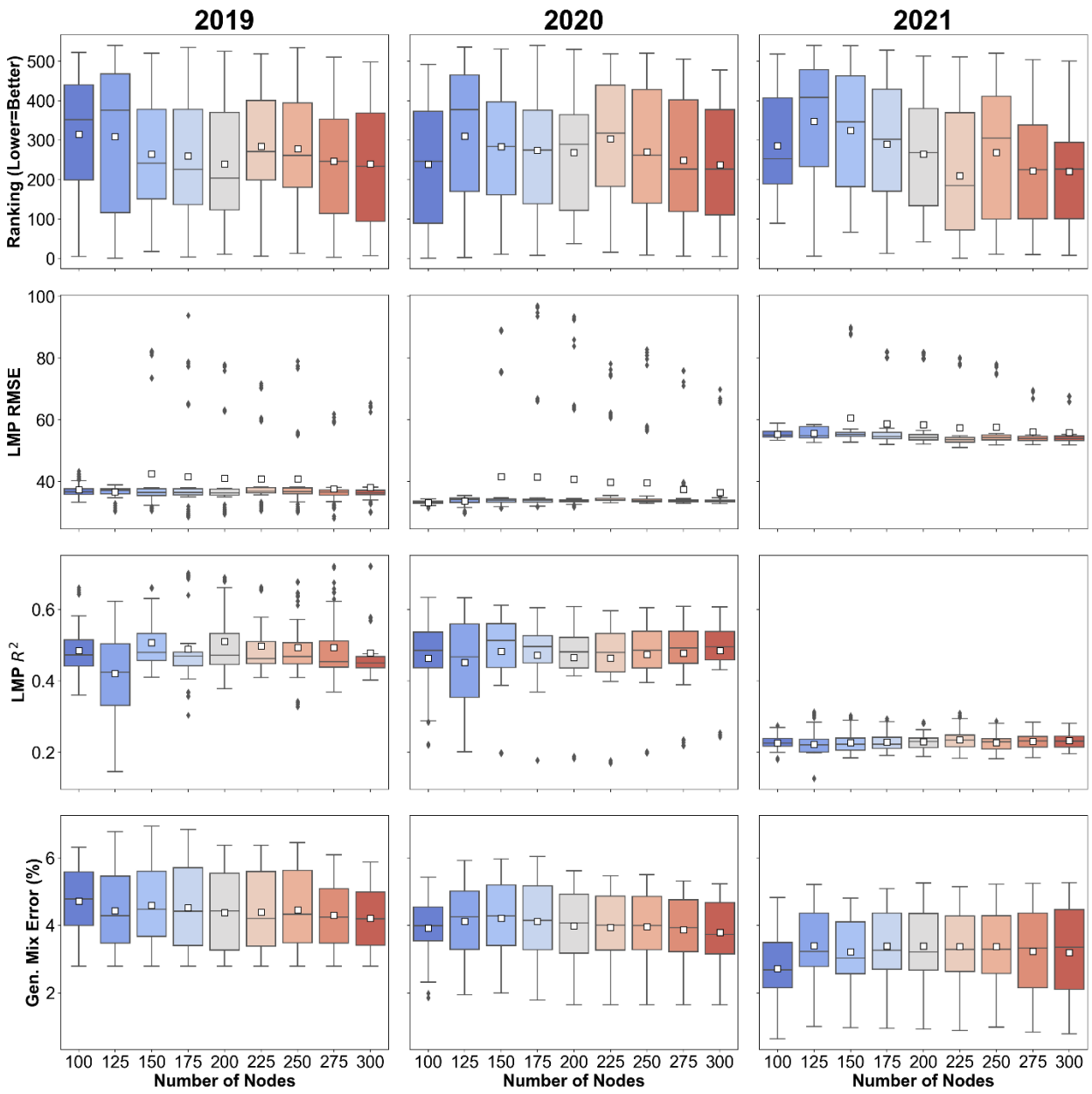

Figure 42: Effect of changing number of nodes on model rankings as well as three model selection metrics

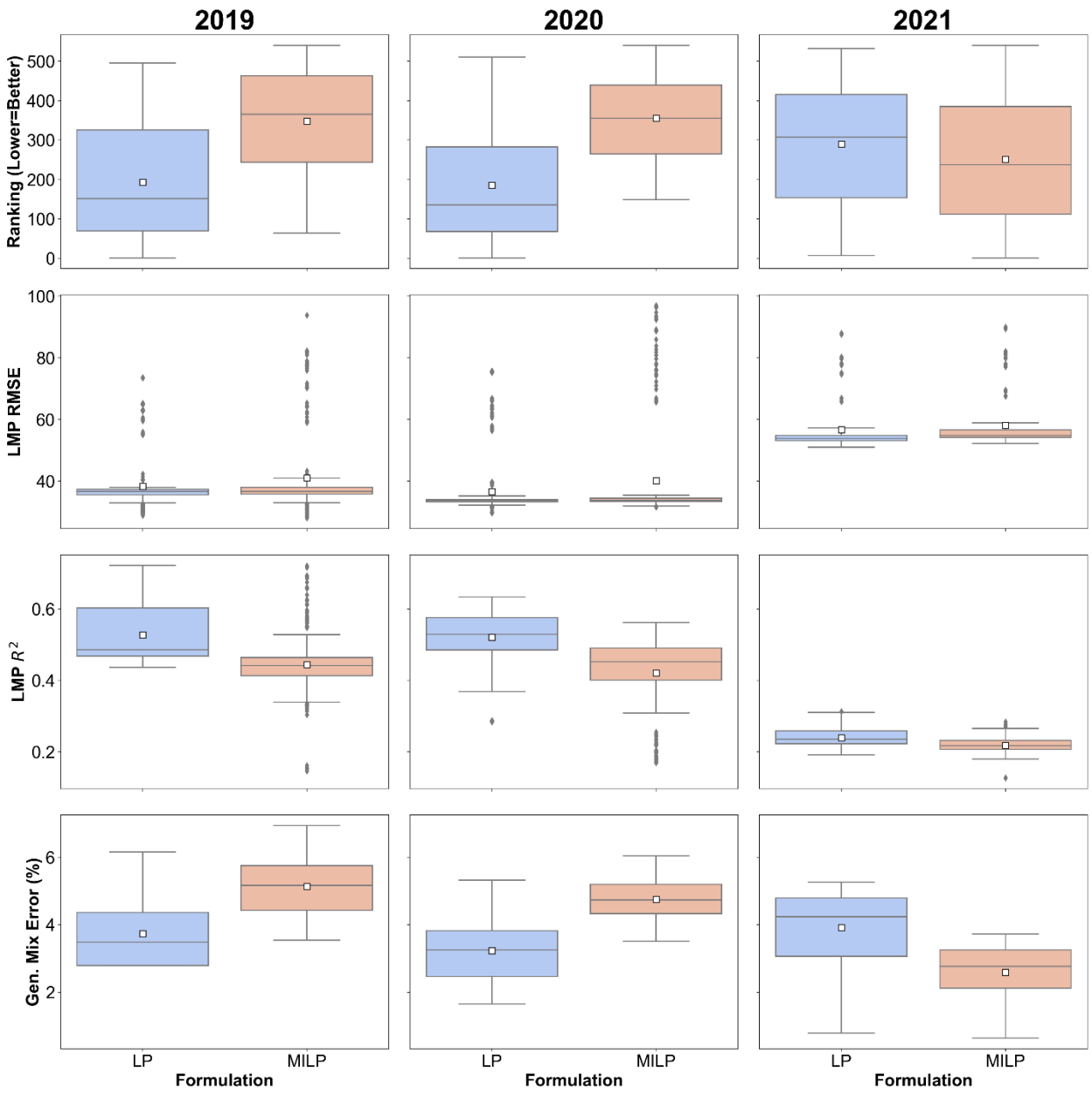

Figure 43: Effect of changing model formulation on model rankings as well as three model selection metrics

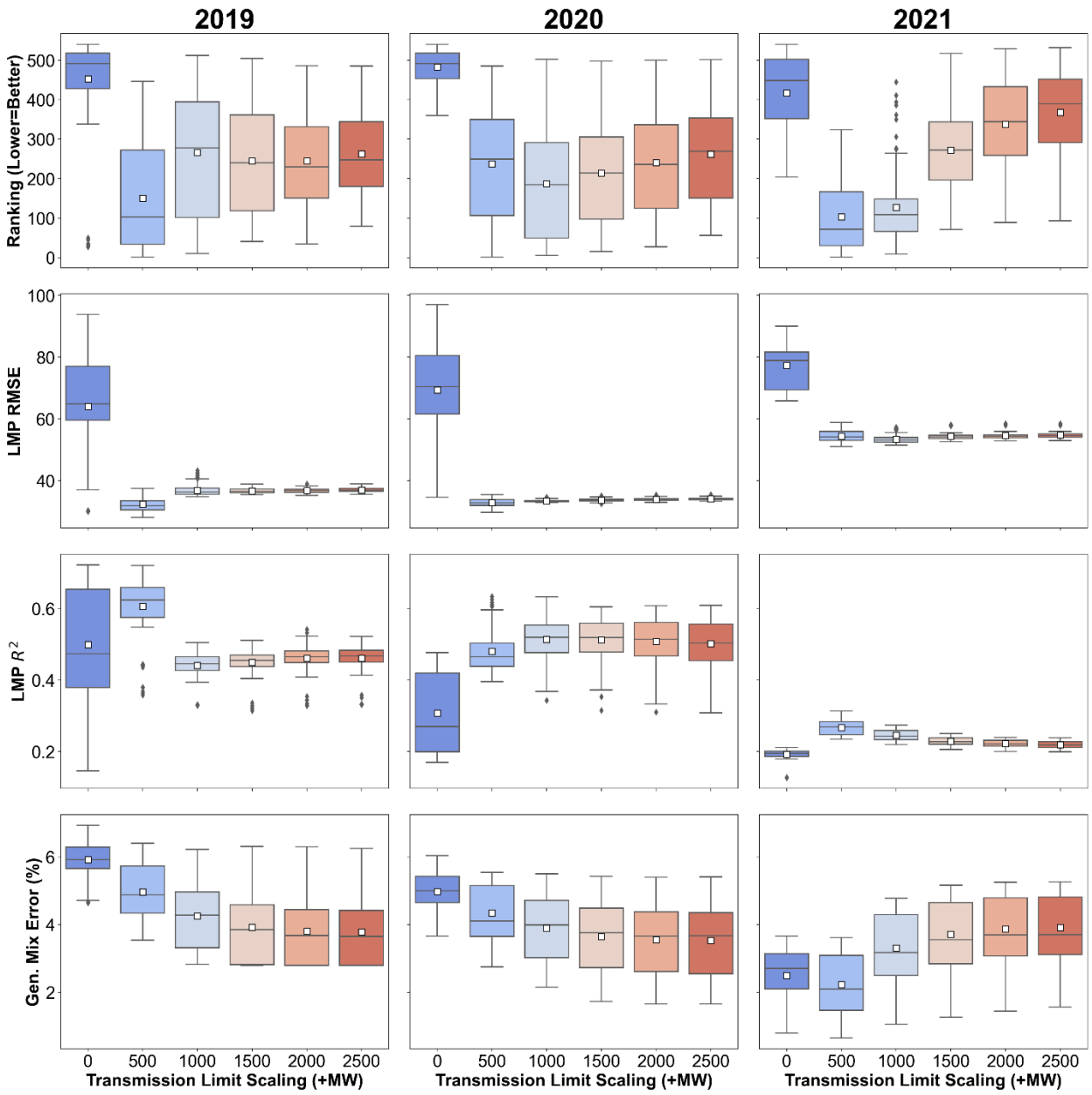

Figure 44: Effect of changing transmission limit scaling on model rankings as well as three model selection metrics

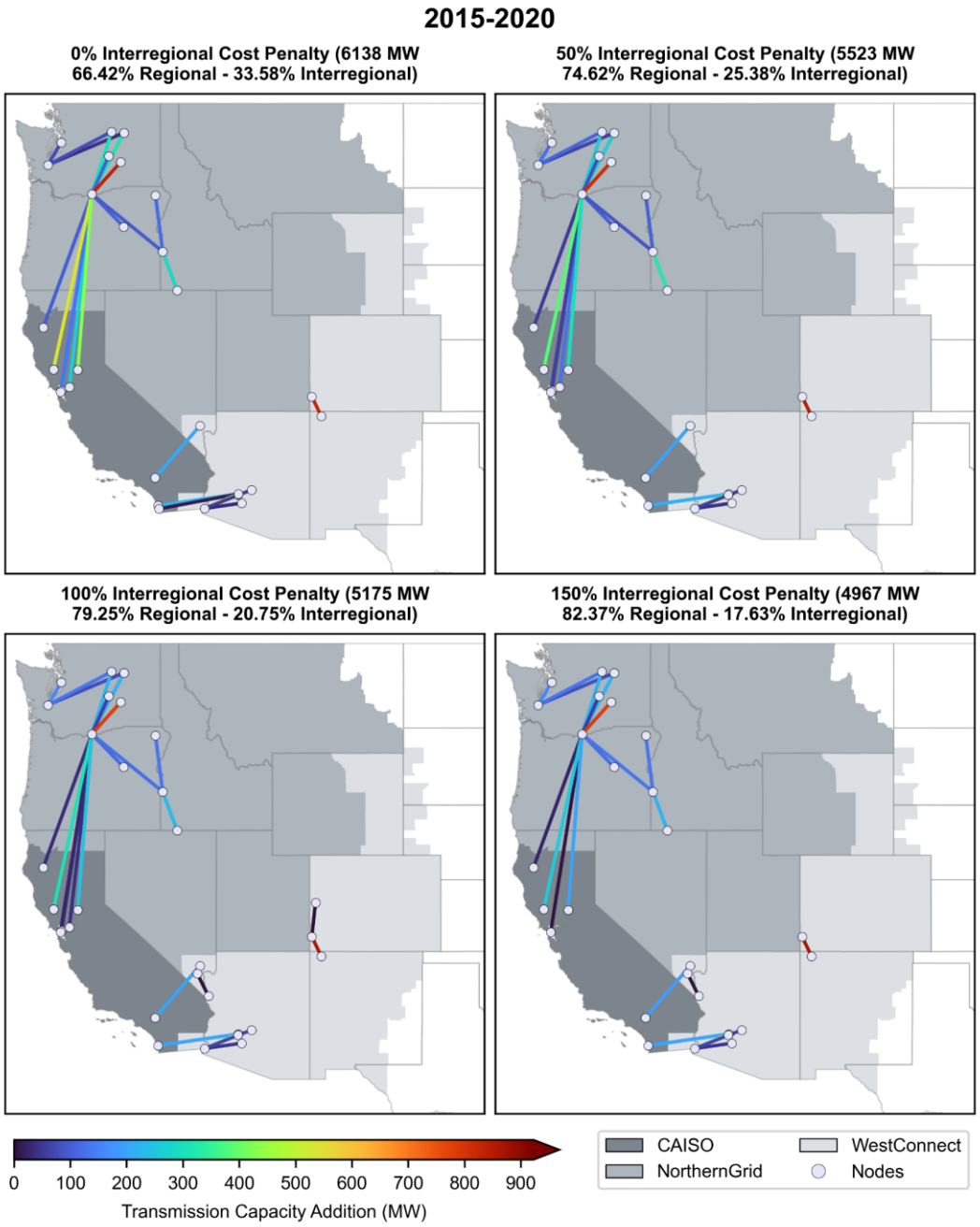

Figure 45: Transmission capacity additions with 0%, 50%, 100%, and 150% interregional cost penalties. Total transmission capacity addition as well as the shares of regional and international transmission investments can be seen in parenthesis.

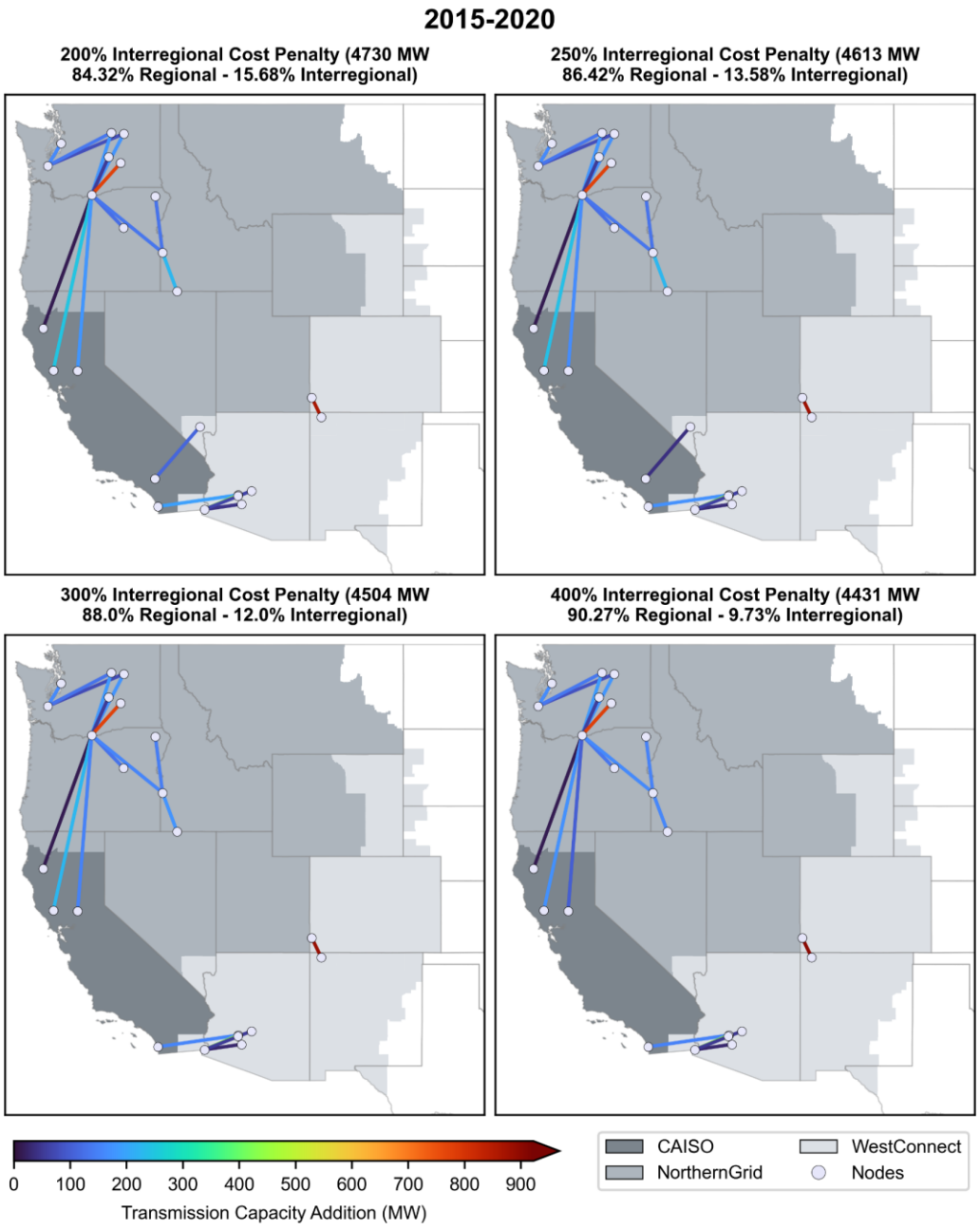

Figure 46: Transmission capacity additions with 200%, 250%, 300%, and 400% interregional cost penalties. Total transmission capacity addition as well as the shares of regional and international transmission investments can be seen in parenthesis.

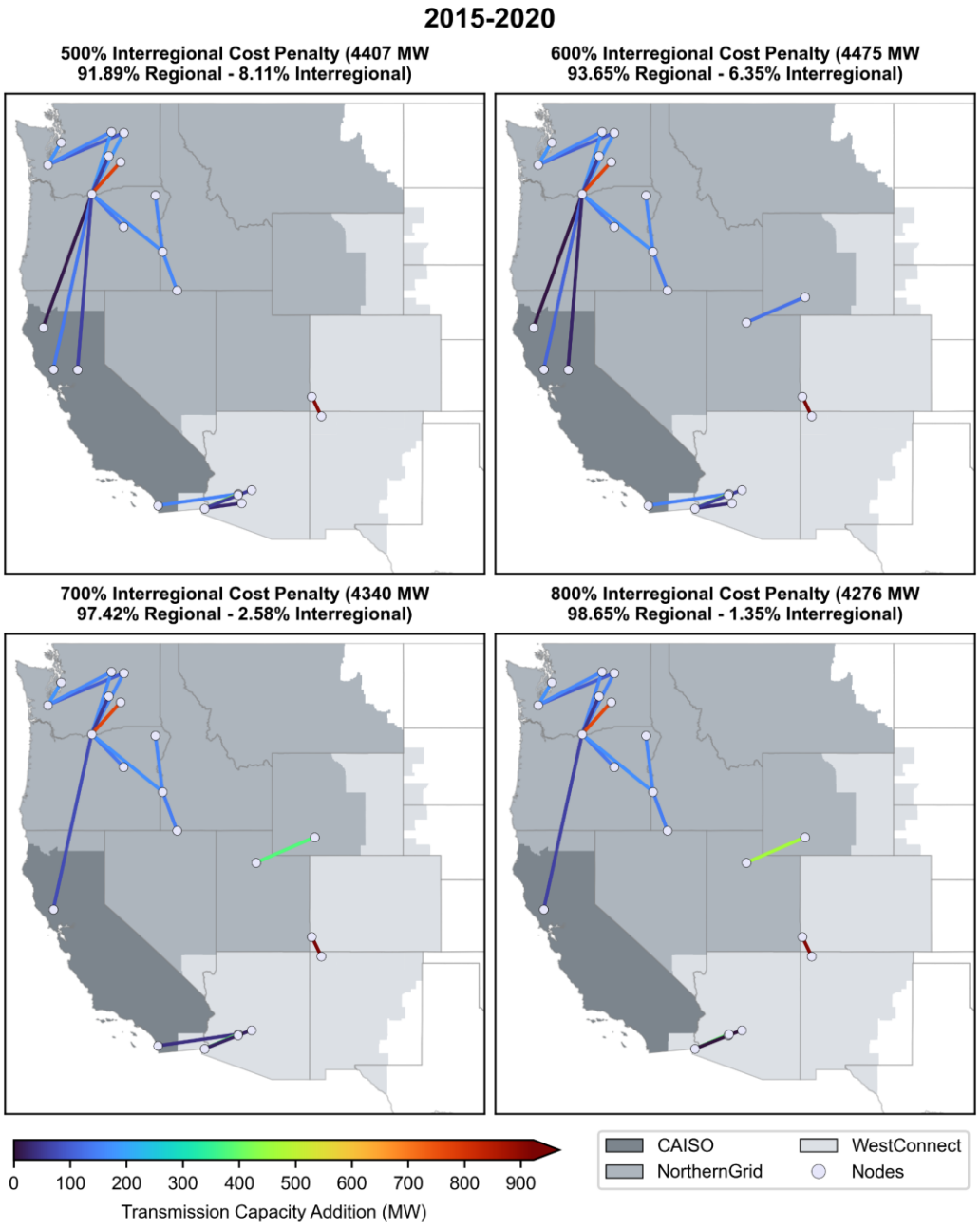

Figure 47: Transmission capacity additions with 500%, 600%, 700%, and 800% interregional cost penalties. Total transmission capacity addition as well as the shares of regional and international transmission investments can be seen in parenthesis.

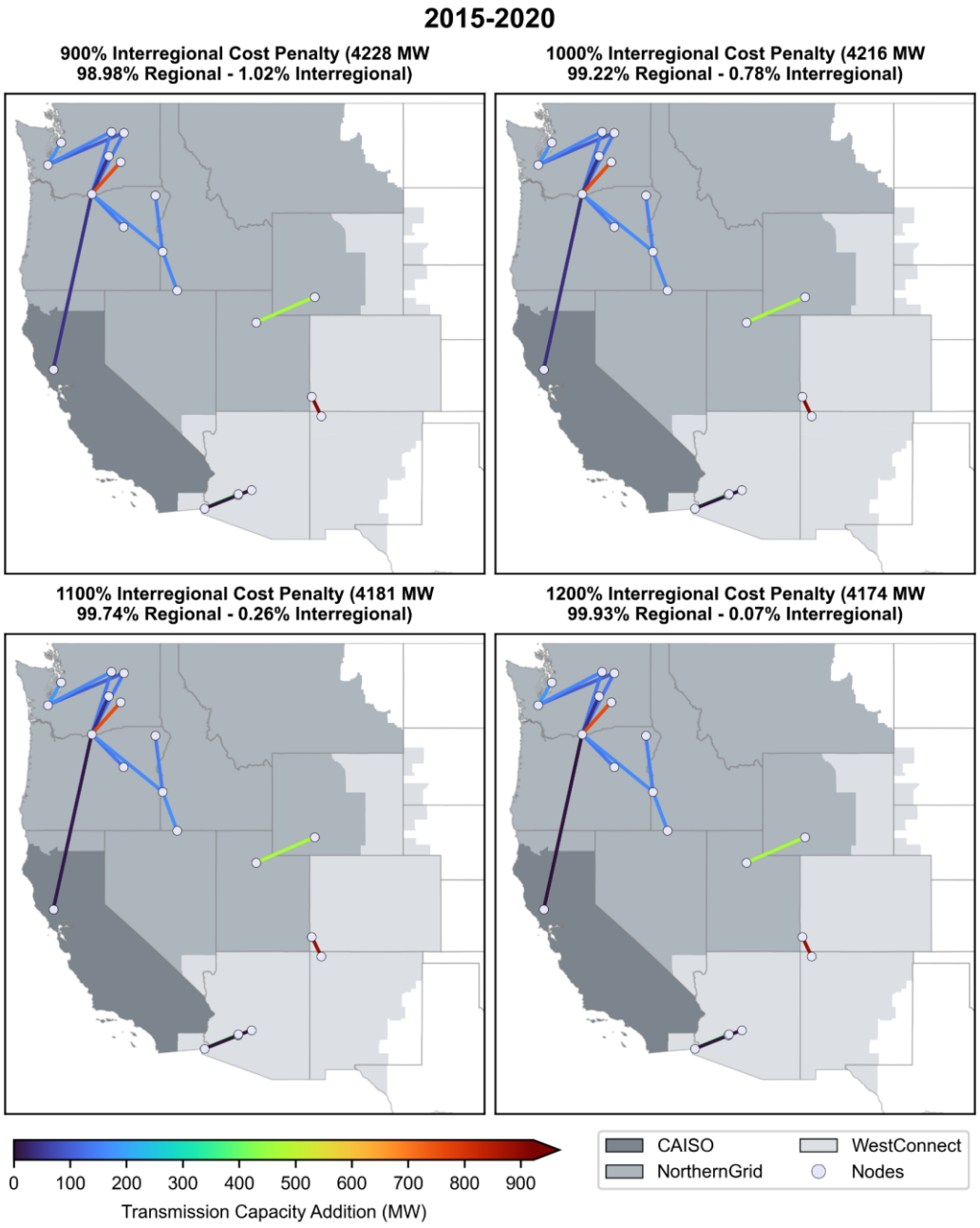

Figure 48: Transmission capacity additions with 900%, 1000%, 1100%, and 1200% interregional cost penalties. Total transmission capacity addition as well as the shares of regional and international transmission investments can be seen in parenthesis.

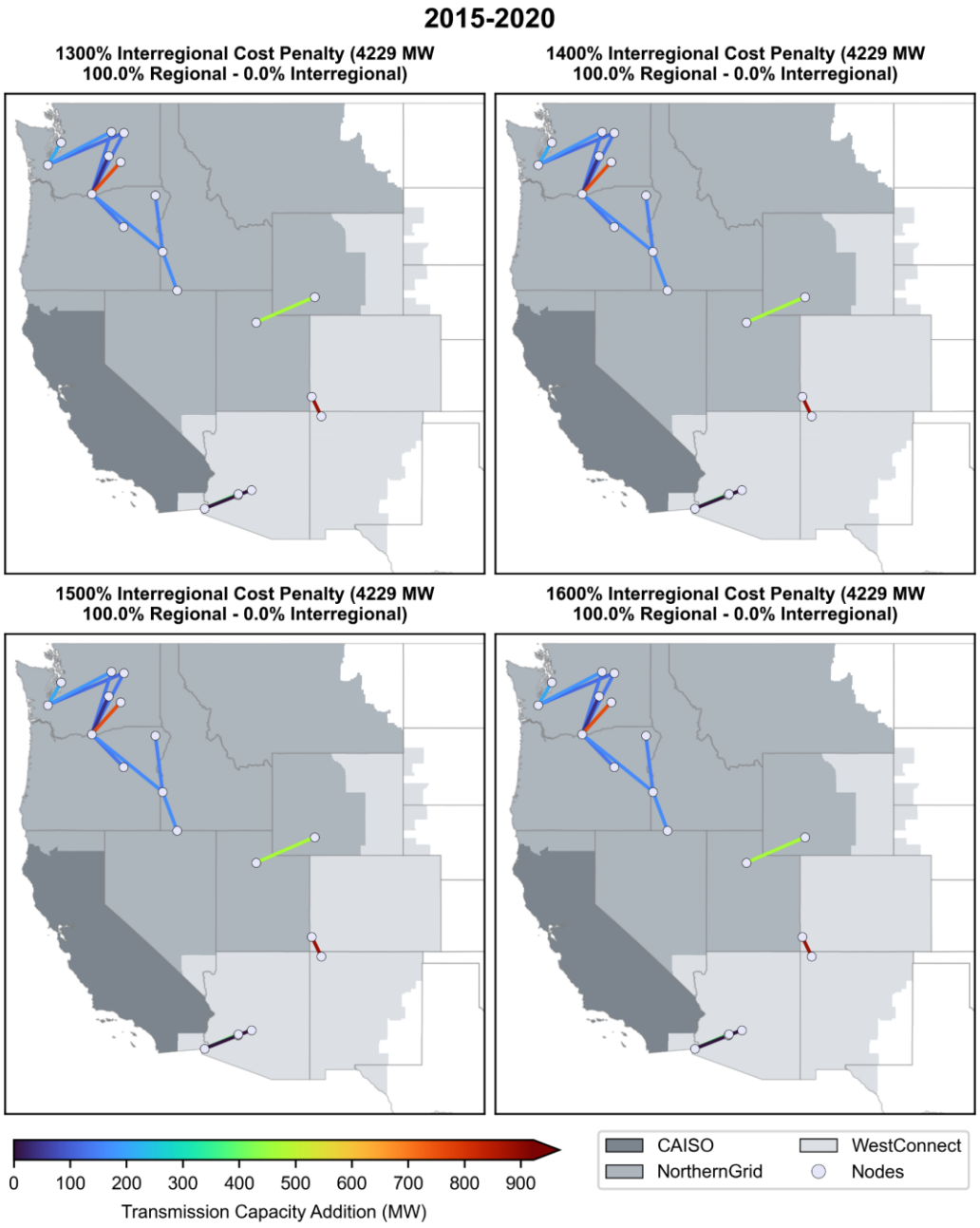

Figure 49: Transmission capacity additions with 1300%, 1400%, 1500%, and 1600% interregional cost penalties. Total transmission capacity addition as well as the shares of regional and international transmission investments can be seen in parenthesis.

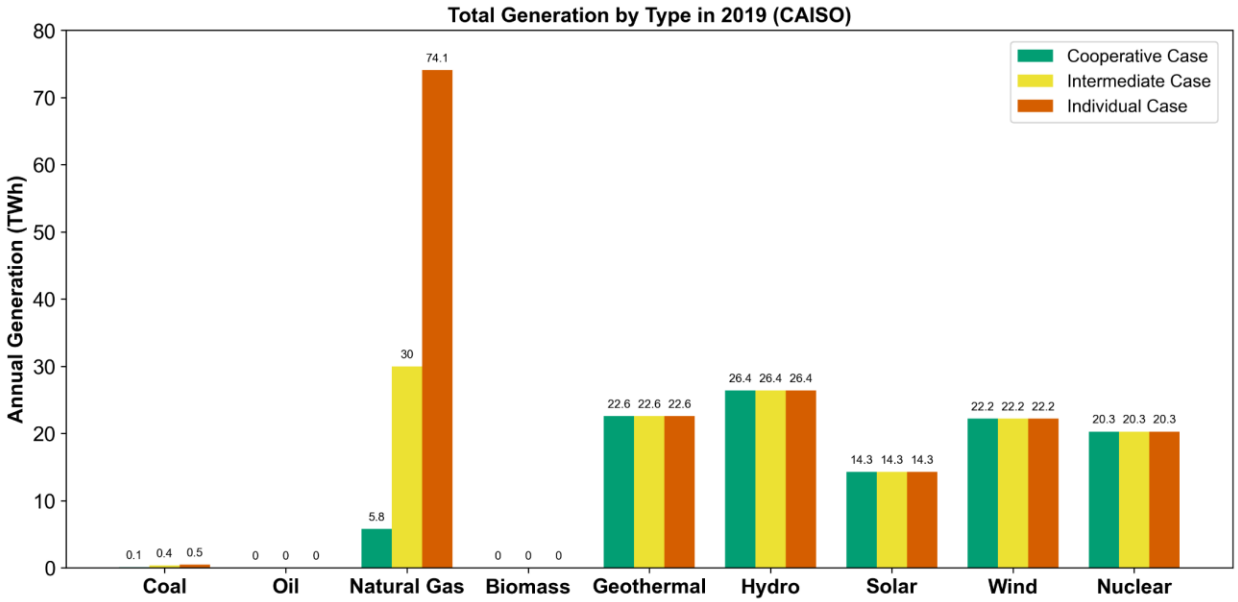

Figure 50: Total annual generation by type in CAISO in 2019. Colors designate the three TEP scenarios.

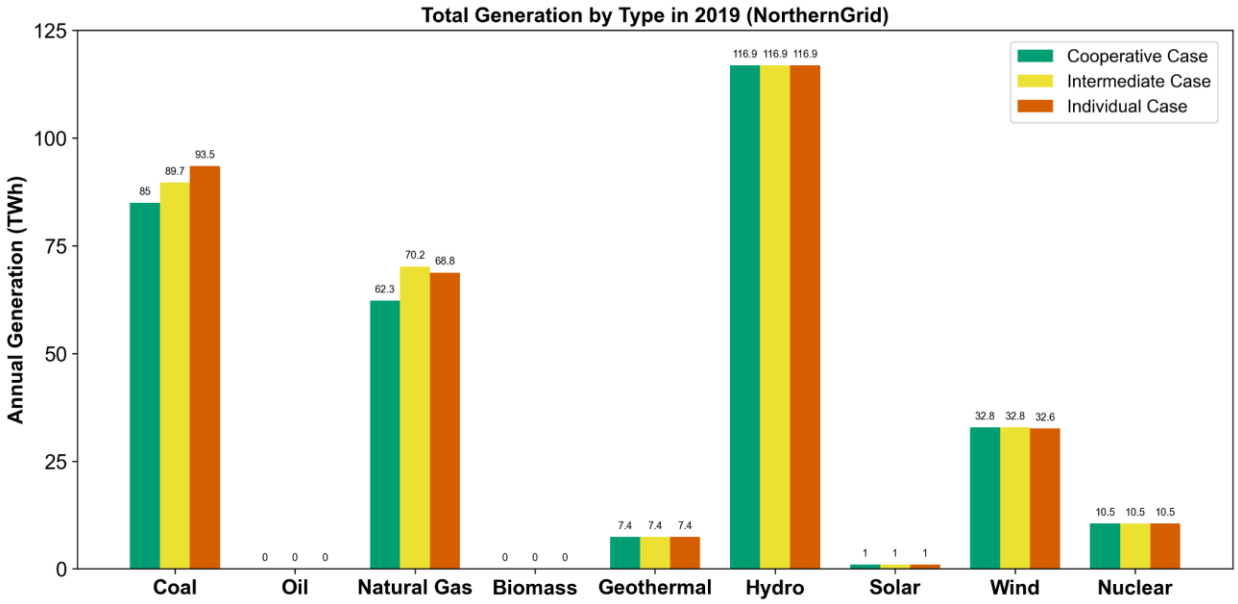

Figure 51: Total annual generation by type in NorthernGrid in 2019. Colors designate the three TEP scenarios.

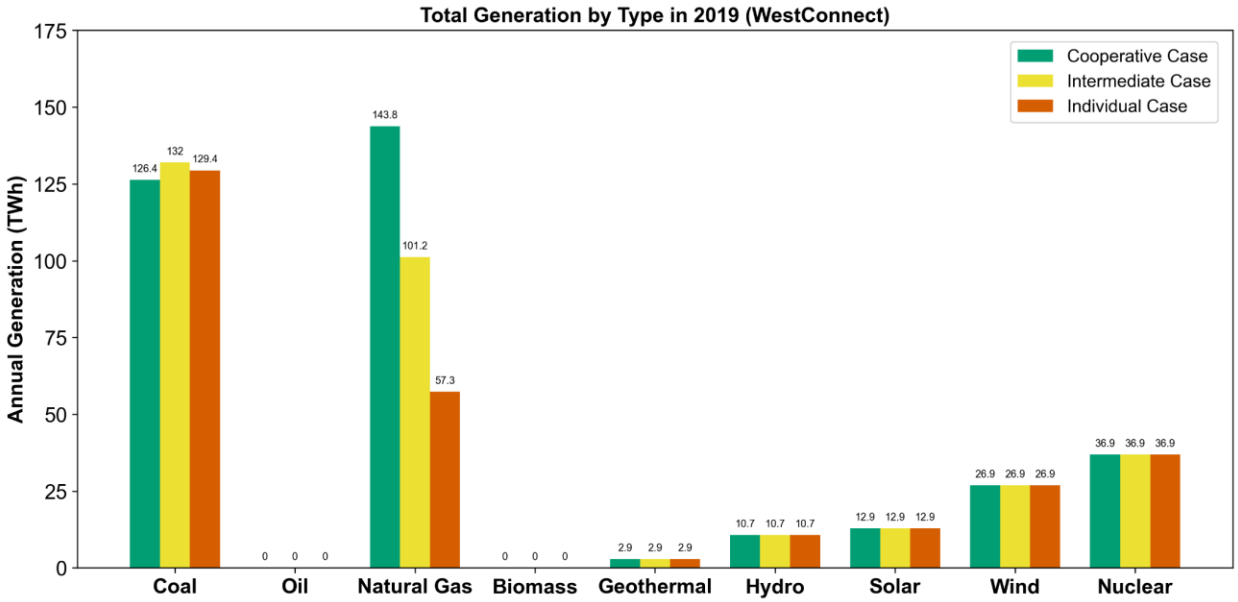

Figure 52: Total annual generation by type in WestConnect in 2019. Colors designate the three TEP scenarios.

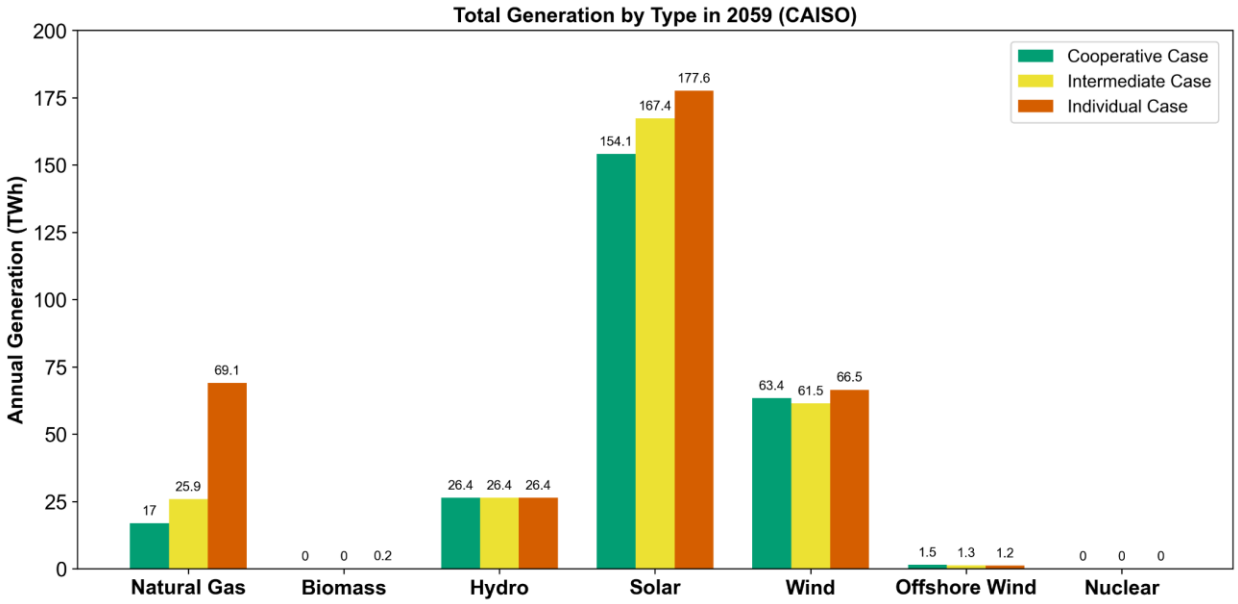

Figure 53: Total annual generation by type in CAISO in 2059. Colors designate the three TEP scenarios.

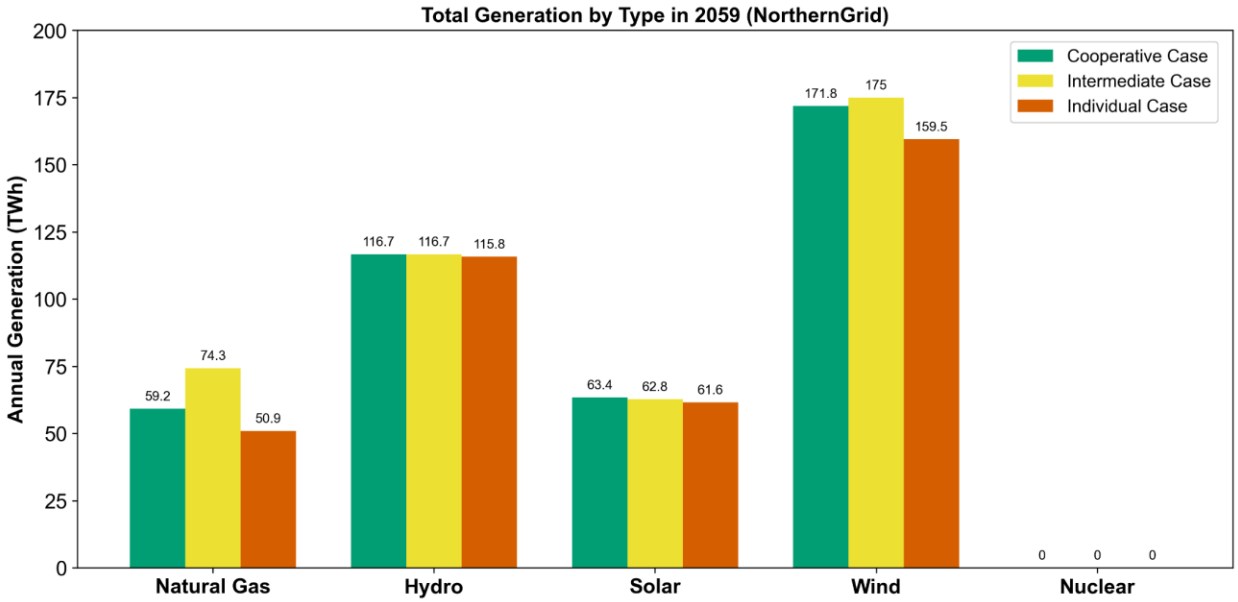

Figure 54: Total annual generation by type in NorthernGrid in 2059. Colors designate the three TEP scenarios.

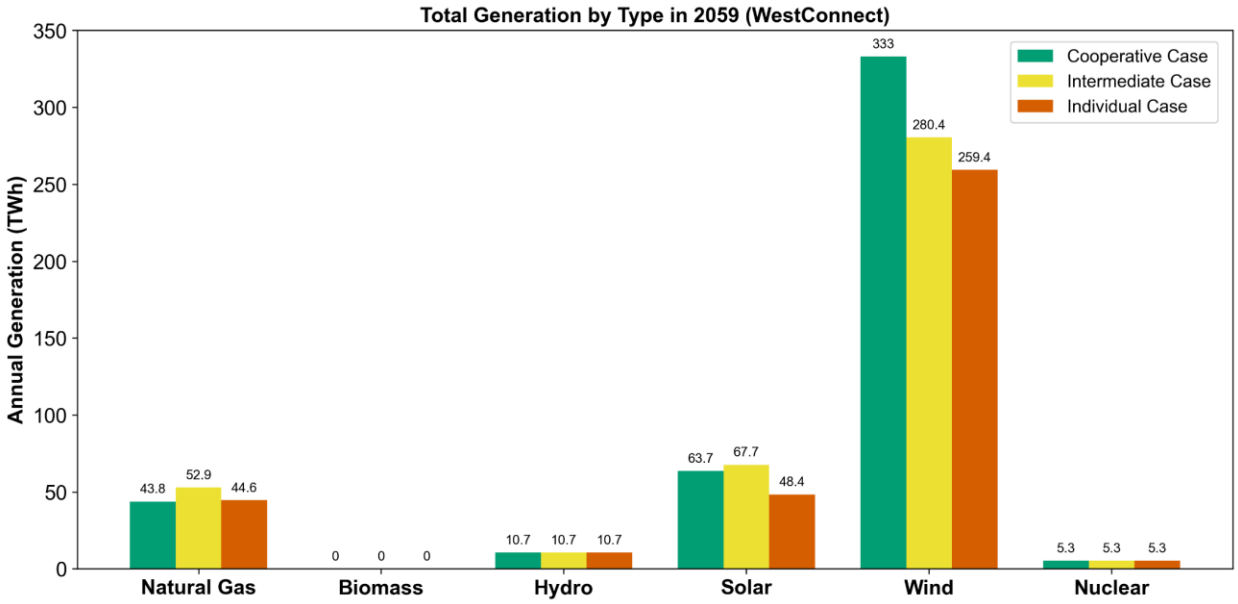

Figure 55: Total annual generation by type in WestConnect in 2059. Colors designate the three TEP scenarios.

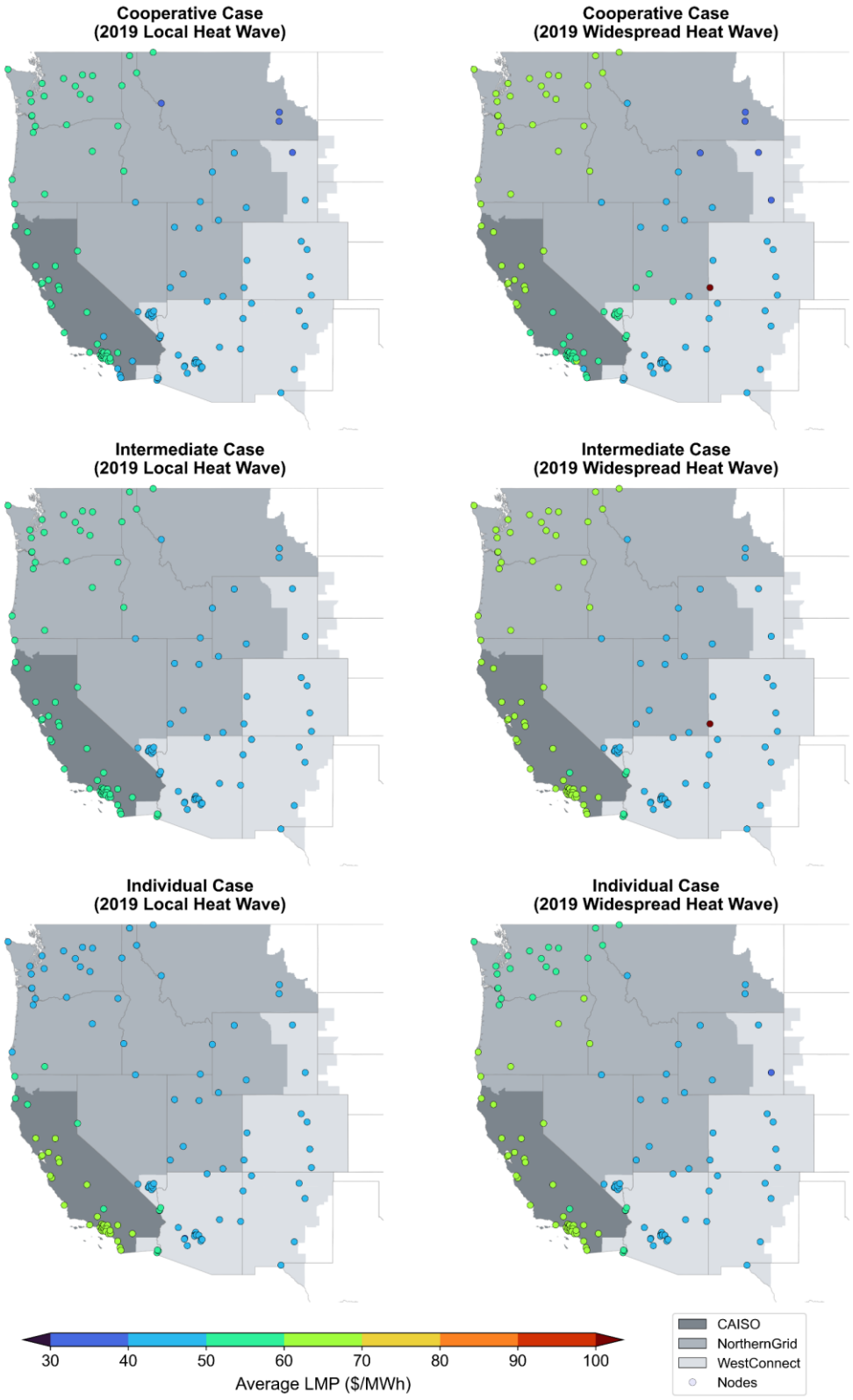

Figure 56: Map of nodal LMPs during local and widespread heat waves under different scenarios in 2019. Colors designate the hourly average LMPs throughout the heat waves.

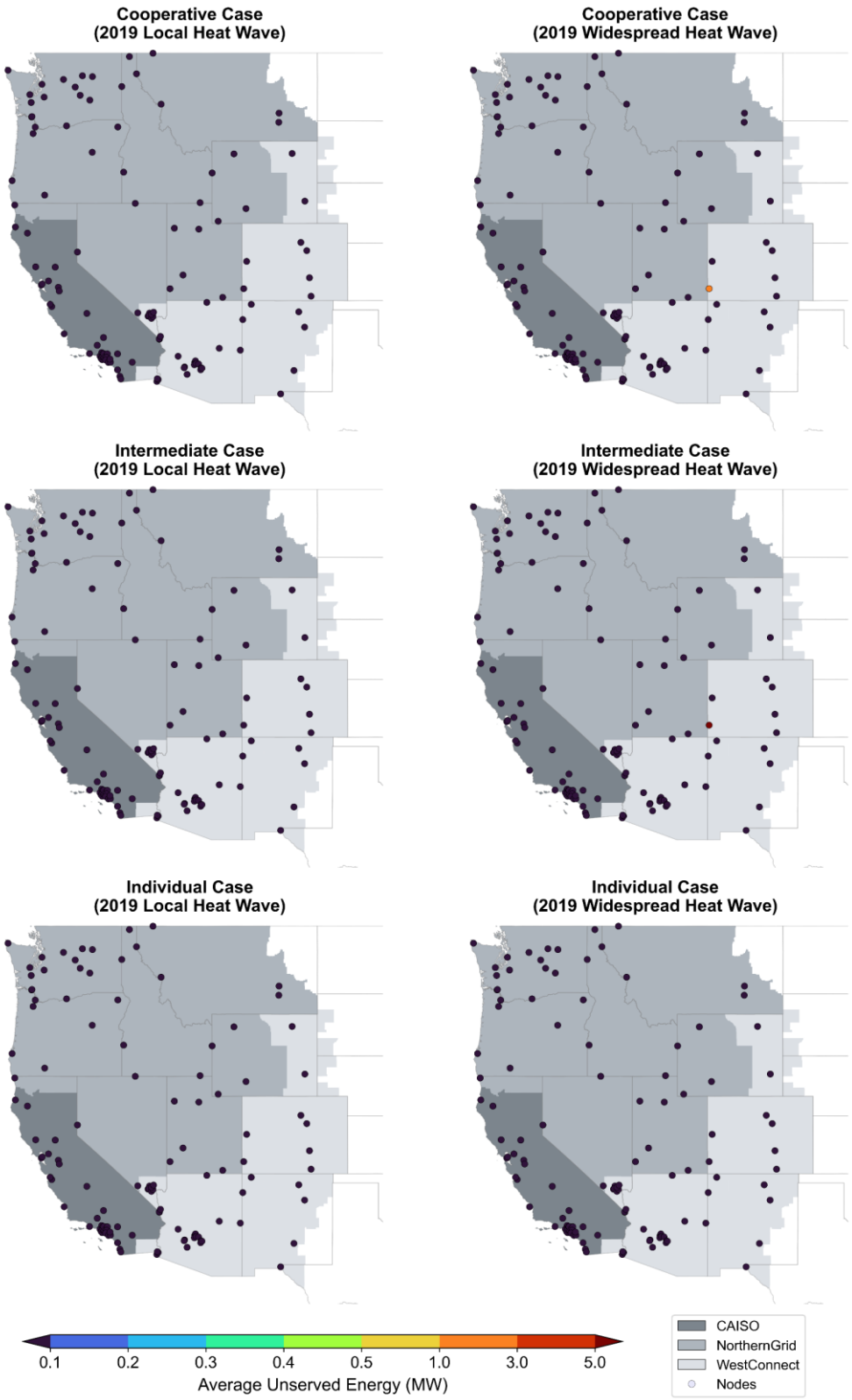

Figure 57: Map of nodal unserved energy during local and widespread heat waves under different scenarios in 2019. Colors designate the hourly average unserved energy throughout the heat waves.

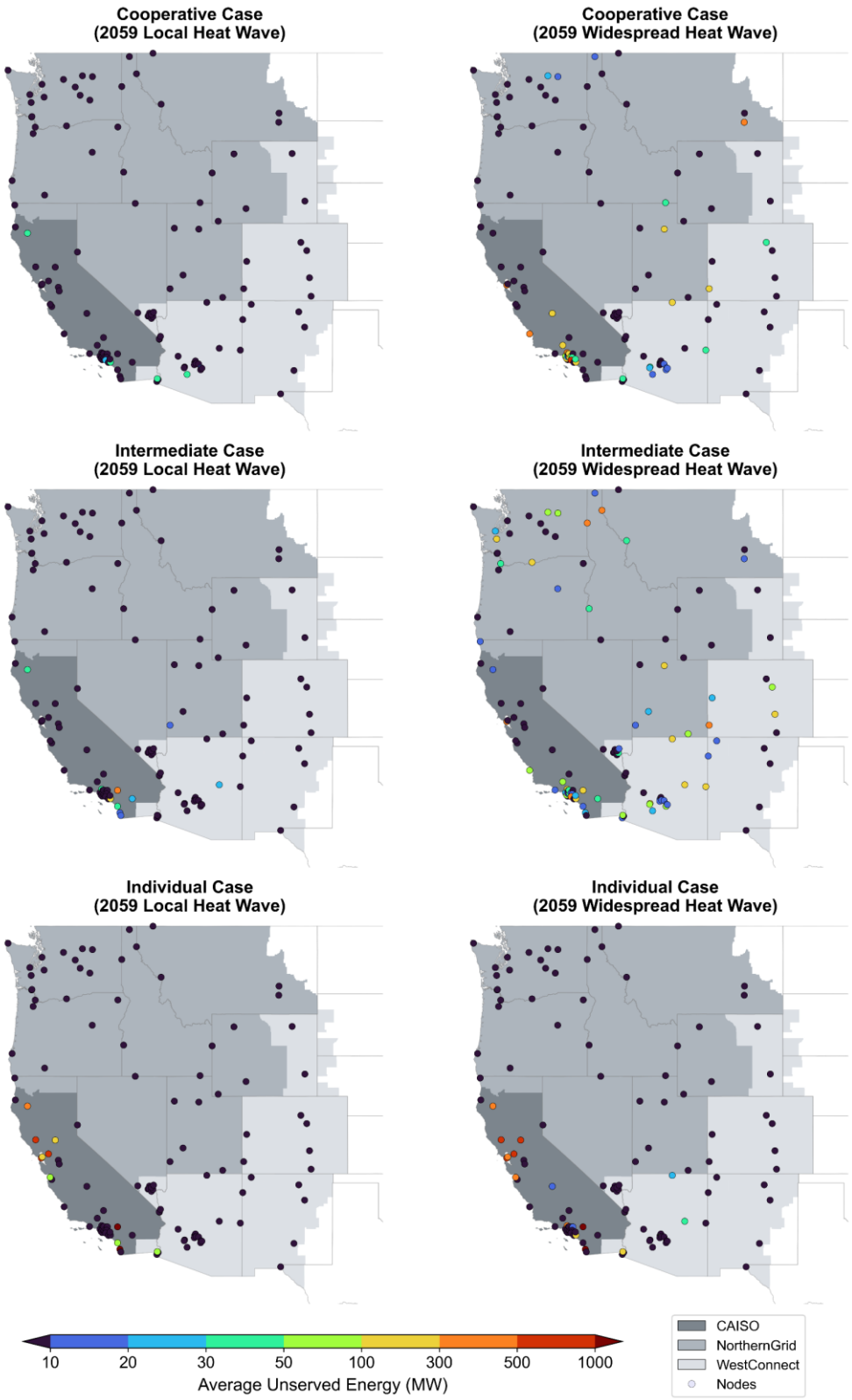

Figure 58: Map of nodal unserved energy during local and widespread heat waves under different scenarios in 2059. Colors designate the hourly average unserved energy throughout the heat waves.